Clemson University
TigerPrints

All Dissertations | Dissertations

8-2022

Protection of Microgrids: A Scalable and Topology Agnostic Scheme With Self-Healing Dynamic Reconfiguration

Phani Harsha Gadde
Clemson University, pgadde@g.clemson.edu

Follow this and additional works at: https://tigerprints.clemson.edu/all_dissertations

 Part of the Controls and Control Theory Commons, and the Power and Energy Commons

Recommended Citation

Gadde, Phani Harsha, "Protection of Microgrids: A Scalable and Topology Agnostic Scheme With Self-Healing Dynamic Reconfiguration" (2022). *All Dissertations*. 3123.
https://tigerprints.clemson.edu/all_dissertations/3123

This Dissertation is brought to you for free and open access by the Dissertations at TigerPrints. It has been accepted for inclusion in All Dissertations by an authorized administrator of TigerPrints. For more information, please contact kokeefe@clemson.edu.

Protection of Microgrids : A scalable and topology agnostic scheme with self healing dynamic reconfiguration

---

A Dissertation
Presented to
the Graduate School of
Clemson University

In Partial Fulfillment
of the Requirements for the Degree
Doctor of Philosophy
Electrical Engineering

---

by
Phani Harsha Gadde
August 2022

Accepted by:
Dr. Sukumar Brahma, Committee Chair
Dr. Johan Enslin
Dr. Ramtin Hadidi
Dr. Shuangshuang Jin

Abstract

Momentum towards realizing the smart grid will continue to result in high penetration of renewable fed Distributed Energy Resources (DERs) in the Electric Power System (EPS). These DERs will most likely be Inverter Based Resources(IBRs) and will be an integral part of the distribution system in the near future. The drive towards resiliency with these IBRs will enable a modular topology where several microgrids are tied together, operating synchronously to form the future EPS at the distribution level.

Since the microgrids can evolve from existing distribution feeders, they will be unbalanced in load, phases, and feeder impedances. A typical control strategy of a conventional inverter that follows the grid voltage and frequency while injecting positive-sequence current can lead to undesirable performance for the unbalanced systems, especially in the islanded mode of operation. So, the dissertation will first focus on the control aspect of IBRs in an unbalanced system. Acceptable operating conditions with stability against disturbances and faults are the primary focus. For the proper functioning of these microgrids, there is a need for grid-forming inverters that can enable acceptable performance and coexist with conventional grid-following inverters that supply only positive-sequence currents. In addition to the control objectives, limiting inverter output during faulted or overload conditions with a current limiter is essential. These control objectives can be implemented in both the synchronous reference frame (dq coordinates) and the natural reference frame (abc coordinates). Hence a comparison study is performed to understand the merit of each implementation related to this specific topology.

As 100% IBR-based microgrid becomes an integral part of the distribution system, the issues and challenges arising from its implementation should be addressed for successful operation. Designing reliable protection is one of the significant challenges for microgrids. Most microgrid protection schemes found in published literature suffer from a lack of generality. They work well for

the assumed topology, including the type and placement of sources. Other generic protection schemes tend to be too complicated, expensive, or both. To overcome these drawbacks, a topology-agnostic, scalable, and cost-aware protection based on fundamental principles is developed that works in the presence of high penetration of inverter-based resources (IBRs). The protection system includes primary and backup. It also implements stable automatic reconfiguration of the healthy sections of the system after clearance of fault, thus increasing resilience by self-healing. The scheme is validated in PSCAD for primary and backup protection and reconfiguration on the IEEE 123-node feeder in grid-connected and islanded modes with 15 IBRs connected to the system.

As the designed protection scheme requires communication between protective devices and the microgrid controller, the method must be validated in real-time with cyber-physical co-simulation for a successful demonstration. In this regard, a Hardware-In-the-Loop (HIL) platform between a simulated power system model using RTDS and physical protective devices is built. In the HIL platform, the primary protection of the scheme is programmed in SEL 421-7 relay, and backup protection is programmed in MATLAB on a generic computer acting as a microgrid controller. The IEC 61850 models are used to communicate between the SEL-421-7 relay and RTDS, whereas TCP/IP communication connects the microgrid controller to RTDS. The focus of the work is to demonstrate the co-simulation platform with communication links established using both protocols and validate the proposed scheme in real-time on the IEEE 123 node distribution feeder. The IEC 61850 and TCP/IP communications configuration are discussed as the interface requires proper hardware and software setup. The real-time performance indicates the Hardware In the Loop (HIL) framework as a competent testing environment for the developed protection scheme for microgrids.

In summary, a scalable and topology agnostic protection scheme with self-healing dynamic reconfiguration is developed for microgrids. Clear guidelines for implementation of the proposed scheme on any microgrid topology are also described.

Dedication

To my parents and wife for always loving and supporting me.

To all my teachers, for shaping my intellect and career.

Acknowledgments

I thank my adviser, Dr. Sukumar Brahma, for his unconditional support in carrying out the research and writing the dissertation. Without his abundant knowledge and professional experience in power system protection, I might not have accomplished my research work. Besides being my adviser and mentor, he helped hone my writing skills. With his input, I conveyed my ideas to others in technical manuscripts lucidly and rationally. I would also like to thank him for his patience and dedication of time in steering me on the right path and for continuously motivating me during difficult times. Additionally, I would like to thank Dr. Johan Enslin, Dr. Ramtin Hadidi, and Dr. Shuangshuang Jin for their time and effort in serving on my advisory committee and for providing me with valuable feedback.

I want to thank the Real-Time Protection and Control of Energy Systems (RT-PACE) lab for providing the equipment and excellent working environment. I thank all the lab members for their support and encouragement during my research at Clemson University.

I extend thanks to my family members, as I would have accomplished none of my achievements without their understanding, love, and support, especially my son Viraj, who kept my spirits up with his innocent actions and smiles.

Lastly, I would like to acknowledge the US Department of Energy for providing financial support for this Ph.D. dissertation research. This work is supported by the U.S.Department of Energy's Office of Energy Efficiency and Renewable Energy(EERE) under the Solar Energy Technologies Office Award Number DE-EE0008774, sub-award 20190382-01-CLE. Any opinions, findings, conclusions, or recommendations expressed in this material are those of the author and do not necessarily reflect the views of the financial supporters.

Table of Contents

List of Tables

List of Figures

Chapter 1

Microgrid System

1.1 Introduction

Electric power distribution system is undergoing a rapid topological transformation with the penetration of renewable energy sources. These sources are expected to provide substantial load support reliably within microgrids, both in grid-connected and islanded modes [1]. California and Hawaii have experienced the highest penetration of DERs in the United States, and are also targeting to achieve 100% renewable generation by the year 2045 [2], making it entirely possible to have just IBRs feeding microgrids. It is also now being conceived that an island will not include a synchronous diesel generator at all; rather the island will be formed by a commercially available grid-forming inverter, with other inverters supporting or following in a droop based control to keep the voltage and frequency at rated values [3]. The intermittent behaviour of the solar and wind energy generation will be compensated with large scale battery storage [2], interfaced with inverter(s). As well known, one of the obstacles for the aggressive implementation of smart grid technologies is the financial overhead on stakeholders in replacing the existing topological infrastructure. So, the transition from a traditional grid to the future microgrids can only be seen as progressive implementation that involves the use of existing infrastructure as much as possible. Therefore, microgrids will evolve from existing distribution feeders, inheriting their topological idiosyncrasies, most notably, substantial unbalance in phases, load, and feeder-impedances.

There is ample amount of literature on stability analysis of inverters and protection of microgrids. In [4],[5] a microgrid with a mix of PV inverters and synchronous diesel generators is

analyzed along with short circuit analysis and development of protection schemes. But no insight is provided on the inverter control schemes or the effect of unbalanced loads. In [6] the stability and resiliency of a microgrid is studied using a PQ droop controller and an overload mitigation controller. However, the study and demonstration is performed on a balanced system and the topology of the microgrid is treated as a parallel combination of inverters connected to a single bus, which is not realistic. In [7] the response of the inverters to unbalanced network is studied, and a negative sequence voltage cancellation control is proposed to balance out the voltage output of a standalone inverter. In [8] the authors worked on an unbalanced microgrid, but the microgrid is treated as single bus with one three phase inverter, one single phase inverter, and loads connected in parallel. In both these papers the multi-inverter interaction that occurs in a microgrid is not mentioned or validated. In [9] an IEEE 13-bus feeder based microgrid model is developed, but phasor models of PV and wind turbine are used for demonstrating the voltage regulation problem in microgrids. The drawback of the phasor models is that they do not capture the dynamics, and the possible stability issues with multiple inverters connected to a feeder. Survey of existing literature reveals that published work has focused on a single inverter control in a microgrid, particularly while addressing unbalanced conditions in islanded mode, e.g., [10]. But in reality, multiple inverters will be connected in a microgrid and their interactions need to be taken into consideration. Also, conventional grid-following inverters are designed to not inject zero sequence or negative sequence currents [11], which are common in unbalanced systems and during unbalanced faults. This design-aspect of inverters is not given attention in majority of the literature. This chapter, therefore, focuses on developing a stable microgrid test bed that incorporates an unbalanced distribution feeder, multiple inverters modeled in detailed time-domain representation using Proportional-Integral (PI) controllers, capable of sharing load without any communication, able to operate in grid-connected and islanded modes, capable of handling transition between these modes, and remain stable under dynamics created by change in load, as well as faults.

1.2 Overview of Inverter Model

The overview diagram of the inverter model is shown in Figure. 1.1. This block is implemented in both grid-forming and grid-following control design. The difference is the grid-forming inverter (GFI) generates an internal reference of three-phase balanced voltages (Reference Gener-

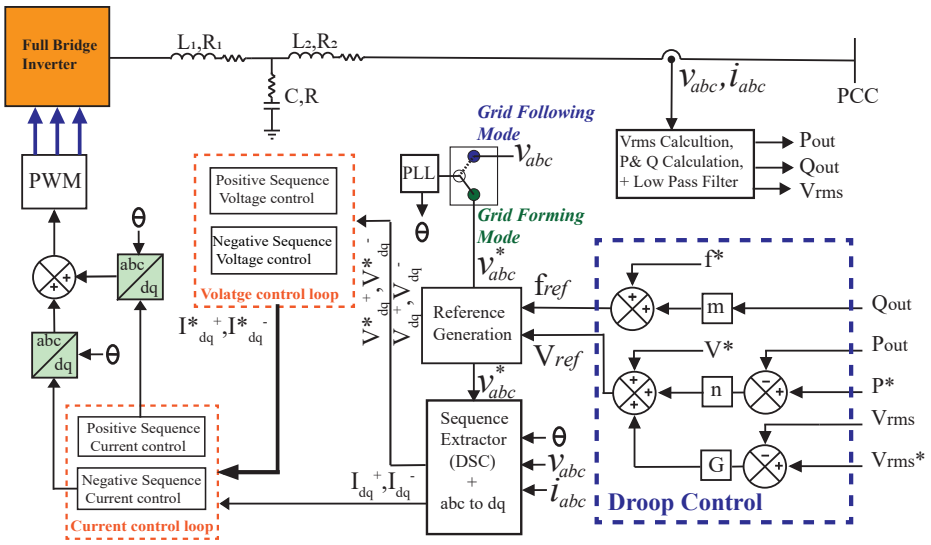

Figure 1.1: Inverter control diagram with PI controller.

ation block in the figure), whereas the grid-following inverters use the voltages measured at their terminal for reference. To facilitate co-existence of multiple inverters, a PQ droop control block is added. Though positive sequence control is most commonly and universally used in existing literature, the negative sequence control block is included and needed to enable separate controlling of sequence components originating due to unbalanced grid. The novelty of this approach, therefore, lies in its universal applicability - power shared among multiple inverters in an unbalanced distribution system in all modes of operation, including transition, while faithfully representing the control objectives of the present generation of commercial inverters. The GFI control design is based on [3], whereas the robust universal power sharing design is adopted from [12],[13] (although the papers demonstrate this only for parallel inverters at a single bus), as this design does not get effected by different output impedances of inverters operating in parallel and can share power irrespective of the X/R ratio of the network. This PQ droop control block will generate the references required for the voltage and inner current control loop. The variables inside the control diagram shown in Figure. 1.1 uses per unit values of voltage, current, and frequency throughout.

1.3 Compensation for Voltage and Current Unbalance

In grid-connected mode the negative and zero sequence currents are supplied by (the usually strong) grid source, which helps keep the voltages balanced within mandated limits. However,

simulation studies, confirmed by field results [14] and experimental results in laboratories [11] have shown that voltages in islanded mode can get highly unbalanced, especially because the inverters are designed to suppress negative sequence currents (zero sequence currents can still be sourced by keeping the grid-side of the interconnecting transformers YG). In order to address this problem, the GFI is allowed to generate negative sequence currents and stabilize the voltages in negative sequence voltage blocking mode, whereas the grid-following inverters are operated in the conventional negative sequence current blocking mode. These designs are shown in Figure. 1.2, Figure. 1.3a, and Figure. 1.3b

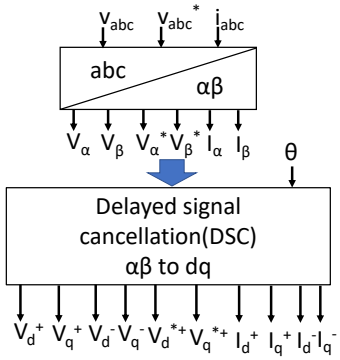

Figure 1.2: Sequence extraction block using DSC.

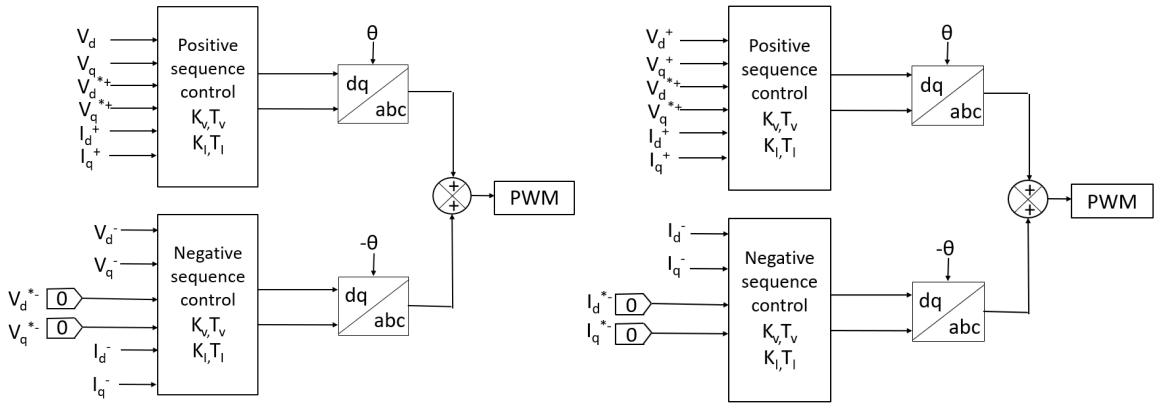

Figure 1.3: (a) Negative sequence voltage blocking controller, (b) Negative sequence current blocking controller.

As shown in the Figure. 1.2, voltage and current signals are converted into $\alpha\beta$ frame and then decomposed into positive and negative sequence components using Delayed Signal Cancellation (DSC) method [15]. The sequence components are then converted from $\alpha\beta$ to dq frame. Positive

sequence components V_d^+, V_q^+ are dc quantities in synchronous frame, but negative sequence components V_d^-, V_q^- will be rotating at 120 hz in opposite direction in synchronous frame. Therefore, to convert the negative sequence components into dc quantities for use in PI controllers, a synchronous frame rotating in opposite direction is taken when converting from $\alpha\beta$ to dq quantities. Figure. 1.3a shows the Negative Sequence Voltage Blocking(NSVB) scheme for balancing the output voltages. Both positive and negative sequence control will have two sets of PI controllers for voltage and current loops. The outputs of voltage PI controllers are the input reference to the current controllers. The PI controllers for voltage and current loop will try to match the reference variables and reduce the negative sequence output voltage to zero by bringing the steady state error to zero. K_V, T_V and K_I, T_I are the PI control parameters. The control block of Negative Sequence Current Blocking(NSCB) of the inverter is as shown in Figure. 1.3b, and follows the same principle to balance the currents, the difference being the negative sequence control in the NSCB scheme does not have the voltage loop, and the current reference of zero is directly fed to the inner current loop of the PI controllers, as shown in the block diagram.

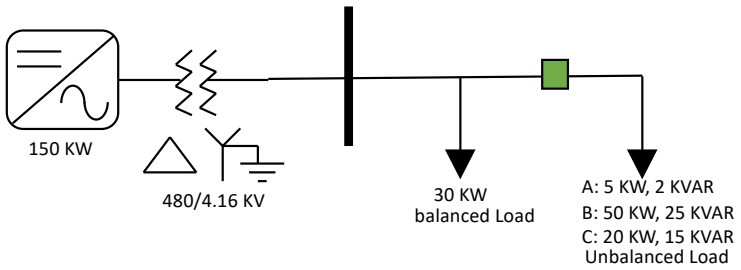

Figure 1.4: Test setup for demonstrating inverter control system.

The test setup to demonstrate the control system performance is as shown in Figure. 1.4. When the unbalanced load is connected to the inverter at 0.3 s, if the inverter is employing the conventional NSCB scheme, the negative sequence currents will be suppressed, resulting in highly unbalanced voltages, as seen in Figure. 1.5. However, if the NSVB scheme is used, as proposed for the GFIs, the voltages will be balanced, but the inverter will need to supply the negative sequence currents, as shown in Figure. 1.6.

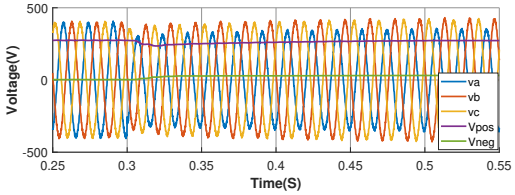

(a) Voltage Output

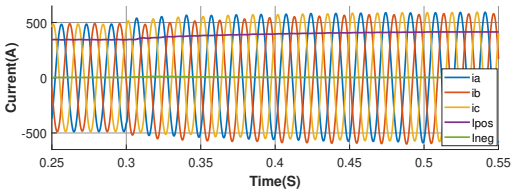

(b) Current Output

Figure 1.5: Inverter Output for NSCB control.

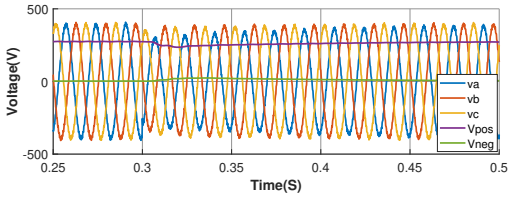

(a) Voltage Output

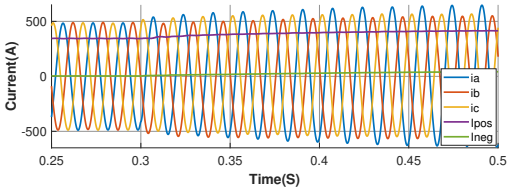

(b) Current Output

Figure 1.6: Inverter output for NSVB control.

1.4 Microgrid test system - 13 bus feeder

In order to replicate the unbalanced distribution system islands fed by 100% or extremely high penetration of IBRs, IEEE 13-bus feeder [16] is chosen as the test system. This is simulated in complete detail in PSCAD. This feeder has a significant unbalance in load, phase impedances, and number of phases. The one-line diagram of the feeder is shown in Figure. 1.7. The total load on the system is 3158+j1588 KVA (total 3534 kVA), including capacitor banks. The sources at bus 650, 633, 675 and 680 are simulated to have the capability of 1500, 1000, 800 and 800 kVA (total 4100 kVA), respectively, to have ample capacity for islanding. The feeder has a 600 kVar three-phase capacitor bank at bus 675, and a 100 kVar single-phase capacitor bank at bus 611, which are both modeled. Note that the reactive power provided by these banks is not enough to feed the entire system, so the inverters will be operated at unity power factor (typical practice) only under grid connected mode, and not in islanded mode. In islanded mode, GFI connected to bus 650 will act as a leader by providing voltage and frequency reference for rest of the grid following inverters 2, 3, 4. The GFI will be used to compensate the unbalance in voltage, and other inverters will only generate positive sequence currents, as they participate in sharing of real and reactive power. Zero sequence currents will be sourced from YG connected secondaries of interconnecting transformers, as mentioned before.

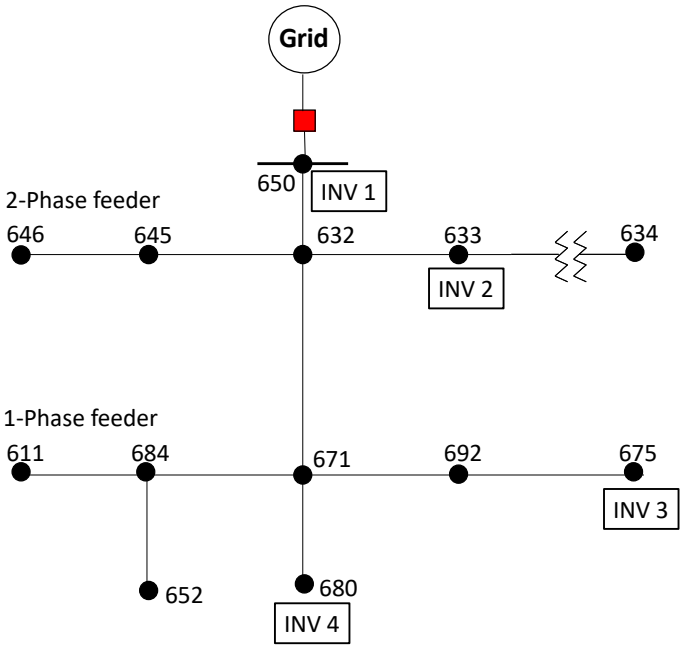

Figure 1.7: IEEE 13-bus distribution feeder with four inverters.

Table 1.1 lists the locations and ratings of inverters in the test system, and Table 1.2 lists the control and filter parameters of inverters.

Table 1.1: Locations and Ratings of Inverters.

Inverter No.	***Bus No.***	***Rating(KW)***
1	650	1500KW
2	633	1000KW
3	675	800KW
4	680	800KW

1.5 Simulation Results

A simulation was run that changes the topology from grid-connected to islanded mode at 1 s into the simulation. Figure. 1.8a shows the power sharing and a stable transition to islanded mode, while Figure. 1.8b shows the corresponding voltages and currents at the inverter terminals. In grid-connected mode, all inverters are acting in the grid following mode. Notice from Figure. 1.8a, all inverters are operating at rated output with unity power factor, and the excess real power

Table 1.2: Controller and Filter Parameters.

Parameters	K_V	T_V	K_I	T_I	$\boldsymbol{m}$	$\boldsymbol{n}$
Values	0	0.05	1	0.05	1	0.05
Parameters	***L1,R1***	***C,R***	***L2,R2***			
Values	$800\mu H$ 0.01Ω	$1000\mu F$ 0.01Ω	$800\mu H$ 0.01Ω			

is being fed back into the grid. When the microgrid is islanded, Inverter 1, which is GFI, gets into the grid-forming mode, stabilizing and balancing the voltages (Figure. 1.8b), while inverters 2, 3, 4 share real and reactive power, but only output balanced currents.

A second simulation was run to show the stability against a step increase in load at bus 632 (phase A:100+j45 kVA, phase B:100+j25 kVA, phase C:10+j7 kVA), while running in islanded mode, implemented at 0.5 s into the simulation. Power plots are shown in Figure. 1.9a, showing that the increased load is shared seamlessly by all four inverters. Voltages and currents shown in Figure. 1.9b illustrate the roles of GFI and grid following inverters are maintained as designed.

Finally, a three-phase fault was created in the islanded grid on bus 671 at 0.5 s, and removed at 0.6 s. The power plots shown in Figure. 1.10 illustrate the system recovers to pre-fault conditions in a reasonable time-frame. Similar results were also observed for a single line to ground fault.

1.6 Summary

In this chapter, a microgrid system using the IEEE 13-bus feeder is developed that can replicate the behavior of an unbalanced distribution system fed by 100% IBRs. A GFI is designed to replicate the role of a conventional synchronous generator in a microgrid to maintain the voltage and frequency reference to the grid-following inverters in an islanded microgrid. Also, the feature of the commercial grid-following inverters to not inject zero sequence or negative sequence currents is also implemented. In the islanded mode, GFI is shown to act as a master inverter in balancing out the voltages in a microgrid; the other grid-following inverters are shown to inject purely balanced output currents. A robust universal PQ droop method is used for power-sharing between the inverters, and stable operation of four inverters is shown in grid-connected and islanded modes, including transition, as well as for changes in load and faults in the islanded mode. In the next chapter, these control objectives will be implemented in natural reference frame using Proportional-Resonant (PR)

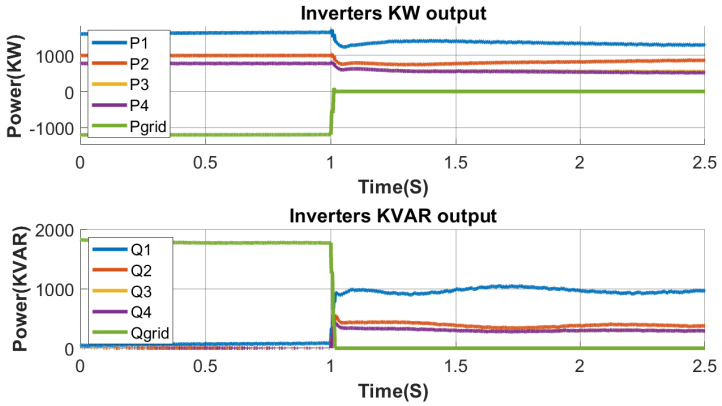

(a)

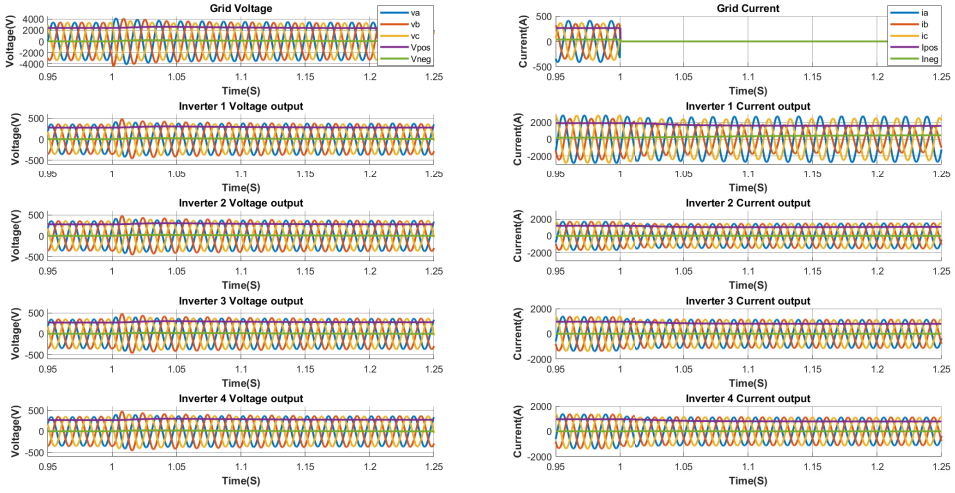

(b)

Figure 1.8: (a) Power output response for islanding operation, (b) Inverter voltage and current response to transition from grid-connected to islanded mode.

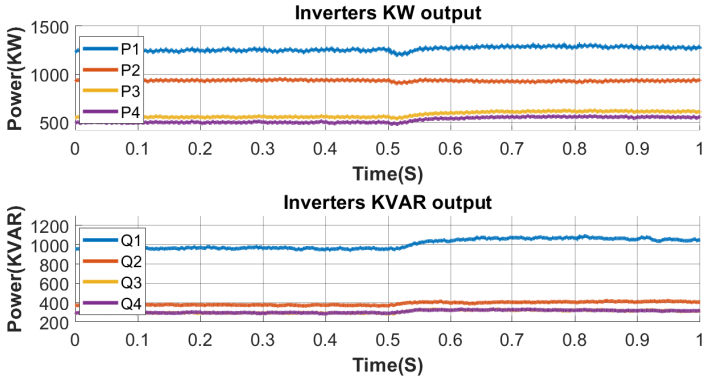

(a)

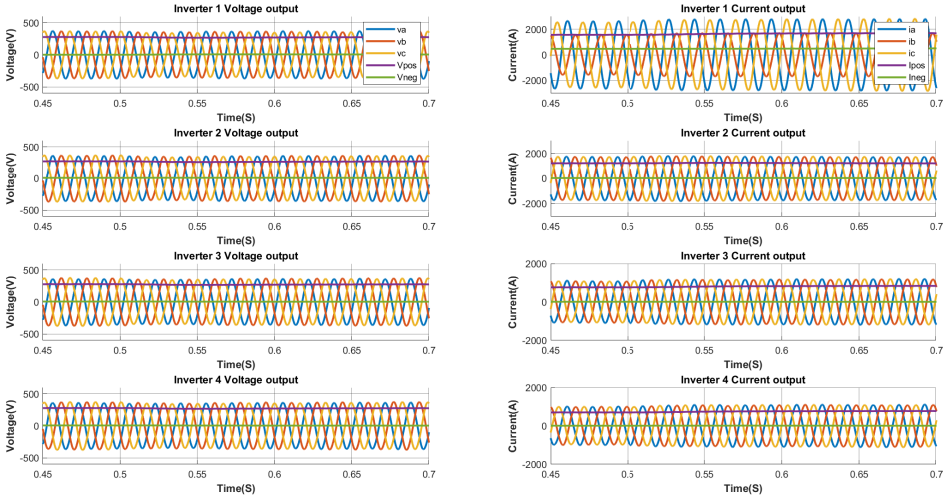

(b)

Figure 1.9: (a) Power output response for unbalanced step increase in load in islanded mode, (b) Inverter voltage and current response to unbalanced step increase in load in islanded mode.

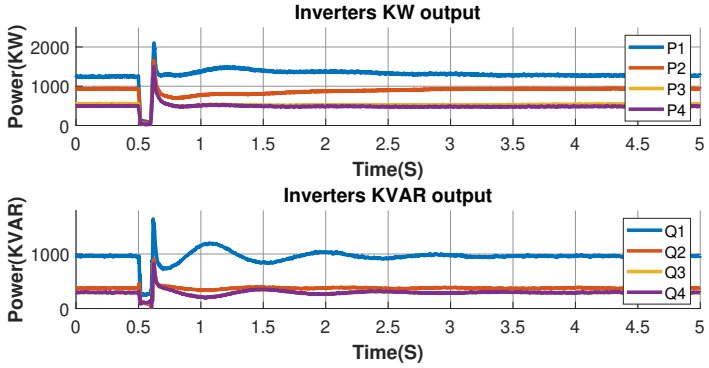

Figure 1.10: Response to three phase fault in islanded mode.

controllers and compared against the implementation with PI controllers.

Chapter 2

Comparison of PR and PI Controllers for Implementing the Inverter Model

2.1 Introduction

The design of the inverter is mainly dependent on the system configuration, and inverter features like grid support with voltage regulation, low voltage ride-through (LVRT), and fault ride-through (FRT) [1]. In [6, 8], the stability, and resiliency of a microgrid are studied using a PQ droop controller and an additional overload mitigation controller. However, it did not consider the control aspect of dealing with an unbalanced system. In [7], the response of an inverter to an unbalanced network is studied and proposed a negative-sequence voltage cancellation control to balance out the voltage output of a standalone inverter. However, the control system is implemented only in the synchronous reference frame(dq coordinates). So, the implementation in the natural reference frame(abc coordinates) and a comparison to understand each implementation's merit is needed. Also, the model of conventional grid-following inverters should be designed not to inject zero-sequence or negative-sequence currents [11], which exist in unbalanced systems and during asymmetrical faults.

In a microgrid, where different types of IBRs based on different technologies and power ratings are interconnected, a hierarchical control architecture is assumed, as shown in Figure. 2.1, with

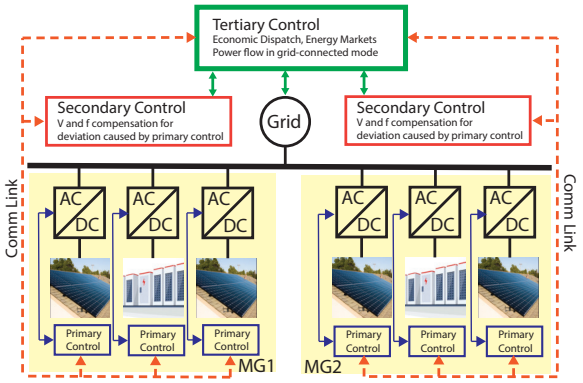

Figure 2.1: Hierarchical control architecture for microgrids.

primary, secondary, and tertiary control to increase reliability, efficiency, and controlability[17]. The tertiary control can be part of the Energy Management System(EMS) at the utility end for solving several objectives like economic dispatch, energy markets, exchanging information with distribution system operators (DSOs) and taking care of power-flow in grid-connected mode. Secondary control can be the microgrid controller correcting the voltage and frequency deviations caused by primary control, using slower controllers and low bandwidth communication [18]. The communication link between primary and secondary control enables sending set-points to primary control and receiving information about IBR capacity and status. At the primary control level, the droop controllers manage the power-sharing among the IBRs in a microgrid by implementing droop equations, not requiring any communication between the IBRs. The voltage and current controllers in the primary control are responsible for regulating the inverter output variables. These controllers should have high bandwidth and performance to guarantee a fast time response under all operating conditions[3]. The focus of this chapter is at the primary control level. The control structure for primary control using PI controller is discussed in chapter 1. In this chapter, the more traditional PI controller is compared with the proportional-resonant (PR) controller showing the simulation results using PSCAD on an unbalanced system. Acceptable performance under unbalance with stable response to disturbances and faults in all operating modes are the focus of this study. This chapter also introduces fault modeling to the design with a current limiter and discussed in section 2.2.4.

2.2 IBR model implementation with PR controller

The PI controller has a well-known shortcoming of the inability to track a sinusoidal reference with zero steady-state error. Overcoming this drawback requires a transformation from the natural reference frame (*abc* coordinates) to the synchronous reference frame (*dq* coordinates), increasing the complexity and cost of the implementation [19]. Also, PI control has poor disturbance rejection capability and the inability to remove low-order harmonics [20] due to bandwidth limitation and requires additional low pass filters in the control system, which adds delay. One way to increase bandwidth is to have a high proportional gain. But, the system's stability becomes a critical issue with higher gains, primarily when LCL filters are used to attenuate the high-frequency switching ripple. The stability problem is challenging to solve as higher gains could excite resonance and lead to instability [21].

Among other controllers, the PR controller is a promising solution to achieve zero steady-state error for a sinusoidal input. Having an infinite gain around the resonance frequency, i.e., the fundamental frequency of 60Hz, a PR controller offers superior performance in sinusoidal reference tracking and also in disturbance rejection. In this chapter, the design and implementation of a PR based controller for both outer voltage and the inner current loop are proposed and evaluated vis-a-vis the PI-based controller. The block diagram of the inverter model with the PR controller is shown in Figure. 2.2. Components of the control diagram are discussed in the following sections, and distinctions from the PI-based design shown in Figure. 2.3 are highlighted.

2.2.1 Droop Control for Power Sharing

As discussed earlier, for primary control, the robust universal droop power-sharing design is adopted from [12, 13], as this design does not get affected by different output impedances of inverters operating in parallel and can share power irrespective of the X/R ratio of the network. This PQ droop control block will generate the reference V_{ref} and f_{ref} using the calculated inverter output power P_{out}, Q_{out} and output voltage V_{rms}. This droop control is the same for both PI and PR based implementations and has shown excellent performance in [22]. However, for PR control, the droop control can eliminate the need for a separate phase-locked loop (PLL) in the system, as droop control also acts intrinsically as PLL[23] for locking on to the grid. Unlike the PI controller, a PR controller does not need a PLL to generate θ for the conversion of *abc* to *dq* quantities. All

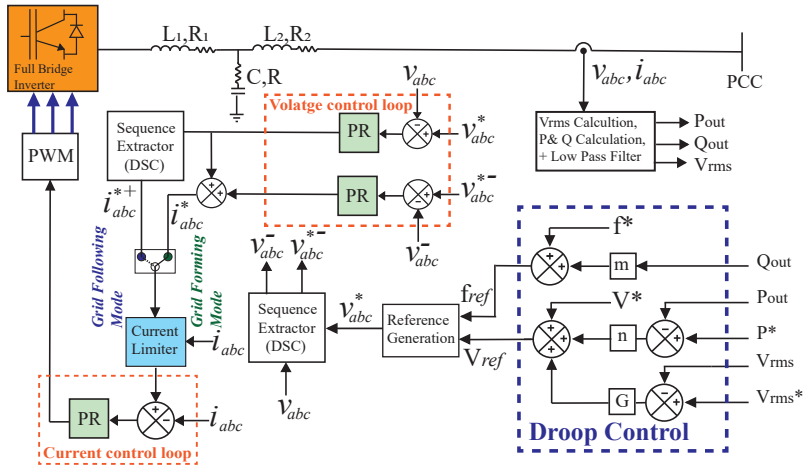

Figure 2.2: Inverter control diagram with PR controller.

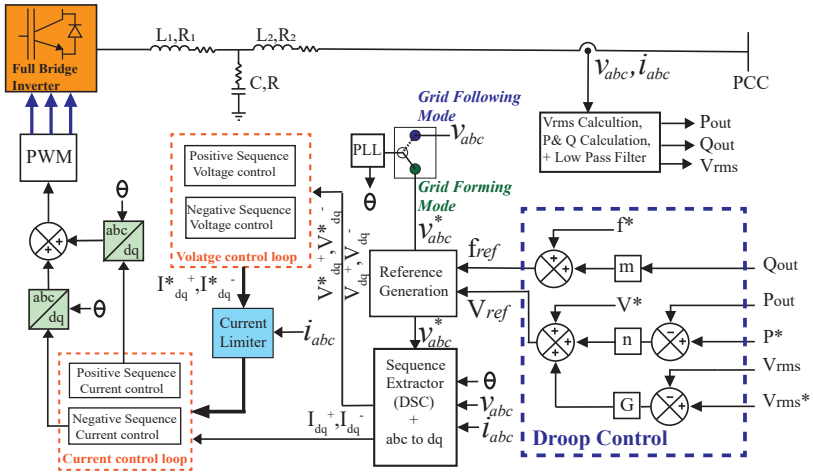

Figure 2.3: Inverter control diagram with PI controller with current limiter.

the signals inside the control blocks use per-unit values of voltage, current, and power, with the reference signals having a $*$ superscript. The voltage and current loop descriptions are discussed in the following sub-sections.

2.2.2 Controller Transfer Function

The transfer function of the practical PR controller is given by (2.1), which can be mathematically derived by transforming an ideal synchronous frame PI controller to a stationary frame. It achieves high enough gain at the ac fundamental frequency, i.e., 60Hz, ω= 377 rad/s, to force

the steady-state error to zero, and no phase shift and gains at other frequencies. In (2.1) K_p is the proportional gain, K_i is the resonance gain, and $\omega_C = 0.5$ rad/s is the cut-off frequency of the controller.

$$G_{PR}(S) = K_p + K_i \frac{2\omega_C S}{S^2 + 2\omega_C S + \omega^2} \tag{2.1}$$

The transfer function of the PI controller is given by (2.2), where K is the proportional gain and T is the integral time constant of the controller.

$$G_{PI}(S) = K + \frac{1}{ST} \tag{2.2}$$

2.2.3 Control Scheme for Voltage and Current Unbalance

In grid-connected mode, the negative-sequence and zero-sequence currents are supplied by (the usually strong) grid source, which helps to keep the voltages balanced within mandated limits, and the inverters are designed to suppress negative-sequence currents. However, zero-sequence currents can still be sourced by keeping the grid-side of the interconnecting transformers as Y-G. In islanded mode, due to the lack of grid-source, this design can lead to highly unbalanced voltages [24]. In order to address this problem, the grid-forming inverter is allowed to generate negative-sequence currents and stabilize the voltages in islanded mode. The grid-following inverters are still operated in the conventional negative-sequence current blocking mode.

For the grid-forming inverter, as shown in Figure. 2.2, the Voltage reference v^*_{abc} generated from the reference generation block provides an inherent negative-sequence blocking. The negative-sequence component extracted from the output voltage v_{abc} is compared against the negative-sequence component of v^*_{abc} for negative-sequence voltage blocking (NSVB) in the islanded mode of operation. The summation output of the voltage loop produces an unbalanced current reference i^*_{abc}. These reference currents once passed through the current limiter block, are compared against the output currents i_{abc} to generate the modulation signals. The external loop controls the grid voltage to match its reference value, while the internal control loop regulates the current supplied by the inverter. In contrast, in the PI controller implementation, the NSVB scheme for balancing the output voltages requires decomposition of v_{abc}, v^*_{abc} into positive and negative-sequence components using Delayed Signal Cancellation (DSC) method [15] and conversion to respective dq

quantities. Both positive and negative-sequence control will have two sets of PI controllers for voltage and current loops. The outputs of positive-sequence voltage control are the reference input to the positive-sequence current control and the same for negative-sequence control loop[22].

For grid following inverters, as shown in Figure. 2.2, The output current reference from the voltage loop is decomposed into positive and negative-sequence components using the sequence extractor block (DSC method). For negative-sequence current blocking (NSCB), the output currents i_{abc} are then compared against the positive-sequence reference currents i^*_{abc}, to suppress the negative-sequence currents in the output. The same principle is followed for PI controller implementation for NSCB, but the difference is that it has two separate current controllers. The negative-sequence current control with negative-sequence output current I^-_{dq} is compared against zero reference, and the positive-sequence current control with positive-sequence output current I^+_{dq} is compared against I^{+*}_{dq}, which is the output of the positive-sequence voltage loop.

2.2.4 Current Limiter

The inverter's current output has to be limited to prevent damage to semiconductor switches during an overload or short circuit condition. There are multiple methods proposed in the literature for the current limiting of inverter output, like the instantaneous saturation limit or predefined latched limit [25]. A simple but new strategy for limiting currents is proposed in this section. The block diagram of the current limiter (shown in Figure. 2.2 and Figure. 2.3) for PR and PI-based controllers are shown in Figure. 2.4a and 2.4b, respectively. The only difference is, in PI controller based implementation, the reference currents I^{*+}_{dq} and I^{*-}_{dq} are converted back to abc quantities. The RMS values are extracted from phase currents i_{abc} and i^*_{abc}, and the maximum value of the three phases is compared against the predefined limit $ILimit$ based on the rating of the inverter to determine the fault status. When a fault is detected, the reference currents are then multiplied by a factor before sending it to the current control loop. For the model in this paper, the $ILimit$ chosen for both types is 1.5 pu, so the multiplication factor will be $(1.5/Iref_{Max})$, as shown in Figure. 2.4. $Iref_{Max}$ is the peak of the maximum of the reference currents i^*_{abc}.

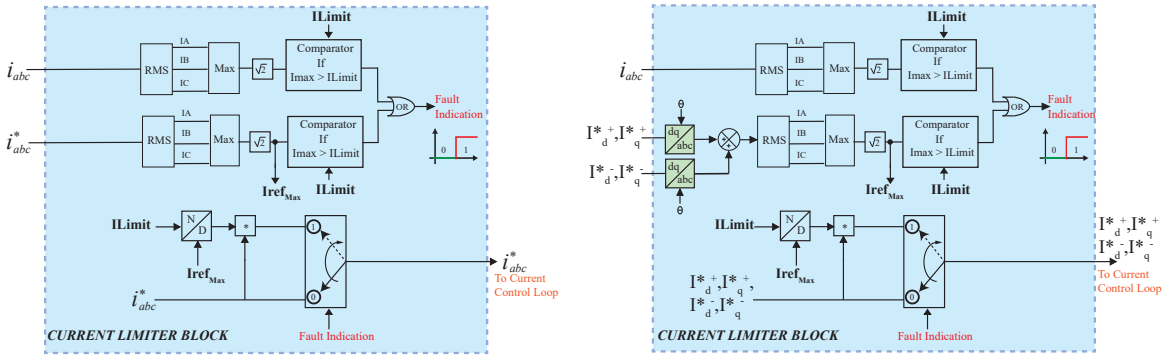

Figure 2.4: Current limiter block: (a) Current limiter for PR based control, (b) Current limiter for PI based control.

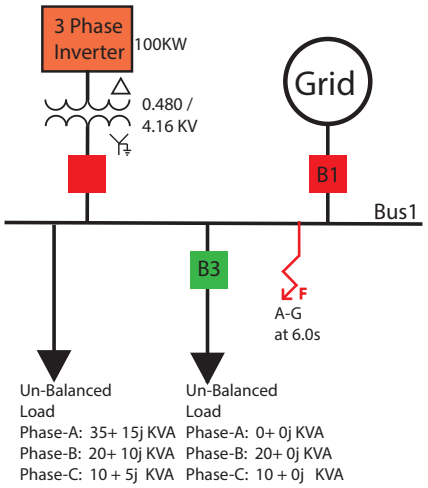

Figure 2.5: Test system for comparison study.

2.3 Performance comparison of PR and PI based controllers

The test system for the comparative study of the two controllers is shown in Figure. 2.5. It is designed to behave as an unbalanced microgrid. The load on the system and inverter capacity are selected to avoid overload in the islanded mode of operation. The inverter under test is rated at 480 V, 100 kW, and interfaced via a Δ/Y-G transformer to the grid. Initially, breakers B1 and B2 are closed, making the system unbalanced and grid-connected. The sequence of events created in the simulation are shown in Table 2.1, effected by appropriate opening and closing of breakers. The inverter's performance with the PR controller is compared against the 'PI-1' and 'PI-2' controllers. 'PI-1' is the inverter model with the filter parameters the same as the PR controller, and accordingly

tuned control parameters, whereas 'PI-2' is with the updated filter parameters, and accordingly tuned control parameters for improved stability and better dynamics (refer to Table 2.2). The comparison between PR and PI-1 gives insight into the actual difference in the controllers' dynamic response. In contrast, comparison with 'PI-2' is made to include an improved PI design, which comes at the cost of a bulkier filter.

Table 2.1: Sequence of Events in Simulation

Event No.	***Description***	***Time in simulation***
1	Islanding	2s
2	Unbalanced Step Load	4s
3	L-G Fault for 0.2s, $R_f = 1.0\ \Omega$	6s

Table 2.2: Controller and Filter Parameters

PR	Kp_V	Ki_V	Kp_I	Ki_I	$\boldsymbol{m}$	$\boldsymbol{n}$	$\boldsymbol{G}$
Control Parameters	1	100	1	300	2	1	2
Filter Parameters	***L1,R1***	***C,R***	***L2,R2***				
	$3500\mu H$ 0.1Ω	$800\mu F$ 0.4Ω	$100\mu H$ 0.01Ω				
PI-1	K_V	T_V	K_I	T_I	$\boldsymbol{m}$	$\boldsymbol{n}$	$\boldsymbol{G}$
Control Parameters	0.2	0.1	0.4	0.2	2	1	2
Filter Parameters	***L1,R1***	***C,R***	***L2,R2***				
	$3500\mu H$ 0.1Ω	$800\mu F$ 0.4Ω	$100\mu H$ 0.01Ω				
PI-2	K_V	T_V	K_I	T_I	$\boldsymbol{m}$	$\boldsymbol{n}$	$\boldsymbol{G}$
Control Parameters	1	0.1	0.5	0.05	2	1	2
Filter Parameters	***L1,R1***	***C,R***	***L2,R2***				
	$3500\mu H$ 0.5Ω	$1500\mu F$ 0.8Ω	$100\mu H$ 0.01Ω				

2.3.1 Islanding Operation

The system is islanded at 2.0s into the simulation by opening breaker B1. The results of this event are shown in Figure. 2.6. The current waveforms in Figure. 2.6c-e show that when the system is grid-connected, the inverter operates in the grid-following mode and supplies balanced currents. When islanded, the inverter supplies unbalanced currents by operating in the grid-forming mode. Figure. 2.6a shows that the settling time of the bus voltage is lower for the PR controller, resulting in faster recovery to a stable operating state after islanding. Also, the voltage overshoot is

less for the PR controller than both 'PI-1' and 'PI-2'. Figure. 2.6b shows the NSVB performance after islanding is superior with the PR controller.

2.3.2 Step Load

The results for event-2 are shown in Figure. 2.7. A step-load of considerable unbalance is done by closing Breaker B3 at 4s into the simulation. The results were clearly showing better performance for the PR controller. The voltage dip of Bus1, as shown in Figure. 2.7a is higher for the PI controller because of the overshoot caused by the proportional gain, and it takes a longer time to settle. It can be seen that the dynamics are improved with the updated filter and control parameters. However, that comes at the cost of increased values of filter components and a damping resistor. Again, from Figure. 2.7b-e the negative-sequence voltage suppression takes a longer time for the PI controller.

2.3.3 Fault Response

The results for event-3, an A-G fault on Bus1 at 6s into the simulation (in islanded mode), are shown in Fig: 2.8. The Fig: 2.8a shows the PR controller limits the current to 1.5 pu within two cycles, resulting in faster thermal protection of switches. The PI-1 controller cannot limit the current to 1.5 pu even within 0.2s, as shown in Fig: 2.8b and Fig: 2.8c shows that the PI-2 controller can limit the fault current within four cycles.

2.4 summary

The purpose of this chapter is to gain insight into the performance of PR and PI based controller designs, as relates to inverters used in highly unbalanced microgrids, in both grid-connected and islanded modes. The control strategy and controller design of the inverters are discussed and tested. It is seen that both designs enable stable steady-state and dynamic operation in both modes under disturbances, faults, and also in transition of modes. However, the PR controller's dynamic performance is superior under all test cases, even when the PI controller performance is enhanced by choosing bulkier filters. The dynamic performance, coupled with the PR design's lower computation burden due to not needing the change of reference frames, makes the PR-based design suitable for unbalanced microgrids. Since it was observed that the detailed switching models (both PI and PR)

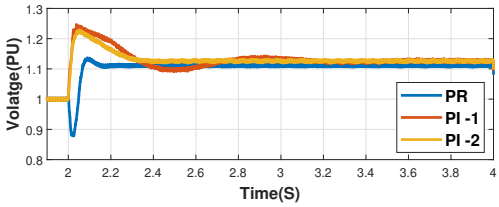

(a)

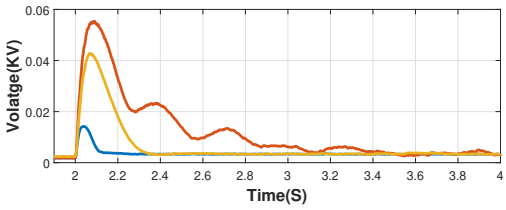

(b)

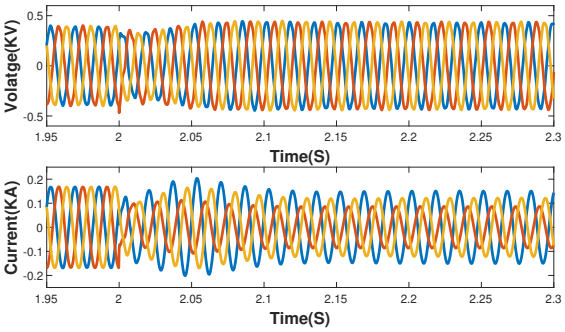

(c)

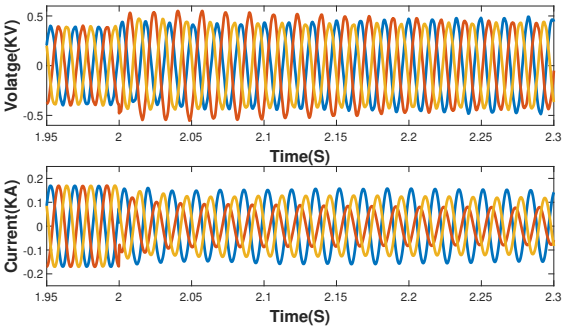

(d)

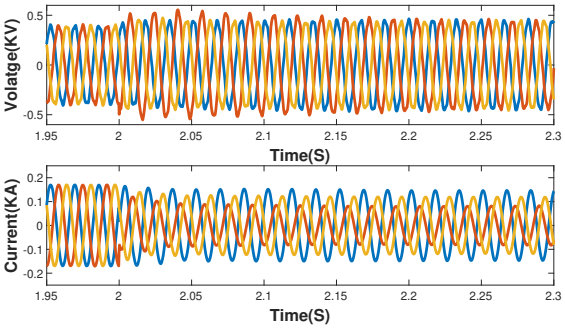

(e)

Figure 2.6: Inverter response to islanding operation at 2s: (a) voltage at Bus1, (b) negative-sequence component of inverter voltage, (c) inverter voltage and current with PR controller, (d) inverter voltage and current with PI-1 controller, (e) inverter voltage and current with PI-2 controller.

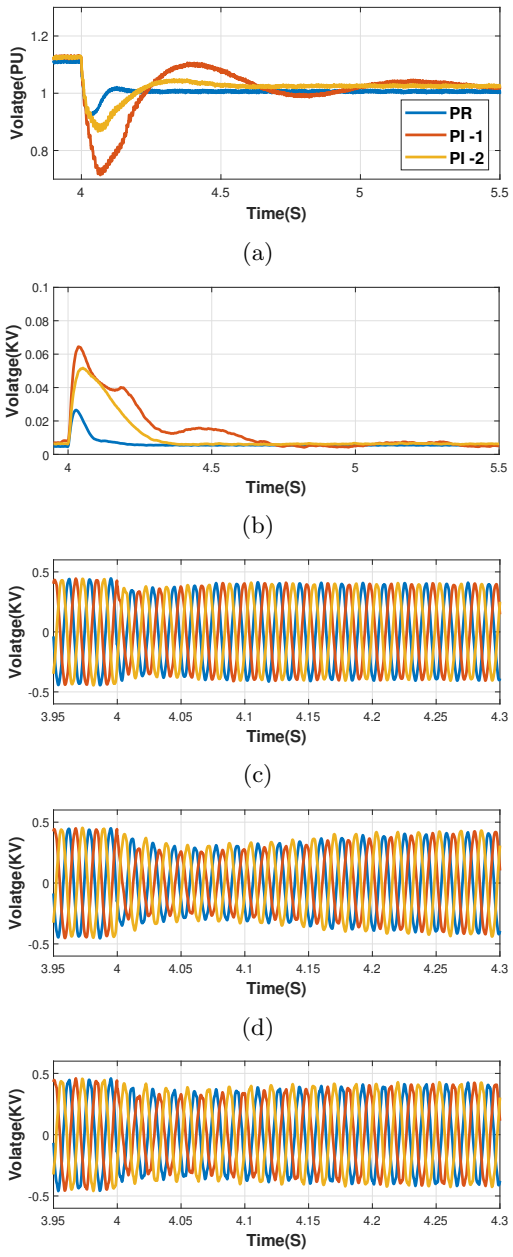

Figure 2.7: Inverter response to step load at 4s: (a) voltage at Bus1, (b) negative-sequence component of inverter voltage, (c) inverter voltage with PR controller, (d) inverter voltage with PI-1 controller, (e) inverter voltage with PI-2 controller.

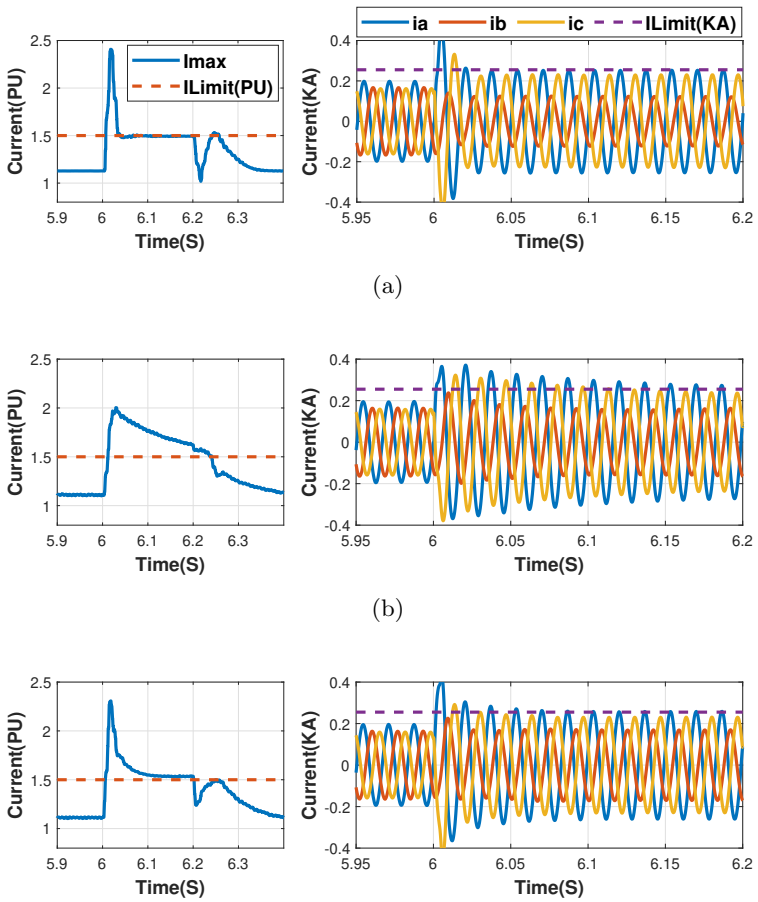

(a)

(b)

(c)

Figure 2.8: Inverter response to A-G fault at 6s: (a) current output of inverter with PR controller, (b) current output of inverter with PI-1 controller, (c) current output of inverter with PI-2 controller.

as chosen in this study result in significant computation time, average models will be developed and used for large microgrids and real-time testing in the following chapters. The PR based average IBR models are used to construct the IEEE 123 node feeder microgrid system with multiple inverters. This larger test system will be used as the baseline for validating the protection scheme proposed in the next chapter.

Chapter 3

Topology-Agnostic, Scalable and Self-Healing Protection Scheme for Microgrids

3.1 Introduction

The United States Department of Energy (DoE) defines microgrids as "a group of interconnected loads and distributed energy resources within clearly defined electrical boundaries that acts as a single controllable entity with respect to the grid. A microgrid can connect and disconnect from the grid to enable it to operate in both grid-connected or island mode"[26]. This is a rather broad definition that can cover many topologies that can vary in size, infrastructure, source types, and complexity. Due to this, a wide variety of test systems and prototypes have been proposed to test the protection schemes for microgrids [27]. Survey papers have been published to summarize the pros and cons of a large number of protection solutions proposed for microgrids with a specific assumed topology and source characteristics [28], or those already operating in North America [29]. The solutions utilize either single or a combination of conventional protection schemes like overcurrent, undervoltage, distance and differential, plus some schemes that are unconventional for distribution systems based on harmonics [30], voltage-transients [31] and traveling waves [32]. Numerous solutions depend partially or heavily on communications used for the adaptive setting of relays [33],

or more complicated multiagent [34, 35], multilayered [36] protection schemes, and learning-based relays [37].

Although these schemes illustrate success in protecting microgrids, the solutions are mostly valid for the specific topology tested in the paper or too complicated to implement for different system configurations [38]. Among the proposed schemes, adaptive protection scheme is often seen as a promising and cost-effective solution, where the relay settings are modified depending on the mode of operation of a microgrid. First, there will still be a cost involved of additional breakers and relays for better selectivity, if the feeder is protected by fuses and reclosers. Additionally, the success of the adaptive schemes is heavily dependent on the fault current limits imposed by inverters. In [39], authors apply adaptive settings to existing protective equipment in a 15-bus microgrid with simple topology. They assume inverters can supply twice their rated current. They conclude that "more complex systems are most likely to require more sophisticated solutions involving communications". Moreover, the adaptive settings calculated will not work if inverter fault currents are restricted to the more traditional limit of 1.1 to 1.2 pu of the inverter's rating. In addition, authors had to perform extensive time-domain simulations to perform short circuit studies due to lack of phasor domain short circuit models for accurate short circuit studies of unbalanced multi-source distribution systems. These needed to be performed after every topology change and proved to be computationally extremely expensive, requiring use of a super-computing facility at authors' institution.

To overcome the drawbacks of the previously proposed protection schemes for microgrids, a general, scalable, topology-agnostic, and self-healing protection scheme is proposed that can be used for any number, location, and nature of sources. The proposed scheme offers primary and backup protection in both grid-connected and islanded modes. The scheme includes an automated feeder reconfiguration that reconnects the subsystems into as few islands as allowed by the topology, thus adding the self-healing feature that strengthens resiliency. The scheme also allows a compromise between performance (selectivity) and cost (number of circuit breakers and relays) so that the scheme can be employed for any real-world distribution system, urban or rural.

Chapter 1 and chapter 2 discuss the detailed, time-domain models of grid forming and grid following inverters capable of operating in both grid-connected and islanded modes. These models are needed to construct the microgrid system to test the protection scheme. The models are performance tested on the IEEE 13-bus feeder in PSCAD [22] and in real-time [40]. In this chapter, averaged models are developed that offer comparable dynamic performance but facilitate

faster simulation. Using these models, the IEEE 123-node feeder [41] is integrated with 15 IBRs. The proposed protection and reconfiguration scheme described in Sections 3.3 and 3.4 are tested on this feeder. Results are described in Section 4.2 to show stable operation (power-sharing), reliable primary and backup protection, and automatic, stable reconfiguration of the healthy parts of the system in both grid-connected and islanded modes.

3.2 The conception of the proposed protection scheme

The protected system (microgrid) is conceived to be divided into multiple zones separated by breakers, as shown in the IEEE 123-node feeder in Figure. 3.1a, with a zonal view shown in 3.1b. An additional source at node 251 is assumed to be connected through a breaker, which is an alternate feed to bolster resiliency. The Red breakers in Figure. 3.1b indicate closed status, maintaining the radial nature of the system. This system will be used later for testing the proposed scheme. A "zone" is defined as the smallest part of the system with a clearly defined physical boundary that can be isolated from the rest of the system by opening appropriate circuit breakers (e.g., breakers B3 and B4 will isolate Zone 3). An island could be one zone or a combination of multiple zones functioning together, isolated from the grid. (e.g., opening breakers B3 and B5 and closing breaker B4 will create an island consisting of Zone 3 and Zone 4). An "area" is an entire network over which the protection scheme is conceived - in this case it is the 123-node feeder. This configuration offers the flexibility between selectivity and cost. In the limiting case, a zone could be one feeder section (maximum selectivity but a maximum number of breakers are required), or an entire area (offering no selectivity, but it is the least expensive). This idea also lays the groundwork for the scalability feature. Besides, as microgrids cannot really function reliably without communication enabled control, it is assumed that fiber is running along with all feeders, and a controller for the entire area resides at the Substation $SS1$. As will be described in Section 3.3, while the primary protection relay resides at the zonal level, the backup protection and reconfiguration scheme (self-healing feature) reside in the area controller, thus effectively merging protection and control. Centralized Protection and Control (CPC), which is well established for substations [42] is assumed to exist between measuring devices, circuit breakers, and protection functions. This assumption is valid because of the relatively small physical expanse of an area. The following sub-sections describe the microgrid components, their attributes, and their models.

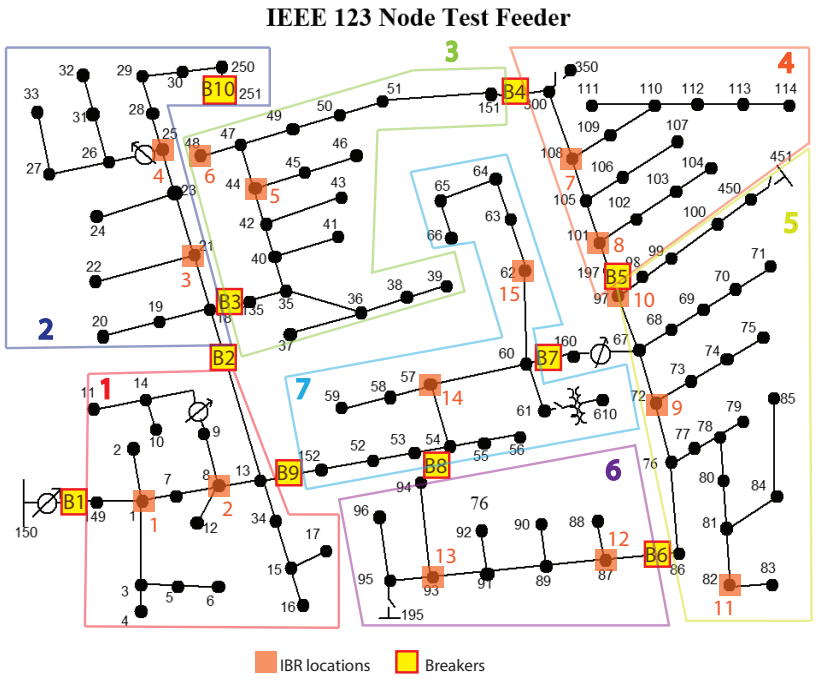

(a)

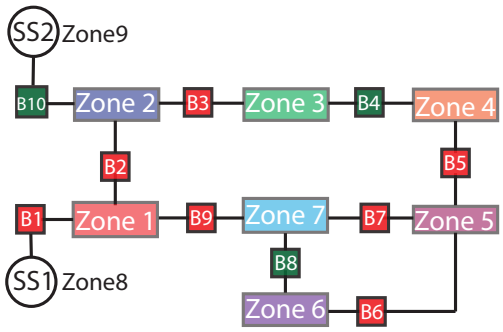

(b)

Figure 3.1: IEEE 123 node feeder: (a) zone formation and IBR placement, (b) simplified zonal view of the test system.

3.2.1 Components in Microgrid

3.2.1.1 IBR inverter Model

In [40], the performance of the PR based IBR control topology discussed in chapter 2 is described on the IEEE 13-bus feeder with 4 IBRs, constituting 100% IBR penetration to create the worst-case scenario. The inverters are shown to exhibit controlled and stable responses to disturbances and faults in grid-connected and islanded modes. This stable behavior and robust fault ride through feature are foundational to the reconfiguration function. In islanded mode, one inverter operates in the grid forming mode. It performs grid functions of keeping voltages balanced and frequency regulated while supplying unbalanced currents. The rest of the inverters operate in the grid following mode, only supplying positive sequence currents. All inverters limit their current to a low value, comparable to their continuous rating (1.1 pu for grid following and 1.5 pu for grid forming were chosen in this study), thus replicating the commercial inverter design [43]. It is also shown that simulation of the PR topology is faster than the more popular Proportional Integral (PI) topology that implements controls in the dq reference frame. However, simulating the switching model results in high memory requirements and computational complexity, which makes its implementation infeasible when multiple inverters are simulated. For the power system side analysis with time frames in the range of fundamental frequency (in ms), an averaged model can suffice. Except for harmonic analysis on the ac side output of the inverters, which is not the goal here, an averaged model of the inverter can replicate a detailed switching model and faithfully represent the dynamics of the inverter[44], [45]. Therefore, the PR topology is further reduced to an averaged model.

For deriving the averaged model, consider the single-phase switching leg of the inverter as shown in Figure. 3.2a, the PWM output pulse S1 will turn on the upper switch, and S2 will turn on the lower switch. It should be noted that the status of the upper and lower switches are conjugates of one another, i.e., $S2 = (1 - S1)$.

$$S1 = \begin{Bmatrix} 1 \ when D(t) > T(t) \\ , \\ 0 \ when D(t) < T(t) \end{Bmatrix}$$

where $D(t)$ is the sinusoidal modulation waveform and $T(t)$ is triangular carrier. The switching model expression for the output voltage v_o is given in (3.1), where V is the dc bus voltage.

$$\begin{aligned} v_o &= S1 * V + S2 * (-V) \\ &= S1 * V + (1 - S1) * (-V) \\ &= V * (2 * S1 - 1) \end{aligned} \tag{3.1}$$

The switching model expression for the dc-side current i_{dc} is given in (3.2)

$$\begin{aligned} i_{dc} &= S1 * i_o - S2 * i_o \\ &= S1 * i_o - (1 - S1) * i_o \\ &= i_o * (2 * S1 - 1) \end{aligned} \tag{3.2}$$

The switching model equations (3.1) and (3.2) are averaged with the assumption that the dc bus voltage V does not change rapidly because of the large capacitor typically connected to the dc bus, and can be considered constant across the switching period. Also, on the output side, ac current i_O is varying slowly because of the inductor in the filter component, and can be treated as constant over the switching period. This assumption holds good in this case, as the ac side current is varying at 60Hz, and the dc side current varies at switching frequency, which is in the order of kHz (7.2 kHz used in this study).

The PWM duty cycle follows the sine function and its average continuous expression is given by (3.3).

$$d(t) = 0.5 + 0.5 * \sin(2\pi f * t) = 0.5(1 + D(t)) \tag{3.3}$$

From [46] and (3.3) the averaged model expressions for the output voltage and dc side current are given by (3.4) and (3.5), respectively.

$$v_o(t) = (2 * d(t) - 1) * V = D(t) * V \tag{3.4}$$

$$i_{dc}(t) = (2 * d(t) - 1) * i_o = D(t) * i_o \tag{3.5}$$

Here, $D(t) \in [-1, 1]$ and $d(t) \in [0, 1]$. The switching leg's averaged model is shown in Figure. 3.2b. The averaged model of the inverter does not bypass the control system of the inverter as shown in Figure. 3.2c, d. To compare its dynamic performance against the detailed model, the inverter (rated 100 kVA) was connected to an infinite bus with a local load (of 90+j30 kVA), and a

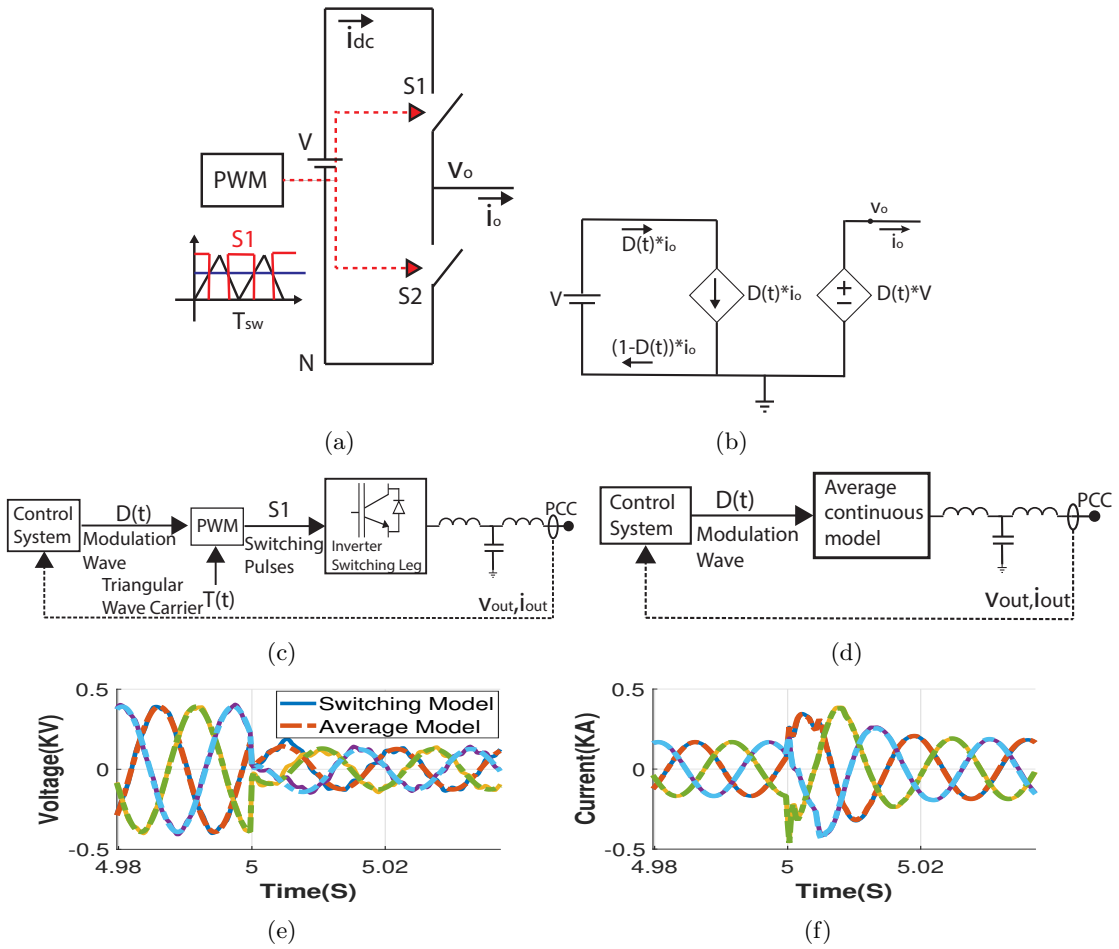

Figure 3.2: Derivation of the averaged model: (a) switching model of the inverter leg, (b) averaged model of the inverter leg, (c) switching model control of inverter, (d) averaged model control of inverter, (e) voltage output comparison, (f) current output comparison.

.

three-phase fault was created at $t = 5s$ on the bus. Figure. 3.2e, f show the comparison of voltage and current responses, respectively, of the switching and averaged models. The averaged model faithfully replicates the dynamics of the switching model. Therefore, the averaged model will be used to simulate IBRs in the test system. Additionally, observe that the fault current is limited to 1.1 pu of its rated value for this grid following inverter. For the grid forming inverter, the current limit is chosen to be 1.5 pu of inverter rating.

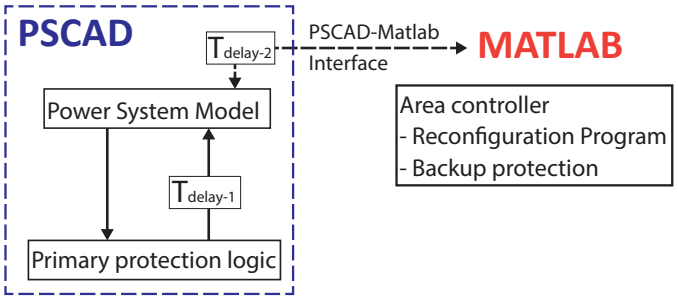

Figure 3.3: Communcation model setup using PSCAD and Matlab softwares.

3.2.1.2 Switchgear

Breakers are conceived as modern reclosers, without having to use the reclosing function. Modern reclosers are equipped with a control box mounted on the same pole as the recloser, which can be compliant with the communication protocol of choice. The control box can be thought of as an Intelligent Electronic Device (IED) that can be programmed to perform different user-defined functions. Since the recloser is equipped with a CT and a VT, and measures voltage and current phasors, different functions related to these phasors can be built into this IED. It is assumed here that the IED can ascertain the direction of current through the breaker, as well as create an undervoltage trigger, since these are the two features used to detect fault and the faulted zone, as will be explained in Section 3.3. Additionally, these breakers will need to connect two live systems while closing, making it necessary to have a check-synchronization (referred to as "sync-check" hereafter) feature [47] built into the IED. This means after getting a closing signal, the breaker will close only when the voltage and frequency differences between two sides are within allowed thresholds. In addition, the IED is assumed to be able to detect breaker failure (failure to open after a trip command). The manual for a commercially available product [48] shows that these capabilities are already available in modern reclosers, thus validating the assumptions made.

3.2.1.3 Communication Model for non-realtime model

Primary and backup protection to be described in section 3.3 are designed using the GOOSE messages in the IEC-61850 communication protocol. The test system and the primary protection are modeled in PSCAD, whereas the backup protection and the reconfiguration scheme that reside in the area controller are coded in MATLAB. For validation of the scheme, at this stage, communications

are modeled through appropriate delays. A delay $T_{delay-1}$ of less than 4 ms is selected to replicate the maximum round trip delay for the GOOSE messages used for primary protection. $T_{delay-2}$ of less than 10 ms is selected for backup signals and less than 100 ms for reconfiguration related messages. For the elements inside PSCAD, delays are modeled using the radio link and time-delay blocks, whereas the PSCAD-MATLAB interface component is used to model delays in backup and reconfiguration, as shown in Figure. 3.3. In the next stage of the proposal, communication will be co-simulated with hardware relays in the loop on RTDS.

3.2.2 Protection Scheme Formulation

Primary protection is designed for a zone, and the logic resides in one zonal relay (a relay that overseas and protects a zone) that can be physically located at any of the IBR facilities. The zonal protection receives GOOSE messages from all the breakers that form the zone's boundary and can send GOOSE messages to trip those breakers. GOOSE messages from breakers are published at a rate of one message/second during normal operation and as a burst of messages at 4ms interval when current direction through a breaker changes, a condition, as explained in section 3.3, that could potentially indicate fault. The backup protection is embedded with the area controller and subscribes to GOOSE messages from the breaker IEDs about the breaker status (close/open) and a breaker-failure alert in case a breaker fails to open, or from a relay if it fails to operate, or from the communication protocol if any communication link fails [49]. On receiving any of these alerts the backup protection determines which other breaker(s) need to open to isolate the fault without compromising the whole area. Backup protection can open or close any breaker through GOOSE command, with sync-check being employed at the breaker IED. This addresses both, backup and reconfiguration (self-healing) aspects of the proposed scheme. Figure. 3.4 displays the overview of this overall protection set up for a zone controlled by two breakers B1 and B2. In the worst case scenario, if elements of primary and backup fail simultaneously (extremely unlikely), the fault will persist and all inverters in the area will shut down after certain time determined by the fault ride through requirements.

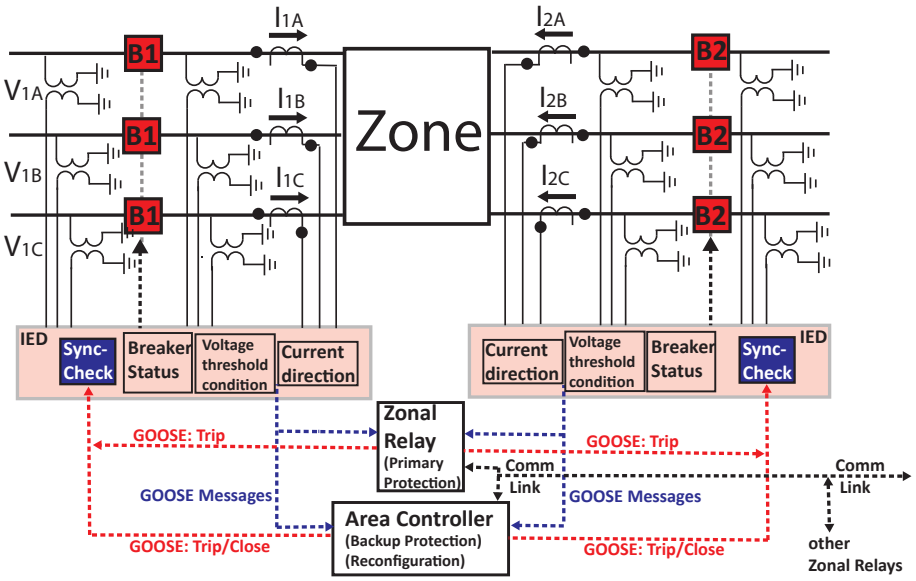

Figure 3.4: Protection and reconfiguration scheme setup.

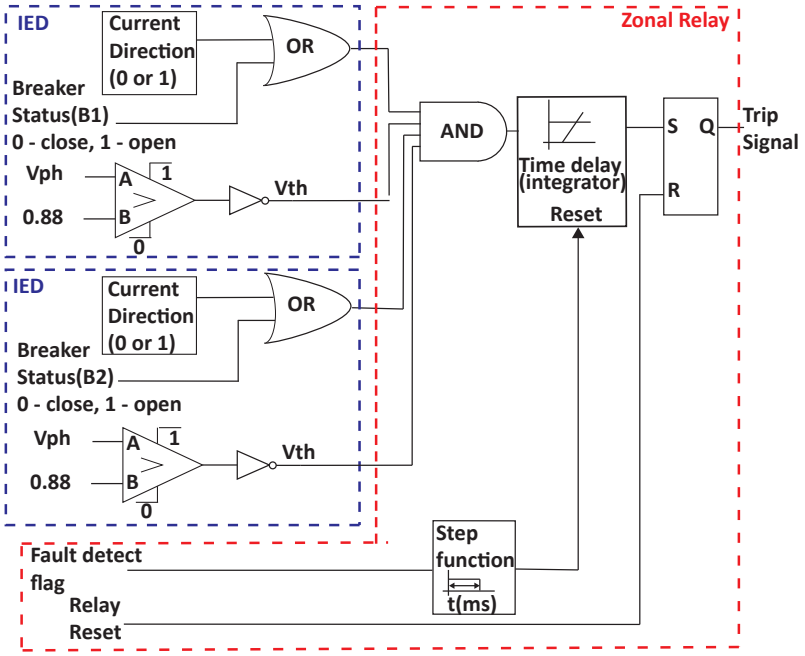

Figure 3.5: Primary protection fault detection logic.

3.3 Protection Scheme Design

3.3.1 Primary Protection

Physics will drive the fault point voltage to a low value regardless of the sources connected to the system. In such condition, the currents will flow **into** the fault point. Therefore, to detect a fault in any zone, two conditions need to be met: 1) current direction in at least one phase should be going **into** the zones from all monitoring breakers, and 2) voltage of the corresponding phase(s) should be lower than a selected threshold. Figure. 3.5 shows how this is accomplished using the protection functions in the breaker IED (boxed in dotted blue) communicating with the zonal relay (boxed in dotted red). In the IED, current direction is calculated using the well-established 90-45 directional scheme that uses line voltages as the polarizing quantities for phase units and zero sequence voltage as the polarizing quantity for ground unit [50]. This scheme provided correct results for the extensive testing reported in Section 4.2. However, as the grid standards for IBRs evolve, more certainty in inverter behavior can drive the research into more robust and innovative directional schemes. The current direction input to the OR gate is 1 for current going in to the zone and 0 for current going out. Thus, the output of the OR gate is high if the current is going in, no matter the breaker status. For current going out, if the breaker is closed the output of the OR gate is 0. It is to be noted that a breaker could be open in normal operating conditions if it is creating a loop-flow. Such breaker is to be used for reconfiguration purpose, as will be explained in Section 3.4. For example, breaker B4 is open in Figure. 3.1a (b), meaning fault is detected by the direction and voltage measured **at only one breaker** for Zone 3 (B3) and Zone 4 (B5). Therefore, the output of the OR gate for an open breaker must be kept 1 at all times. The comparator compares the measured voltage against a threshold of 0.88 pu, and the value of signal V_{th} is high if undervoltage condition is detected. Therefore, it is clear that the AND gate in the zonal relay will output 1 only when current is flowing into the zone through all closed breakers defining that zone and the voltage sensed by each closed breaker is below the threshold. The voltage threshold of 0.88PU is selected because the IEEE 1547 standard allows the voltage of healthy islands to go as low as 0.88 pu [1] in the voltage ride-through requirements. This voltage threshold, however, can be user-defined and facilitates sensitivity for the protection scheme. In summary, the proposed protection logic uses voltage monitored directional comparison principle [51].

Activation of AND gate initiates a timer which is set to 50 ms (about three cycles) to

add security to the relay to avoid operation for system dynamics other than fault, like a large load switched on. If fault still exists after 3 cycles, the timer output goes high, thus setting the SR latch output to 1. This trip signal is sent as GOOSE messages to all the zone-defining closed breakers, which will open to isolate the faulted zone. One more security feature was needed to avoid misoperation of relay in a healthy zone. It was observed that when a faulted zone was isolated, voltage across the system (healthy zones) can remain lower for longer than 50 ms. During this period, if a healthy zone was importing power from other zones, or, if the zone had only one controlling breaker, the load current would be flowing in to the zone from all breakers. This would set up an incorrect trip signal for the healthy zone. To avoid this, when a fault is detected in a zone, a fault-detect flag (FDF) is sent out to all other zonal relays. This flag starts a timer which is a step function that goes and remains high for a user-defined time interval (it is taken as 100 ms in this study). During this time, the relay timer is blocked, as the "Reset" input to the timer will be high. Finally, a Relay Reset signal is used to reset the trip signal after the fault in the zone is cleared.

3.3.2 Backup Protection

The backup protection is located in the area controller, and is cognizant of the area's zonal structure using graph theory, with zones as nodes(N) and breakers as branches(B). Based on the topology information and breaker status, an Adjacency Matrix(AM) and a Node Incidence(NI) matrix are built. Two types of AM matrices are built - the static AM matrix based on breaker locations, and dynamic AM matrix based on breaker status. The dynamic AM matrix updates and stores the topology information, whereas the NI matrix updates and stores the branch current direction information. In this section, backup protection is described through construction and usage of these matrices for different conditions created in the 123 node test system shown in Figure. 3.1a. Backup protection can be set to operate after a user-defined time-delay. It is taken as 100 ms for this study.

Consider the test system in the state shown in Figure. 3.6a, with breakers $B4, B8, B10$ open, preserving the radial nature of the system. For this topology, the static AM matrix, shown in Figure. 3.7a, is 9×9, since there are N=9 zones (nodes) in this system (sources are taken as zones for this formulation). The value of the element $(k, l) = 1$ indicates that there is a breaker located between zones k and l. For example, there is breaker located between zone 3 and zone 4, hence element (3,4) is 1. The dynamic AM matrix for this state of the system is shown in Figure. 3.7b.

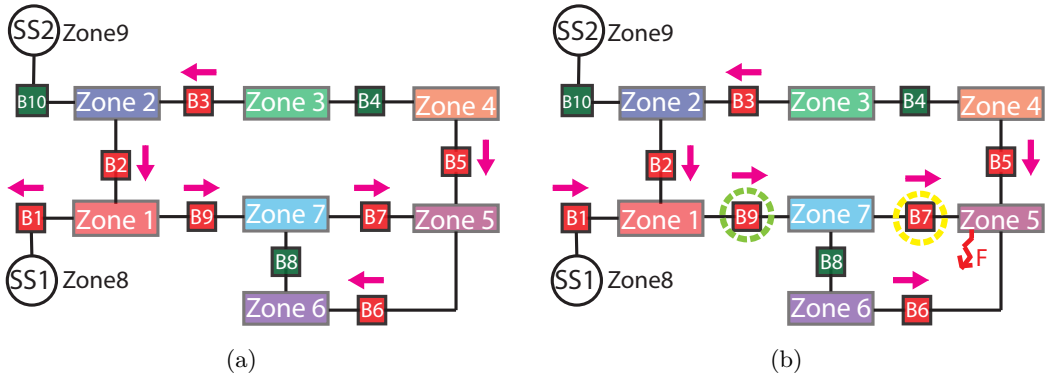

Figure 3.6: Three-phase fault in Zone 5: (a) pre-fault state, (b) fault state.

The value of the element $(k, l) = 1$ indicates that the breaker is closed between zones k and l. For example, element (3,4) is 0 in this case, but element (2,3) is 1.

For the same state of the system, the NI matrix, shown in Figure. 3.7c, is $N \times B$ for each phase, where N=9 (nodes, or zones), B=10 (breakers, or branches). The current directions are mapped to NI matrix with element $(m, n) = -1$ indicating that the current direction in n^{th} breaker is going into the m^{th} zone, and a value of $(m, n) = 1$ indicating that the current is going out of m^{th} node. For example, current in breaker 2 is going in to zone 1, and out of zone 2, so elements (1,2) and (2,2) are -1 and 1, respectively. No connection between a breaker and a zone (including open breakers) create values of 0. For example, elements (3,4) and (4,4) are zero, since breaker $B3$ is open.

Now, when a fault takes place in Zone 5, as shown in Figure. 3.6b, current directions change, but the connection status does not. Therefore, the dynamic AM matrix for the faulted state will remain unchanged, but the NI matrix will be updated to have the values shown in Figure. 3.7d. Three cases that represent failure of primary protection are analysed now to describe how backup protection will respond using the state of the network matrices. Note that controller subscribes to all messages (current direction, breaker status, which includes breaker-failure alert, and undervoltage triggers) published by the breaker IEDs, as seen in Figure. 3.4.

3.3.2.1 Case1- Breaker Failure

When a breaker corresponding to the dynamic AM matrix element (k, l) fails to open, the breaker IED sends this information through the network, and is received by the controller. To determine the appropriate breaker to trip in this case, the backup protection looks for the element

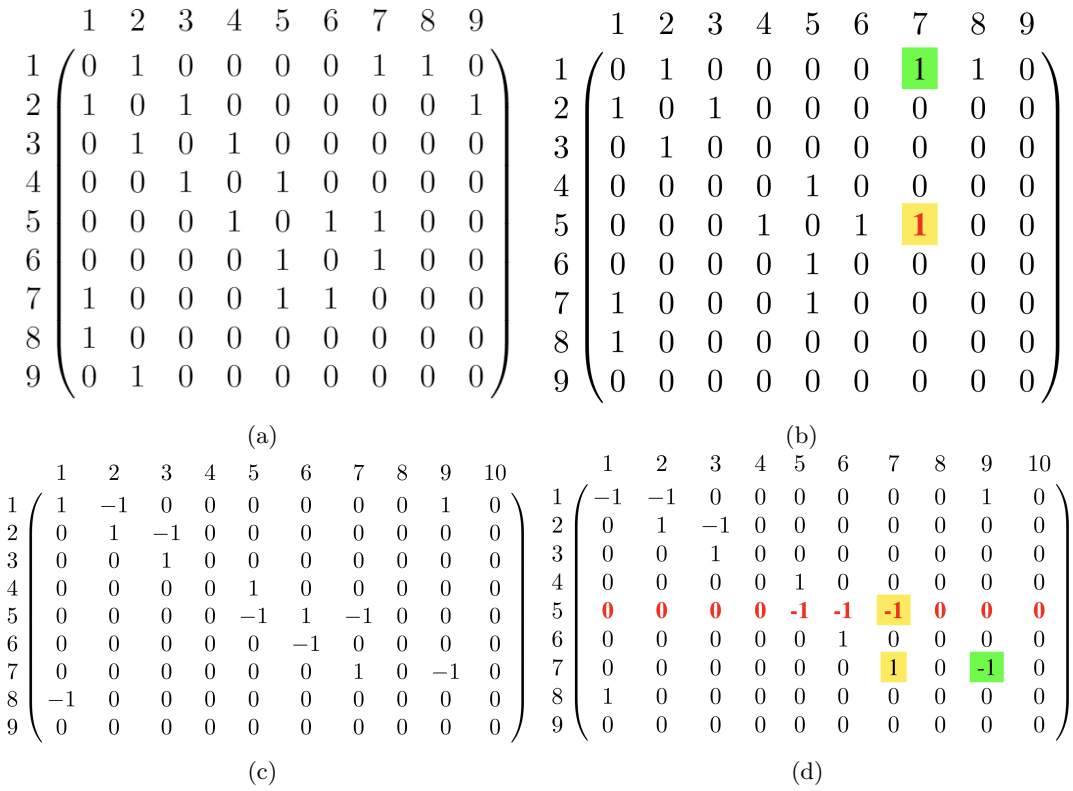

Figure 3.7: Network matrices for conditions shown in Figure. 3.6: (a) static AM matrix, (b) dynamic AM Matrix , (c) NI Matrix for pre-fault state, (d) NI Matrix for faulted state.

with a value of $'1'$ in l^{th} column, and opens the corresponding breaker. For fault in zone 5 as shown in Figure. 3.6b , when the breaker $B7$ corresponding to the dynamic AM matrix element $(5, 7)$ fails, the next breaker to trip is $(1, 7)$, i.e., breaker $B9$ to isolate the fault.

3.3.2.2 Case2- Zonal relay failure

Since the controller subscribes to all the messages published by the breaker IEDs, when a fault occurs in a zone, backup can use the updated NI matrix to determine the faulted zone, using the same logic used by the zonal relay. If the zonal relay fails, it will publish a failure message to the controller, and then the backup protection directly uses the NI matrix to determine the faulted zone (the row with all non-zero elements as -1) and opens the associated zone breakers based on the dynamic AM matrix. In case the relay does not communicate with the controller due to its failure, and backup does not see the trip signal from zonal relay, it concludes that the zonal relay has failed and waits for 100 ms before opening the associated breakers.

For example, in case of a fault in zone 5, row 5 in the NI matrix shown in Figure. 3.7d representing zone 5 is the only row with all its non-zero elements as -1, indicating the zone is faulted and $B5, B6, B7$ are the breakers backup protection will open through GOOSE trip commands.

3.3.2.3 Case3- IED communication failure

A communication failure with an IED at breaker n, which corresponds to element (k, l) in the dynamic AM matrix, will cripple the zonal protection of zone k, and zone l. The communication failure is detected by controller through the built-in failure status mechanisms in the IEEE 61850 protocol. The failure creates invalid measurements for elements in the n^{th} column of the NI matrix. So, these zones k and l are combined as a single region from the backup protection perspective. The elements to monitor for this region will be all non zero elements in k^{th} and l^{th} row except (k, n) and (l, n). When the voltage goes below the threshold, the backup protection uses the NI matrix to determine if the combined region is faulted by checking the current directions using the elements in the associated rows. For the same example of fault in zone 5, When there is a communication failure with IED at $B7$, it cripples the protection of zone 5 and zone 7. So, when the value of all monitored elements in 5^{th} and 7^{th} rows- $(5, 5), (5, 6), (7, 9)$ (elements $(5, 7)$ and $(7, 7)$ are excluded) are $'-1'$, as seen in the NI matrix in Figure. 3.7d, the backup protection will isolate the combined region (zone 5 and zone 7) by tripping breakers- $B5, B6, B9$. The functioning of the backup protection described in this section is captured in a flowchart in Figure. 3.8.

3.3.3 Coordination with Secondary Feeder Protection

Typically, the primary protection described in this section for microgrid needs to backup faults in the secondary network. In traditional distribution systems the transformer feeding the secondary feeder would be protected by fuses on the secondary and primary sides. However, with 100% IBR scenario, fuses may not be reliable, as the fault currents for some faults in islanded mode may not feed enough current to blow the fuse. This is demonstrated with an example. The load at node 48 in zone 3 is 260 kVA, connected through a 300 KVA, 4.16KV/480V transformer, as shown in Figure. 3.9 (a). Transformer primary side fuse (**FP**) is selected as 30T, which should backup for any fault on the secondary feeder not cleared by fuse **FS**. From Figure. 3.9 (b), it can be seen that in case of islanded mode, with only IBR 5 supplying the load, the fuse **FP** will not blow for a fault downstream of fuse **FS**. Even with both IBRs feeding the fault, the fuse takes more than

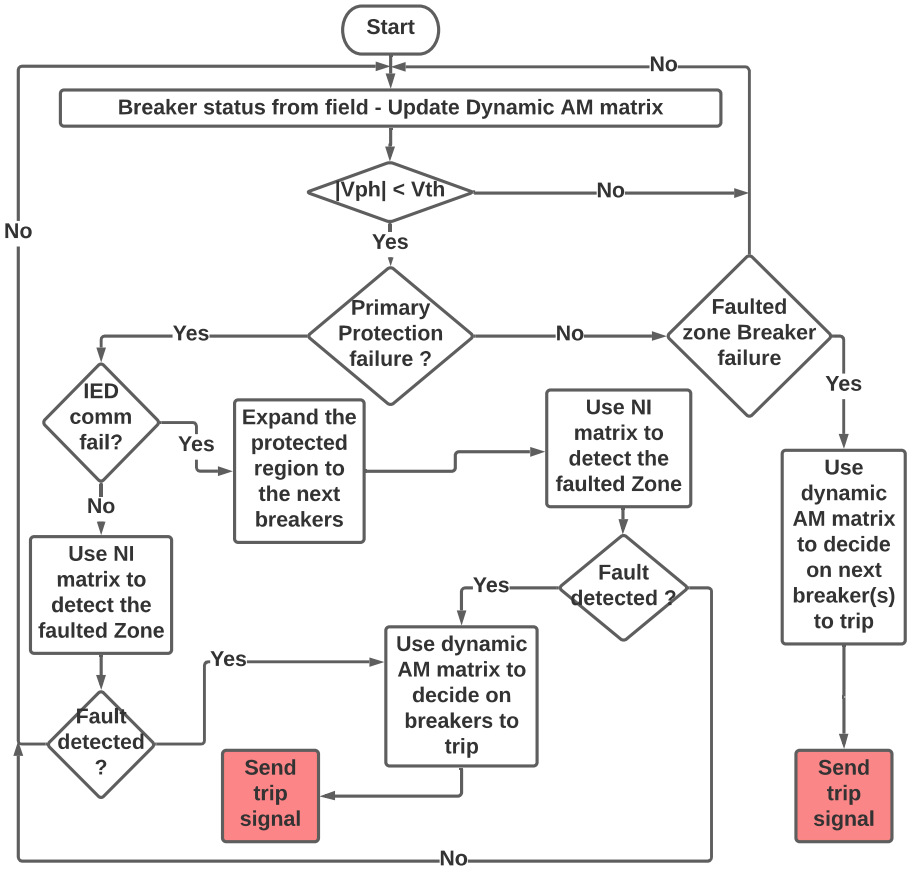

Figure 3.8: Backup protection flow chart.

10 s to blow, which is unreasonable. However, for the example configuration illustrated by Figure. 3.9 (a), the voltage at the zone-breakers **B3** and **B4** dropped well below the setting of 0.88 pu for all fault scenarios depicted in Figure. 3.9 (b). Such studies were performed in all zones, and the voltages of the faulted phases at the boundary breakers of the faulted zone always dipped below 0.88 pu in both, grid connected as well as islanded modes, underscoring the generality of the proposed fault detection technique. It should be noted that in case the secondary network loads (typically houses) have roof-top solar, the secondary network protection has to be redesigned completely due to bi-directional currents, which is not within the scope of this study. However, the primary protection time of 50 ms chosen in this study can be adjusted to backup whatever time is needed to protect the secondary network.

It can be argued that there might be some instances, despite the results reported in this chapter, where a fault in the secondary network will not result in voltages lower than 0.88 pu at the

boundary breakers. In islanded mode, fault drags the voltage down at the fault point, and due to low fault currents in feeders the voltages of all buses in microgrid are brought down to about the same values as the fault voltage, making the proposed voltage-monitored directional comparison scheme very reliable. This phenomenon is demonstrated in [52] for the IEEE 13-node feeder and it was also observed for the IEEE 123-node feeder under test. In grid connected mode, grid provides a large fault current. Therefore, the user has the option to make the scheme more dependable, utilizing the high fault current from grid, by adding the following protection function in the grid-connected mode: "a fault is detected if current through any of the breakers increases suddenly by 200% or more of its steady state value". The current direction can then be used to locate the faulted zone, as proposed in the section 3.3.1. This was verified to be true for all the 210 faults simulated in the grid-connected mode as described in Section 4.2.

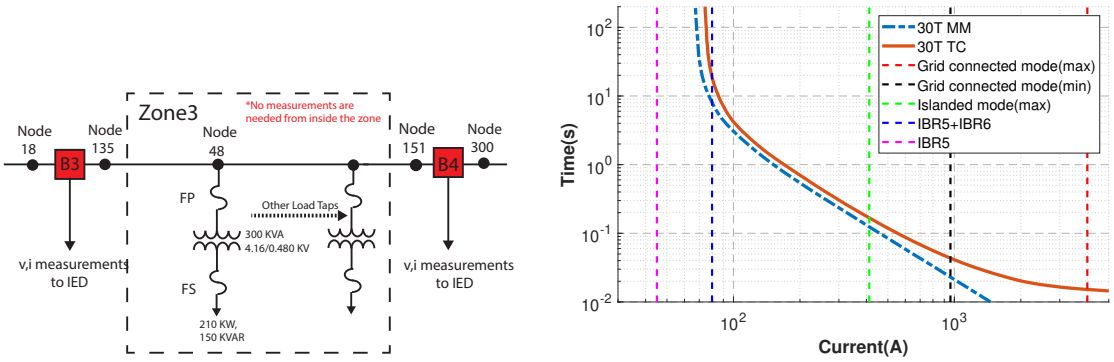

(a) (b)

Figure 3.9: Unreliable performance of a fuse protecting a transformer feeding a secondary feeder: (a) setup, (b) 30T fuse curves with different fault currents.

3.3.4 Security of the Proposed Scheme

Since large currents can result from starting of large motors, or due to transformer inrush, the security of the protection scheme for cold load pickup or transformer inrush needs to be verified. Cold load pickup was simulated by simulating a motor comprising of half the load of each zone. To demonstrate the response, a 300HP induction motor (considered aggregated cold load in zone 2, which forms 50% of the Zone 2 load) is started. The motor is connected via 300 KVA, 4.16 KV/480 V transformer at node 18. The simulation is carried out in both grid connected and islanded mode of operation. The voltage at the boundary breakers **B2**, **B3**, **B10**, and at motor terminal are shown

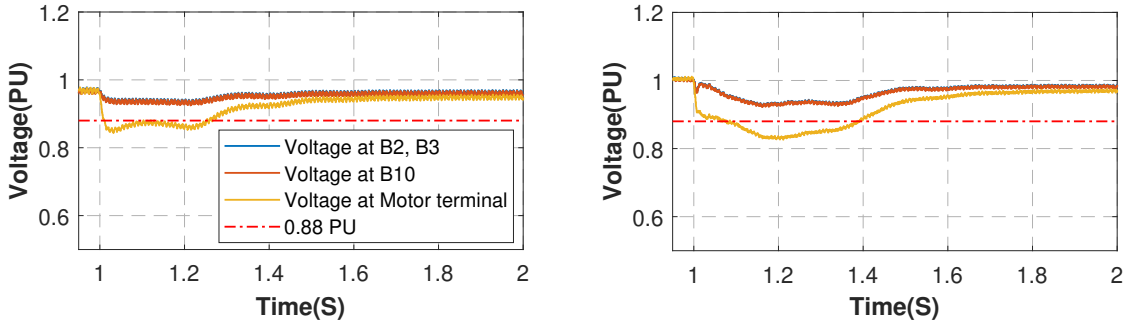

Figure 3.10: Voltage response for a motor starting in zone 2: (a) grid-connected mode, (b) islanded mode.

in Figure. 3.10. It can be seen that the voltage at the motor terminal dips when the motor is started, but the voltage at the boundary breakers did not dip below the threshold value of 0.88 pu. Moreover, most large motors are routinely fitted or can be fitted with power electronic based soft starters [53], which would obviate such misoperation.

The transformer was then energized at a time-instant when the inrush would be maximum (voltage of one phase passing through zero). The voltages at the boundary breakers did not violate the 0.88 pu threshold. This was also observed for some other cases studied at other nodes in the network. It should also be noted that the inrush decays substantially in the three cycles set for the primary protection to operate, thus providing additional security against inrush.

3.4 Self Healing - Dynamic Reconfiguration Scheme

In a radial distribution system, once the protection system isolates the faulted zone, it may leave the healthy downstream zones isolated from the grid source. This is where the reconfiguration scheme will help in the system's self-healing and increase the entire microgrid's resiliency. The reconfiguration scheme is also designed based on graph theory and uses the dynamic AM matrix for finding a connected path between nodes. The well-established breadth-first search (BFS) algorithm [54] is used for finding all the possible paths between two nodes X and Y, with the path-length measured by the number of branches between nodes. When multiple paths are available between nodes, the path with the minimum length is preferred. The static input to the reconfiguration program is the topology information with zone data and breaker locations. This information is

used in constructing the static AM matrix as described in section 3.3.2. The dynamic input to the reconfiguration program is the breaker status from field, which is used in constructing the dynamic AM matrix. The static AM matrix is used in finding available paths between zones using the BFS algorithm. Then, the BFS algorithm applied on the dynamic AM matrix gives the existing paths between zones. The zone data indicates whether each zone is a grid or non-grid node. In Fig. 3.1b, Zone 1 to 7 are non-grid nodes and Zone8 (SS1), Zone9 (SS2) are grid nodes. Whenever there is a topology change, the BFS algorithm uses the dynamic AM matrix to find the path between non-grid nodes and grid nodes to determine which zones are islanded. The aim of the reconfiguration program is to connect these islanded zones back to a grid source. If no path is available to any grid source, then the program minimizes the number of islands formed in the area by closing the available connection-paths between isolated zones. While re-configuring, the program always aims to maintain the radial structure by not allowing more than one path between two zones. It should be noted that after a fault is cleared by primary or backup protection, the faulted zone(s) are considered isolated, and are not included in the reconfigured system. The functioning of the reconfiguration program described in this section is captured in a flowchart in Figure. 3.11.

In the example case of a fault in zone 5, when the protection system detects the fault, the trip signal will open breakers $B5, B6, B7$ and isolates zone 5. The reconfiguration program subscribes to these trip signals and knows the active fault status for the zone. As the reconfiguration program detects the topology change, it looks for islands formed in the area by using the BFS algorithm on the dynamic AM matrix and finds zones that do not have a path to any grid source. In this case, zone 4, 5 and 6 are the islanded zones. Since, zone 5 fault status is known, it is treated as an isolated zone and not included for reconfiguration. The algorithm then checks if grid sources are lost, which is not true in this case. The algorithm then looks for available paths between healthy islands (zone 4 and 6) and the grid node (SS1) using the static AM matrix, and determines the breakers to close for connecting them to grid. In this case, it connects zone 4 and 6 to the grid (SS1) by closing the breakers $B4$ and $B8$ respectively. As another example, if Zone 1 is faulted and isolated, B10 and B4 will close, connecting all other healthy zones to SS2. However, if Zone 1 is faulted and breaker $B2$ fails to open, then backup will open breaker $B3$. In this case, the reconfiguration will result in Zones 3 through 7 being converted to one island by the closing of breaker B4 as there is no path available to both $SS1$ and $SS2$.

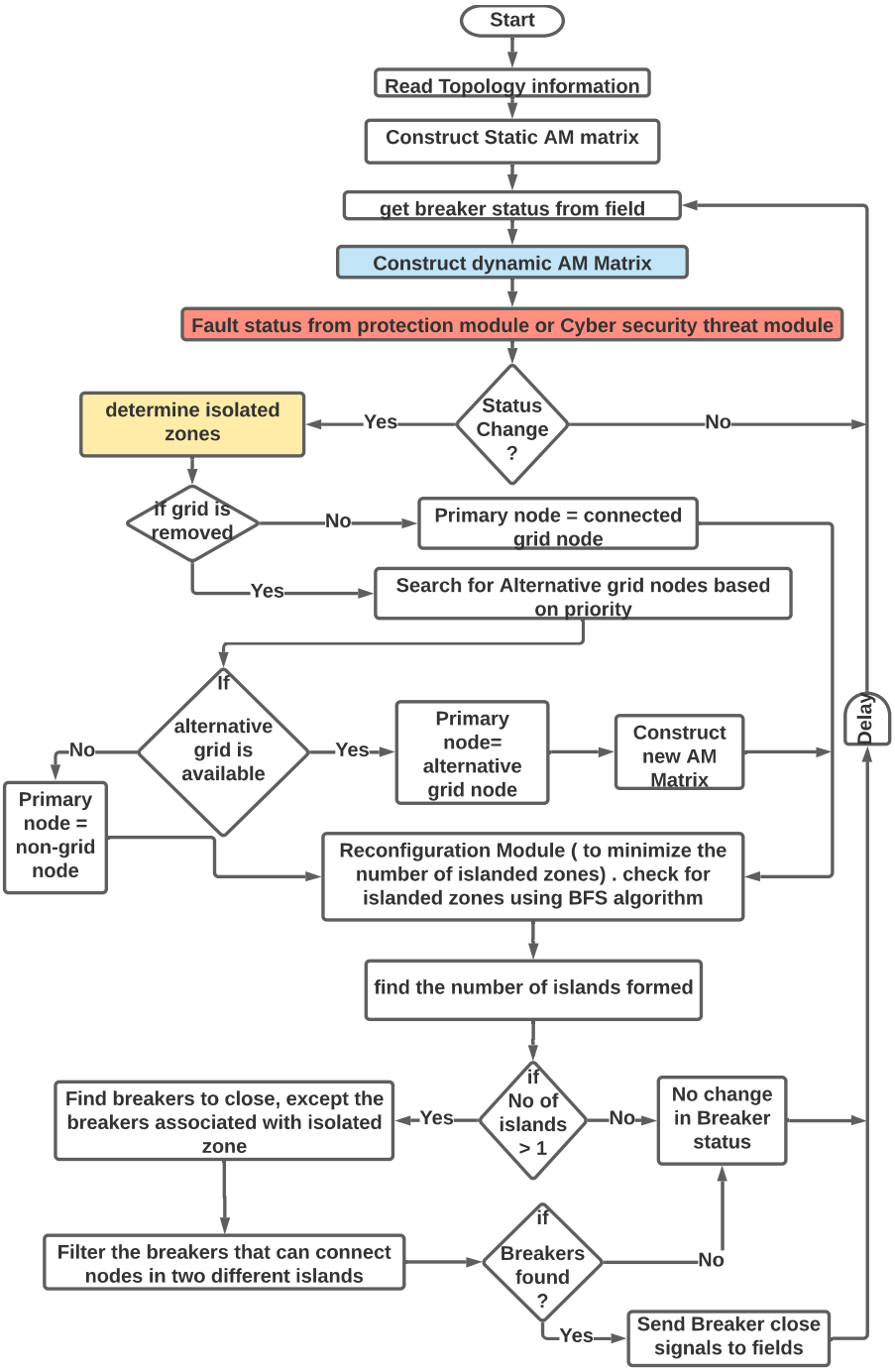

Figure 3.11: Reconfiguration program flow chart

3.5 summary

This chapter describes formulation of primary protection, backup protection and reconfiguration (self-healing) of a microgrid in both, grid-connected and islanded modes, while using only the existing technology. The novel features of this formulation are 1) topology-independence, 2) scalability, 3) cost-awareness. Averaged inverter models used in this study facilitate time-domain simulation of a large number of IBRs, while realistically modeling their steady-state and dynamic behavior. Primary protection is formulated locally within each protection zone to ensure reliability and speed, but backup and reconfiguration are effectively merged with the microgrid controller located centrally. The validation of the protection and reconfiguration schemes will be shown in the next chapter.

Chapter 4

Validation using PSCAD simulation

4.1 IEEE 123 node distribution feeder - Microgrid system

The IEEE 123-node feeder shown in Figure. 3.1a and discussed in Section 3.2 is selected as the test system, as it has all the characteristics of a typical distribution feeder in terms of topology and unbalance. A total of 15 IBRs are added to the system, and their placements with generation capacity expressed as percentage of load in each zone is summarized in Table 4.1. The role of IBRs during islanding (grid forming or following) is also mentioned under the column "Type". For generality, a few zones (zone 3, 5 and 7) are designed to have lower generation capacity and are equipped with a load shedding scheme to test various dynamic scenarios. It sheds predetermined controllable loads if the voltage is less than 0.88 pu or the frequency is below 57 Hz. The values are based on the ride-through requirements for islanded microgrids in IEEE Standard 1553-2018 [1]. Loads to be shed in the zones are shown in Table 4.2.

4.2 Results and Discussion

Different cases are simulated to test the proposed scheme's effectiveness in protection and self-healing of the test system. First, the effectiveness of primary protection scheme is shown by itself

Table 4.1: IBR placement and generation capacity

Zone No.	***Node No.***	***IBR No.***	***Rating***	***Type***	***Generation Capacity***
1	1	1	300 KW	Gform	100%
	8	2	210 KW	Gfol	
2	21	3	240 KW	Gform	100%
	25	4	210 KW	Gfol	
3	44	5	210 KW	GForm	43.8%
	48	6	180 KW	Gfol	
4	108	7	210 KW	GForm	100%
	101	8	180 KW	Gfol	
5	72	9	210 KW	Gform	51.3%
	97	10	180 KW	Gfol	
	82	11	120 KW	Gfol	
6	93	12	180 KW	Gform	100%
	87	13	120 KW	Gfol	
7	57	14	210 KW	GForm	62.3%
	62	15	180 KW	Gfol	

Table 4.2: Load Shedding Scheme Data

Load shed nodes		Preserved Critical Load		
Zone No.	***Node Nos.***	***PhaseA***	***PhaseB***	***PhaseC***
3	35,36,37,38 39,41,43,45 46,49,50,51	125 KW 85 KVAR	105 KW 75 KVAR	105 KW 75 KVAR
5	68,69,70,71, 73,74,75,77, 80,82,84,85,98	145 KW 100 KVAR	130 KW 80 KVAR	130 KW 80 KVAR
7	52,53,58,59, 62,66	115 KW 65 KVAR	130 KW 70 KVAR	70 KVA 50 KVAR

in both grid-connected and islanded modes of operation. Then the backup protection is demonstrated with a test case. Finally, reconfiguration program is demonstrated with test cases.

4.2.1 Fault Detection - Primary protection

To test the primary protection system, a total of 420 faults (divided equally between four types of fault - LG, LLG, LLLG, LL - were created in different zones, half in grid-connected and half in islanded mode of operation. Fault resistances were varied from 0.1Ω to 3Ω. Note that higher fault resistances translated to fault current contribution from grid getting below the load current for many simulated faults, interpreted as high impedance faults. All faults were detected correctly. The time delay setting of the primary protection logic was set to 50 ms (3 cycles) and the time period of the step function for FDF was set to 0.1s (6 cycles).

4.2.2 Backup Protection

Backup protection was tested successfully with all four types of faults taking place in Zone 3 and in Zone 5. Both, breaker failure and the failure of primary protection relay were simulated. Here one of the test cases with a permanent BG fault created in Zone 3 at 1 s into the simulation is used to demonstrate the working of the backup protection. As shown in Figure. 4.1(a), Breaker $B3$ fails to open in the simulation. The breaker IED would send a breaker-failure signal to the area controller. The area controller in this case needs to expand the region to be isolated by opening breaker B2, thus isolating Zone 3 and Zone 2, as seen in Figure. 4.1(a). For this fault, the current directions and voltage measurements in all breakers in three phases are shown in Figure. 4.1(b) and (c), respectively. Before fault, load current in phases A and C are going into Zone 3, but the load current in phase B is going out of Zone 3. This is due to unbalanced loads. After fault it can be seen that only zone 3 has incoming currents from all of its boundary breakers ($B3$) in phase B. Note that the voltage of phase B is well below the threshold at breaker B3. Thus, it is clear the fault is in Zone 3. Using the dynamic AM matrix for these current directions, the backup protection correctly trips the breaker $B2$ at $t = 1.1s$ to isolate the expanded region after the user-defined time delay of $100ms$. The frequency and voltage output of the zones 1, 2 and 3 is shown in Figure. 4.1(d),(e). As seen from the plots, after the breaker B2 opens, the IBRs in zone 2 and 3 shut down, driving the frequency and voltage of those zones to zero, whereas the voltage and frequency of Zone 1 (and the

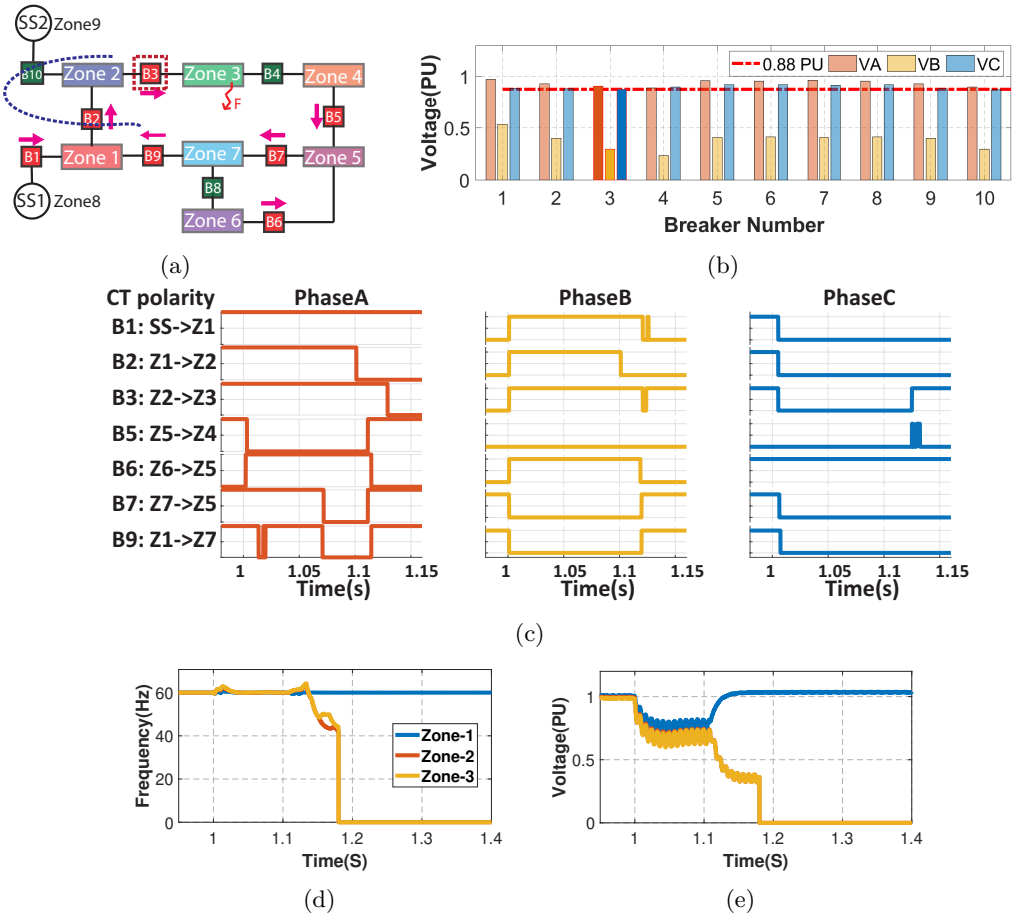

Figure 4.1: Backup protection test case: (a) system with B-G fault in Zone 3, (b) current directions measured by all breakers, (c) fault-voltages measured at all breakers, (d) frequency plots for Zones 1, 2, 3, (e) voltage plot for Zones 1, 2, 3.

rest of the healthy part of the area) recover.

4.2.3 Reconfiguration for self-healing

Reconfiguration program is tested with all possible scenarios in the system that are created by 1) fault in each zone, and 2) isolation of multiple zones. To demonstrate the working of the reconfiguration scheme, two test cases are described here. First, a permanent fault that leads to loss of grid is described. In this case Zone 1 is faulted at $t = 1s$, and is isolated by the zonal relay by sending trip signals to breakers $B1, B2, B9$ at $t = 1.05s$ as shown in Figure. 4.2(a). As a result, the reconfiguration scheme detects the loss of grid source and creation of two islands. The program then finds and closes a path between islands ($Island-1$ and 2) and grid source ($SS2$) by closing

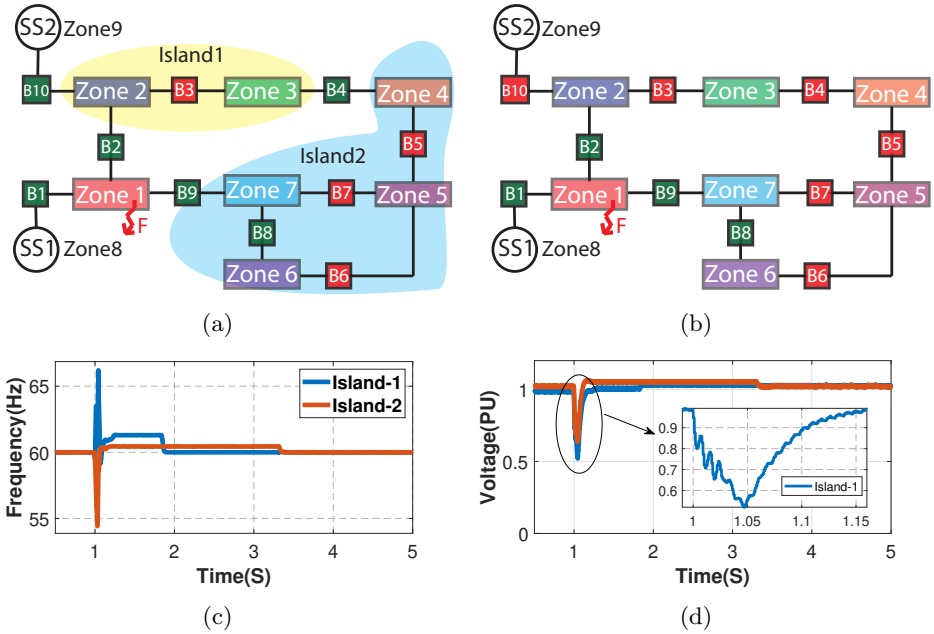

Figure 4.2: Reconfiguration test case1: (a) pre-reconfiguration state, (b) post-reconfiguration state, (c) frequency plot, (d) voltage plot.

breakers $B10$ and $B4$. This operation leads to the post reconfiguration state as shown in Fig .4.2(b). The voltage and frequency plots of the two islands during the event as shown in Figure. 4.2(c),(d) validate stable reconfiguration.It should be noted that close commands are sent to breakers $B10$ and $B4$ at the same time, but the actual closing of breakers depends on when the sync-check conditions are met. In this test case, the actual breaker closing occurred at $t = 1.8s$ for $B10$ and at $t = 3.4s$ for $B4$.

This example also brings out the necessity of the FDF feature built into the main protection, as discussed in section 3.3.1. In Figure. 4.2(d), after the fault is cleared at $t = 1.05s$ by the zonal relay of zone 1, the voltage recovery in zone 2 (Island 1) takes around 60 ms to get above the threshold value of 0.88 pu. During this time, the current direction in Breaker B3 is going in to Zone 2. If the FDF in Figure. 3.5 is not used in the protection logic, then the zonal relay of zone 2 may misoperate since fault-conditions are met. The time taken for a zone to recover after fault depends on factors like inverter's capacity, primary control response, and severity and proximity of the fault. In this case, the FDF signal received by Zone 2 with user-defined time interval (100 ms taken in this study) is applied to reset the integrator in the protection logic to avoid mis-operations during recovery.

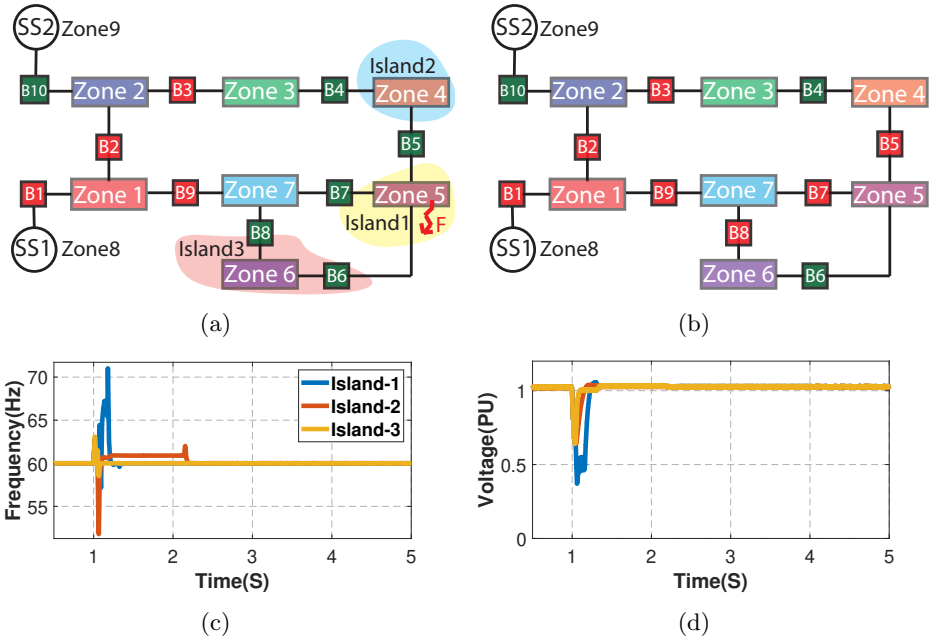

Figure 4.3: Reconfiguration test case2: (a) pre-reconfiguration state, (b) post-reconfiguration state, (c) frequency plot, (d) voltage plot.

The second case demonstrates how the self-healing feature also accommodates temporary faults. For a temporary fault in Zone 5, the protection system isolates zone 5 by opening breakers $B5, B6, B7$, and the primary relay is reset, as per the discussion in section 3.3.1. But, when the fault clears, the voltage and frequency get to healthy levels, effectively leaving three healthy islands ($Island-1$, 2 and 3) as shown in Figure.4.3(a). Since the grid is not lost in this case, the program determines the path and reconnects the healthy zone 4, 5 and 6 back to the grid ($SS1$) by sending close commands to breakers $B5, B7, B8$. The post reconfiguration state is shown in figure Figure.4.3(b). The voltage and frequency plots of this event are shown Figure.4.3(c),(d), respectively. Observe in both cases discussed for reconfiguration, the frequency excursions are unusually high due to the combined effect of fault and islanding. Frequency of Zone 5 (Figure.4.3(c)) shows the worst excursion, because there is also load shedding involved. However, the inverter controls are able to quickly stabilize the frequency. It should be underscored here that the stability of IBR models developed and used in this work is crucial for backup and reconfiguration schemes to be successfully implemented.

4.3 summary

The protection scheme is tested on the highly unbalanced IEEE 123-node feeder with 15 IBRs connected to it. Reliable operation of main and backup protection is demonstrated without the need for any adaptive changes in settings for grid-connected or islanded modes. Backup comprehensively addresses failure of relay, breaker or communication. Reconfiguration scheme is tested to show temporary faults do not result in permanent outage and the test cases for reconfiguration underscore the extremely stable performance of the IBR models under fault, load-shedding and islanded conditions. However, as the protection scheme requires communication between devices, it will be tested on a cyber-physical co-simulation setup with actual communication links in the next chapter.

Chapter 5

Real-time Implementation

5.1 Introduction

The proof of concept for the protection scheme with successful detection and isolation of 420 faults of all types is shown in chapter 4. However, all the analysis is done on IEEE 123 node feeder simulated on non-real-time PSCAD software with simulated communication network delays modeled as a specific value in protective relays (modeled within PSCAD) and microgrid controller (uses PSCAD-MATLAB interface). This is a drawback which can only be addressed by real-time co-simulation of power and communication network (cyber-physical system) with the protective devices interfaced as HIL. This setup is called Control Hardware in the Loop (CHIL) simulation. In this chapter, the authors present such a HIL framework to establish the cyber and physical setup required to test the developed protection scheme in real-time. Usually, in the published literature, the HIL implementation involves the usage of a single communication protocol in testing protective devices/schemes in closed-loop [55, 56]. In this chapter, the authors created a co-simulation platform that uses IEC 61850 and TCP/IP communications to test, analyze, and design a communication-assisted protection and self-healing scheme for microgrids, thus helping to integrate protective devices using different types of protocols. Hence, the novelty lies in two folds: demonstrating a novel communication assisted protection scheme for microgrids in real-time that require different types of communication protocols.

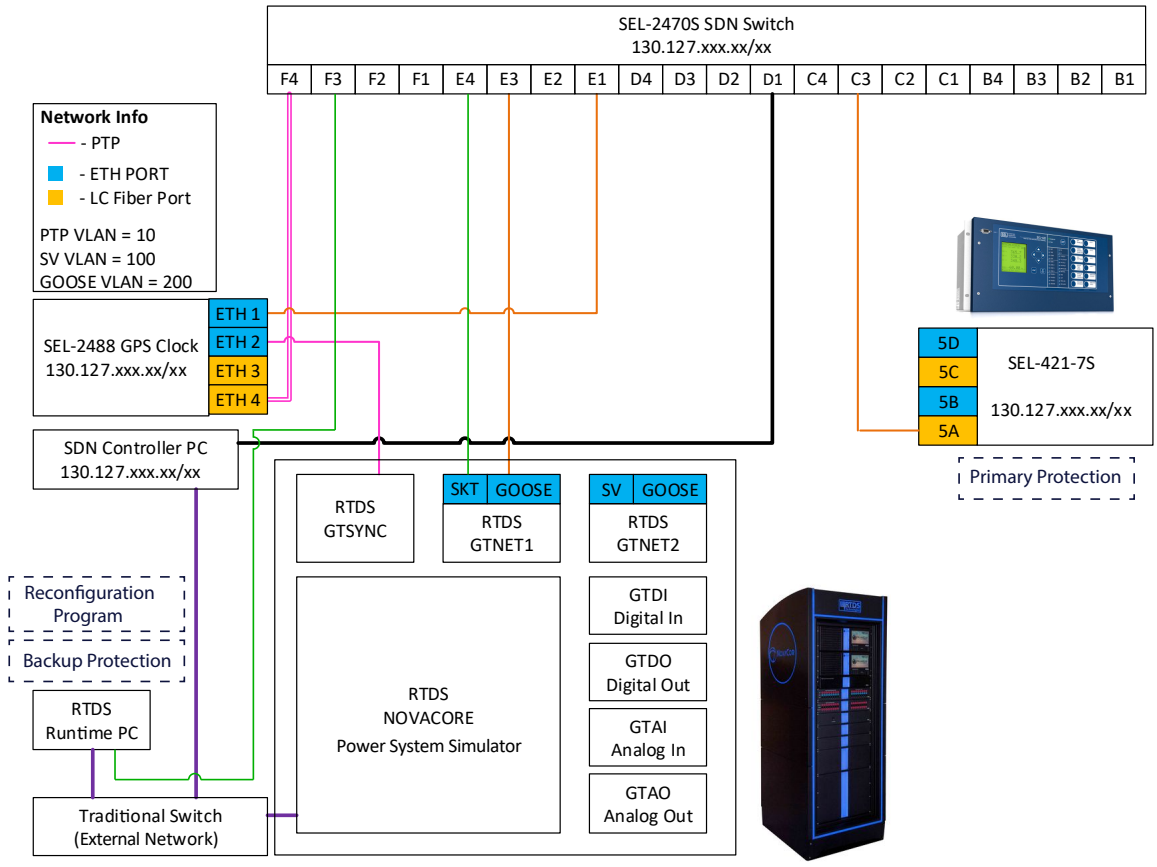

Figure 5.1: HIL setup using RTDS.

5.2 Hardware in the Loop framework

This section will explain the HIL setup, its components and data flow in detail. The HIL setup consists of the RTDS simulator rack, SEL-2470 software-defined network (SDN) switch, SEL-2488 GPS Clock, SEL-421 protection relay, SDN controller PC, and a Runtime PC as shown in Figure. 5.1. The SEL-2470 SDN switch manages the network traffic between the connected devices. The SDN, the GPS clock, and the SEL 421 relays are configured on a local area network (LAN) and managed using the SDN controller PC. The SEL-2488 GPS clock provides the GPS time as a PTP signal to the GTSYNC card and the SDN switch. The GTSYNC card synchronizes the simulator time to the GPS time PTP signal.

5.2.1 Real-time simulator

The RTDS simulator is designed to perform real-time electromagnetic transient program simulations. The processing unit of the RTDS Simulator is called a NovaCor. Each NovaCor contains an IBM Power8 processor with 10 cores, operating at 3.5 GHz, with workstation interface functionality, communication ports, and analog output channels [57]. These 10 cores are used to solve the network solution, network components (i.e., transmission lines, loads, transformers, etc.,) and any controls present in the simulation modeled using its user interface software called RSCAD.

5.2.1.1 Microgrid system on RTDS

The IEEE 123 node test feeder with 15 IBRs is modeled in RSCAD to simulate a microgrid system in real-time. The inverter models are the building blocks of the 100% IBR based microgrids, and use of detailed models with proper control scheme is vital to enable stable system response for different dynamic scenarios. A detailed switching model of a three-phase inverter based on Proportional Resonant (PR) control is developed for the IBR model in chapter 2. The performance of this control topology with a robust droop controller is described on the IEEE 13-bus feeder with 4 IBRs, constituting 100% IBR penetration to create the worst-case scenario [40]. However, for the power system side analysis with time frames in the fundamental frequency range (in ms), an averaged model (with full control scheme) can suffice instead of a detailed switching model of the three phase inverter. The switching legs of the IBR models in [40] are averaged as described in section 3.2.1.1 to reduce the computational burden and run the microgrid model (123 node power system model + 15 IBR models) in real-time with a time step of $150\mu s$. All the inverters operate in GFL mode with unity power factor output and supply only balanced currents when the grid is connected, where the grid source supplies reactive power and unbalance currents. This is achieved by employing negative sequence current blocking (NSCB) in calculating the reference for the current control loop. In islanded mode, one inverter operates in GFI mode. It performs grid functions of keeping voltages balanced while supplying unbalanced currents. This operation is achieved by involving a negative sequence voltage blocking scheme (NSVB) in the voltage control loop. All inverters limit their fault current to a low value for device protection. The value is comparable to their continuous rating (1.1 pu for grid following and 1.5 pu for grid forming were chosen in this study), thus replicating the commercial inverter design [43] in limiting fault currents. The overview of the control diagram of

the three-phase IBR model is shown in Figure. 5.2 and a complete control scheme with a detailed explanation of GFI and GFL mode of operation can be found in section 2.2.

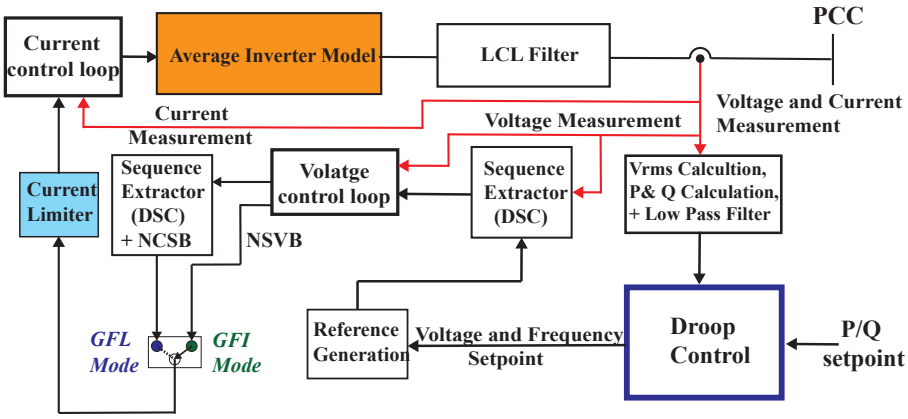

Figure 5.2: Overview of three-phase IBR control.

5.2.1.2 IED model

The developed protection scheme requires current directions, breaker status, and voltage magnitude values from all breaker locations shown in Figure. 3.1a. These measurements and breaker controls needed for the protection scheme are modelled in RSCAD as an Intelligent Electronic Device (IED) for each breaker. The breakers are conceived as modern reclosers without using the reclosing function. Modern reclosers are equipped with a control box mounted on the same pole as the recloser, which can be compliant with the communication protocol of choice. The control box can be thought of as an IED that can be programmed to perform different user-defined functions. Since the recloser is equipped with a CT and a VT, and measures voltage and current phasors, different functions related to these phasors can be built into this IED. In the IED, current direction is calculated using the well-established 90-45 directional scheme that uses line voltages as the polarizing quantities for phase units and zero sequence voltage as the polarizing quantity for ground unit [50]. Additionally, these breakers will need to connect two live systems while closing, making it necessary to have a check-synchronization (referred to as "sync-check" hereafter) feature [47] built into the IED. This means after getting a closing signal, the breaker will close only when the voltage and frequency differences between two sides are within allowed thresholds. In addition, the IED is assumed to be able to detect breaker failure (failure to open after a trip command). The manual for a commercially available product [48] shows that these capabilities are already available in modern reclosers, thus

validating the assumptions made and the IED model created in RSCAD.

5.2.2 Network Interface card for data communication

The GTNETx2 card is used to interface the RTDS to external equipment over a LAN connection using various standard network protocols. The GTNETx2 card can be viewed as a protocol converter accepting packets from the LAN, extracting data from the packets and sending the payload information to the NovaCor processing unit. The GTNETx2 card connects to the NovaCOR via a fiber port. Data from the RTDS Simulation can also be sent into a packet (packet format based on selected protocol) and put out on the LAN where it will be picked up by the devices assigned to accept the data. Each GTNETx2 has the capability of running two protocols simultaneously. In this work, the GTNETx2 card is configured to use GSE/GOOSE and socket(SKT) protocol [57] for the protection application.

5.2.3 SEL-421-7 Relay

The SEL-421-7 relay is a high-speed transmission line protective relay that is compatible with IEC61850 std and features various standard protection logics. SEL provides the acSELerator Quickset software to configure the relay setting either using standard functions or the user can define the custom logic in the place holder called "protection free-form logic settings". As the protection scheme in this dissertation uses a custom logic developed by the authors, sequence timers, math logic blocks, and latches provided in the acSELerator Quickset software are used to program the protection logic developed in chapter 3.3.1 as a custom logic. The current direction measurements and breaker status (Boolean value) are received as GOOSE messages by the relay from RTDS. SEL provides relay word bits called virtual bits (VB) for user configuration. The virtual bits $VBXXX$ are used for mapping the receiving GOOSE messages to the relay. Similarly, SEL provides remote analogs (RA) in analog quantities for user configuration. These remote analogs $RAXXX$ are used for mapping RMS voltages from RTDS. The trip signals of the protection logic are mapped onto protection variables $PSVXX$. The protection variables are part of the Boolean variables provided in the SEL relay. These trip signals are configured to be sent as GOOSE messages to RTDS that will be explained in the below section.

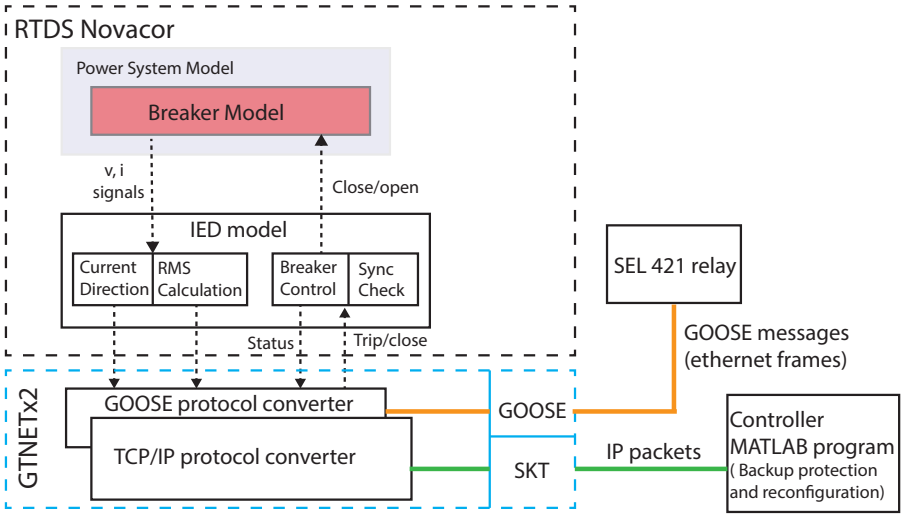

Figure 5.3: HIL data flow from RTDS to protection devices.

5.2.4 IEC 61850 Framework

The IEC 61850 standard was developed by the IEC Technical Committee Number 57 Working Group 10 and IEEE for Ethernet (IEEE 802.3)-based communication in electrical substations and is currently being extended for teleprotection (IEC 61850-90-1). Although developed initially, keeping the substation automation and protection in mind, IEC 61850 also works well for microgrid applications. It provides an efficient and reliable interoperability framework between different field devices in protection applications. The protection applications impose stringent restrictions on messages that communicate fault-related signals, such as the 4 ms end-to-end time limitation imposed on GOOSE messages by IEC 61850 [58], making it a suitable protocol for primary protection. The GOOSE object within IEC 61850 is designed for high-speed protection and control applications. IEC 61850 GOOSE automatically broadcasts messages containing status, controls, and measured values onto the network for use by other devices. GOOSE sends the message several times, increasing the likelihood that other devices receive the messages.

The object-oriented peer-to-peer data exchange capabilities are the most significant properties of IEC 61850 over the other common standards. The Substation configuration language (SCL) is an XML-based configuration language used to support the exchange of configuration data between different tools from different vendors. There are four types of SCL files as follows.

- IED capability description file (ICD).

- System specification description (SSD) file.
- Substation configuration description file (SCD).
- Configured IED description file (CID).

The ICD file describes the capabilities of an IED, including information on LNs and GOOSE. The SSD file describes the single-line diagram of the substation and the required LNs. The SCD file contains all IEDs, communications configuration data, and a substation description. The CID file describes a single instantiated IED within the project and includes address information. For ease of usage, every vendor will provide an editor with a user interface to parse the SCL files. In this case, RTDS has ICT editor [59] and SEL has AcSELerator Architect.

The data model in IEC 61850 follows a hierarchical structure with each physical IED consisting of several logical devices representing physical equipment. Each logical device has several logical nodes (LN). Logical nodes (which are abstract) are the IEC 61850 object-oriented virtual model's primary elements, consisting of standardized Data Objects (DO) and Data Attributes (DA) [58]. Most data objects comprise standard classes involving basic data objects, status, control, and measurement. Each data element consists of several data attributes with a data attribute type that belongs to functional constraints. The proposed protection scheme uses the Generic process I/O (GGIO) LN defined to use for non-standard functions. The calculated direction measurements and breaker status in the IED model described in section 5.2.1.2 are mapped to status information DO-Ind and DA-"stVal". The Analog Input DO-AnIn is used for voltage measurements from the IED model and values are mapped to DA-"mag.f". The trip signals from the relay described in section 5.2.3 are also defined as GGIO LN and mapped to DO-Ind, DA-"stVal".

With the decided data models, the steps to complete the configuration of GOOSE messaging between RTDS and SEL-421 relay is as follows.

1. Using the ICT editor in RSCAD, map the outputs of IEDs (current directions, breaker status, RMS voltages) described in section 5.2.1.2 to correct data models and configure them to publish as GOOSE messages.
2. Export the configured settings as a CID file from ICT editor and import it on SEL Architect.
3. In SEL Architect, Map the DAs to the virtual bits and analog inputs according to section 5.2.3 in the relay. This step will ensure relay subscribing to messages from RTDS.

4. Create GOOSE transmit messages using protection variables (PSVXX) for publishing trip messages.

5. Export the CID file for the SEL relay and import it in ICT editor and configure to subscribe to the trip messages from SEL relay.

The data flow between RTDS and SEL 421 relay for the configured IEC61850 communication is show in Figure. 5.3.

5.2.5 Microgrid controller and TCP/IP link

The TCP/IP is a standard communication protocol that establishes end-to-end communication with acknowledgments ensuring packet delivery. The TCP standard comes with priority settings that can be used to prioritize the protection related data over the network to warrant faster packet delivery. To protect the entire microgrid, the physical network design covering the whole area to yield the 4ms end-to-end latency requirement of IEC61850 can be achievable [60] but can increase the cost of implementation. For the backup protection an extra time delay is available to operate as it is time co-coordinated with primary protection (100ms in this chapter). This makes TCP/IP a suitable protocol to use that can provide a latency of around 10ms to 20ms[61]. The backup protection and reconfiguration logic are programmed in MATLAB on the runtime computer shown in Figure. 5.1. The *tcpclient* object in MATLAB software can be used to represent a connection to a remote host and remote port from MATLAB to read and write data. The remote host can be a server or hardware that supports TCP/IP communication. In this case, RTDS is configured as a TCP server supporting bi-directional data. The server is configured with an IP address and port number to send/receive data. The data flow between RTDS and MATLAB program in microgrid controller (i.e., runtime PC) for the configured TCP/IP is shown in Figure. 5.3. The current directions, voltage values, breaker status and trip signals from primary protection are formatted into a data array and sent as IP packets. The IP packets are read at the runtime computer and the payload is extracted and sent to back up protection and reconfiguration programs. After program execution, the trip signals from backup protection are sent back to the server (RTDS) from MATLAB as IP packets. Similarly, close signals from the reconfiguration program are sent to RTDS from MATLAB.

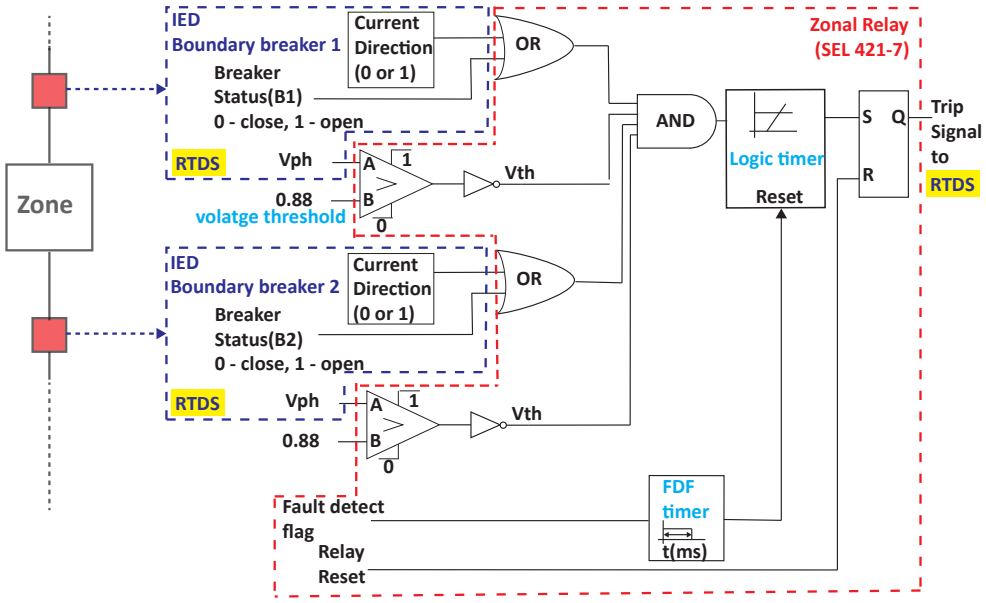

Figure 5.4: Primary protection fault detection logic with two boundary breakers.

5.3 Implementation of the protection scheme

The IEC 60834-1: Teleprotection Equipment of Power Systems defines the fault clearance times for communication assisted protection schemes. The time divisions of the total fault clearing time includes several parts as shown in Table 5.1. If protection applications requires transmitting and receiving information from a remote location, propagation delays for teleprotection needs to be taken into account as well. In summary, the typical fault clearance time can be in the range of 42ms to 180ms. This range can also be seen in grid codes such as [62], which specifies a fault clearing time "shall not be faster than 120ms for medium voltage networks (132KV and below)".

As discussed in section 3.3, The protection scheme includes primary and back-up protection. Three settings are required for the primary protection logic of a zone shown in Figure. 5.4: 1) logic timer, 2) voltage threshold, and 3) Fault Detect Flag (FDF) timer, where the settings used are 2 cycles (33ms), 0.88 PU, and 100ms respectively. The detailed explanation of the logic and flags are given in chapter 3.3.1. Based on the primary protection logic timer, backup protection time delay has to be set by adding the co-ordination time interval (CTI) to logic timer. Unlike conventional protection schemes where CTI includes relay and breaker operation time, the CTI in this scheme should include maximum network latency and operation delays as it involves communication.

The detailed time division of total fault clearance by primary protection is shown with an

Table 5.1: Time allocation for fault clearance according to IEC60834-1

Category	***details***	***time (ms)***
Fault recognition time	-Analog to digital conversion -protection algorithm pickup	10 to 30
Teleprotection	-network latency and propagation delay for teleprotection	2 to 40
Relay decision time	-Trip decision in application -relay operating time	0 to 30
circuit breaker operating time	-circuit breaker trip coil -circuit breaker mechanical movement	30 to 80
Total	Fault clearance time for a protection system	42 to 180

example: a BG fault is applied in zone 1, that has three boundary breakers B1, B2 and B9. The communication setup for the example is shown in Figure. 5.5 (a). The time taken for different operations in ms is shown in Figure. 5.5 (b). The fault is applied at 20ms, where as the relay picked up the fault at 39ms after the voltage went below threshold of 0.88PU. The relay decision time and round trip communication took around 43ms (33ms of time delay + 8ms for round trip communication and relay logic execution) to receive trip signal at the breakers B1, B2 and B9 at 82ms. The breaker opening delay is 35ms, taken from the data sheet of the breaker equipment assumed in the dissertation [48]. So, the total fault clearing time is around 97ms, which is within the IEC 60834 specified range.

Now, considering to have a network that can provide a maximum communication latency of 4ms for for IEC61850 communication and 10ms for TCP/IP, The CTI should be at least: 33ms (logic timer) + (2*4ms) + 10ms = 51ms. The backup time delay has to be set > 35ms (breaker opening time) + CTI = 86ms. In this chapter, the time delay of 100ms is selected for the backup protection allowing enough time for co-ordination with primary protection. For the same BG fault in zone 1, the time of operation in ms for backup protection is shown in Figure. 5.5 (c). The fault is applied at 20ms and backup protection picked up the fault at 39ms after the voltage went below threshold of 0.88PU. The program decision time and round trip communication took around 120ms to receive trip signal at the breaker at 160ms. The 120ms include 100ms time delay, 12ms for execution of backup protection program execution and 8 ms for round trip communication. Considering the breaker opening time, the total fault clearing times is around 174ms, which is within the IEC 60834 range.

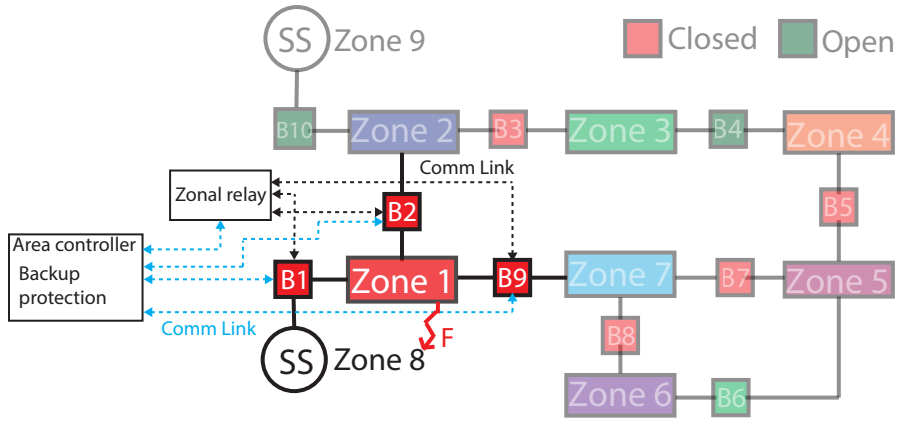

(a)

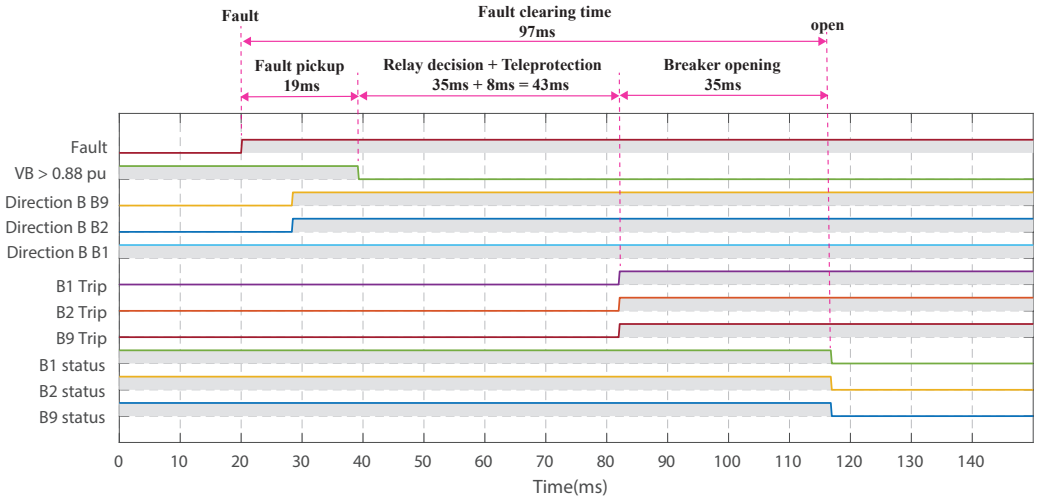

(b)

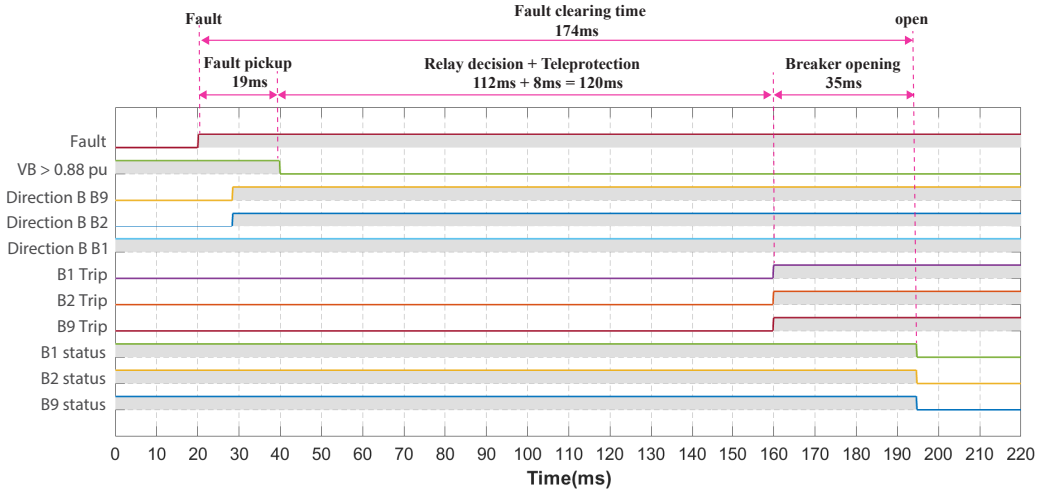

(c)

Figure 5.5: Protection of zone 1: (a) communication setup, (b) operating times of primary protection, (c) operating times of secondary protection.

5.4 Real-time HIL Results

The Protection scheme was tested on the 123 node distribution feeder using the HIL setup discussed in section 5.2. The Following case studies in this section are used for the analysis and validation of the proposed scheme on the co-simulation platform.

5.4.1 Primary Protection

The primary protection logic for all seven zones is programmed in the SEL-421 relay. The protection scheme is tested in real-time for different faults in different parts of the 123-bus feeder in both grid-connected and islanded modes. The response of the scheme in detecting, locating, and clearing the faulted zone at three randomly selected locations on the feeder in grid-connected mode is shown in Figure. 5.6 (a) and islanded mode is shown in Figure. 5.6 (b). It can be seen that in both modes of operation, correct zonal protection is detecting the fault and sending the trip signal. For example, in Figure. 5.6 (a), an AG fault at 200 ms in zone 1 is detected by the zone 1 relay (blue color), and the zone trip signal is received by corresponding breakers B1, B2 and B9 at 255 ms in RTDS run time. The operation time of 55 ms includes the pick up time, relay operation and round trip time communication delay. The actual breaker opens 35ms after receiving trip signal.

5.4.2 Backup Protection

The backup protection is tested for three cases: primary protection failure, breaker failure, and IED communication failure in both grid-connected and islanded modes of operation. As mentioned in the previous section 5.3, to co-ordinate with the primary protection, a time delay of 6 cycles (100ms) is used in the backup protection logic. First, for a primary protection failure, the response of the backup protection for detecting, locating, and clearing the faulted zone at three randomly selected locations on the feeder in grid-connected mode is shown in Figure. 5.7. For example, for an ACG fault in zone 1 at 200ms, the backup protection will trip the breakers B1, B2, B9 at 330ms and isolate zone 1. The operation time of 130 ms includes the 100 ms of time delay plus 30 ms for relay pickup time, backup protection operation and communication delay. Second, for a breaker failure, the response of the backup protection is demonstrated with a test case in islanded mode, as shown in Figure. 5.8(a) and (c). For a BG fault at 200ms in zone 4, when breaker B5 fails to operate (the breaker failure signal is simulated at 285 ms), the backup protection will clear the faulted region

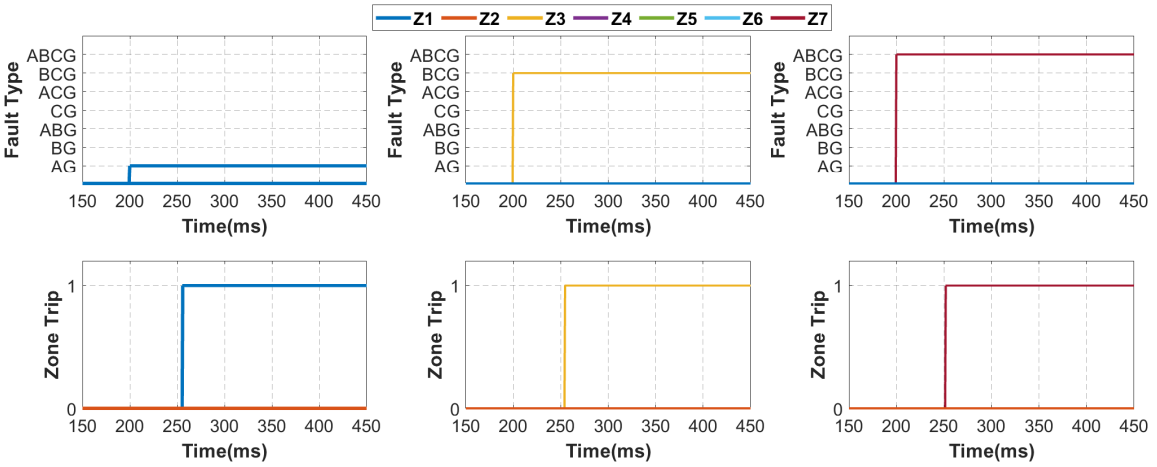

(a)

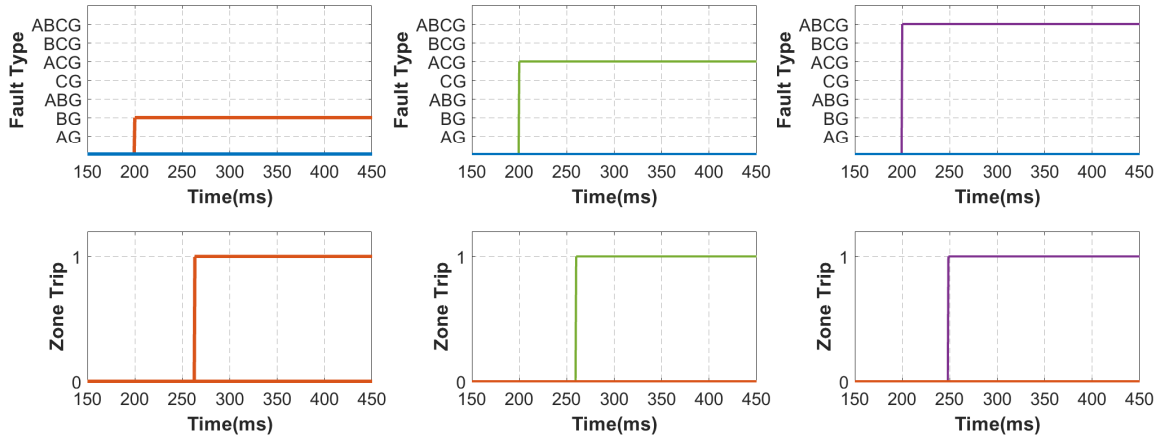

(b)

Figure 5.6: Primary protection response: (a) grid connected mode, (b) islanded mode

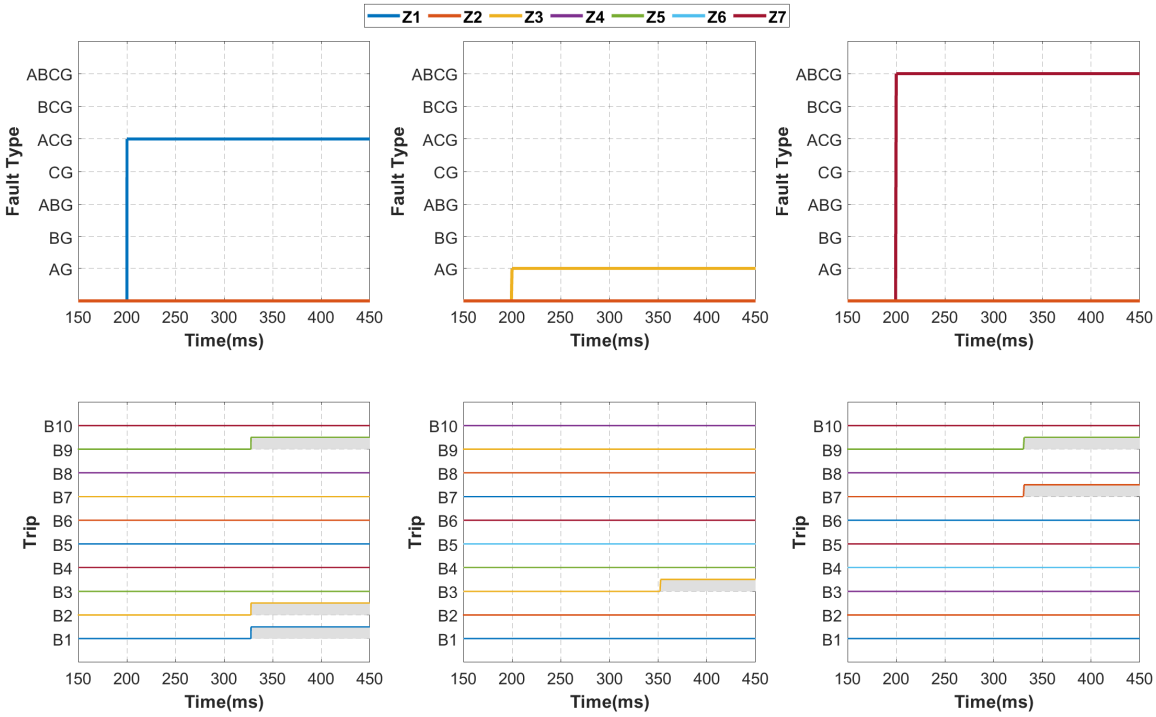

Figure 5.7: Backup protection response to primary protection failure

(zone 4 and 5) by opening breakers B6, B7 at 348ms. The operation time of 148 ms includes the 100 ms of time delay plus 48 ms for round trip relay pickup time, backup protection operation (decide the next breakers to trip for the failed breaker) and communication delay. Third, for an IED communication failure, the response of the backup protection is demonstrated with a test case in islanded mode, as shown in Figure. 5.8(b) and (d). For an ABCG fault at 200ms in zone 4, when breaker B5 fails to operate (the breaker failure signal is simulated at 285 ms) in addition to IED comm failure at B7, the backup protection will clear the faulted region (zone 4, 5, and 7) by opening breakers B6, B9 at 352ms. The operation time of 152 ms includes the 100 ms of time delay plus 52 ms for round trip communication delay, relay pickup time plus backup protection logic operating time in expanding the protection region for the failed IED and deciding the next breaker(s) to trip for the failed breaker. Note that the trip time shown in the figures is the time when the breaker will receive a trip signal.

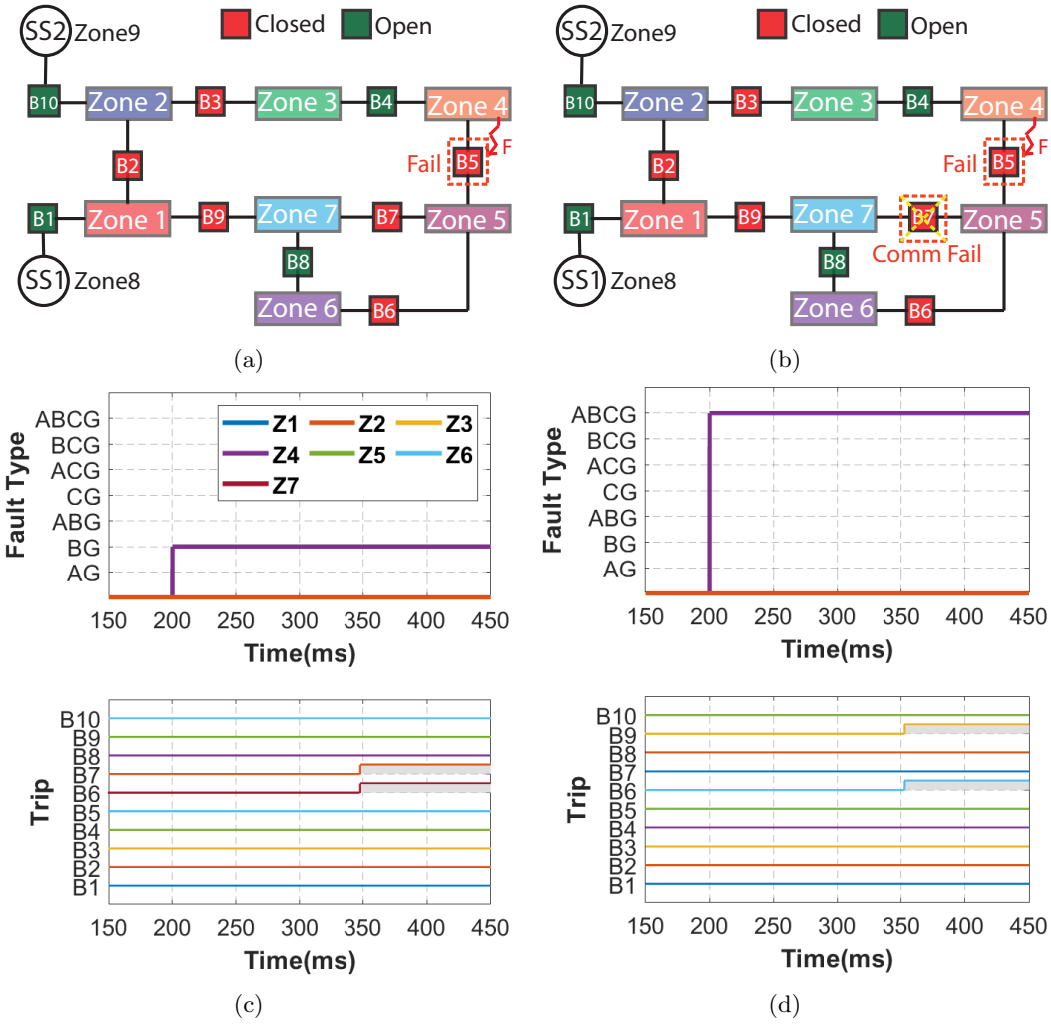

Figure 5.8: Backup protection response to: (a) breaker failure, (b) IED failure

5.4.3 Reconfiguration aided Protection

The first case is to demonstrate the working of the reconfiguration program in self healing the system in the event of loss of grid source. A temporary fault is applied in zone 1 on the base case topology shown in Figure. 5.5 (a) and the zonal relay will isolate the fault by tripping breakers B1, B2, and B9. This action by the protection system leads to the loss of grid source SS1 to the healthy part of the system (i.e. zone 2, 3, 4, 5, 6, and 7). In this case, the reconfiguration program connects the healthy part of the system to an alternative grid source (SS2) by closing breakers B10 and B3. The topology after reconfiguration is shown in Figure. 5.9 (a). The power plots in Figure. 5.9 (c) show stable reconfiguration for this case. As the fault is temporary, zone 1 will be reconnected to the system by the reconfiguration program (after clearing the fault flag manually) by closing breaker B2. The next case is executed on this changed topology in Figure. 5.9 (a).

The second case will exhibit the robustness of the reconfiguration program to work for any topology. A permanent fault is applied in zone 4, and the protection system isolates the fault by opening breakers B4 and B5. This action will lead to the islanding of healthy zones (i.e. zone 5, 6, and 7). The reconfiguration program closes breaker B9 to connect the healthy zones to the grid source. The topology after reconfiguration is shown in Figure. 5.9 (b). The power plots shown in Figure. 5.9 (d) show stable reconfiguration for this case. As the fault is permanent, it can be seen that the IBR 7 and 8 will shut down after they ride through the fault (see the power output goes to zero) in accordance with the requirements of IEEE1547 standard.

5.4.4 Reconfiguration for a fault with equipment failure

Case 1- Resiliency for primary protection relay failure: The first case is to demonstrate the isolation of the faulted zone by backup protection for primary protection failure followed by the reconfiguration program self-healing the rest of the health system. To simulate the scenario, the zone 1 zonal relay is disabled and a temporary fault is applied in zone 1. As the primary protection failed, the backup protection will isolate the fault by tripping breakers B1, B2, and B9. This action leads to the loss of grid source SS1 to the healthy part of the system (i.e. zone 2,3,4,5,6, and 7). In this case, the reconfiguration program connects the healthy part of the system to an alternative grid source (SS2) by closing breakers B10 and B4. The topology after reconfiguration is shown in Figure 5.10 (b). The power plots shown in Figure 5.10 (d) show stable reconfiguration for

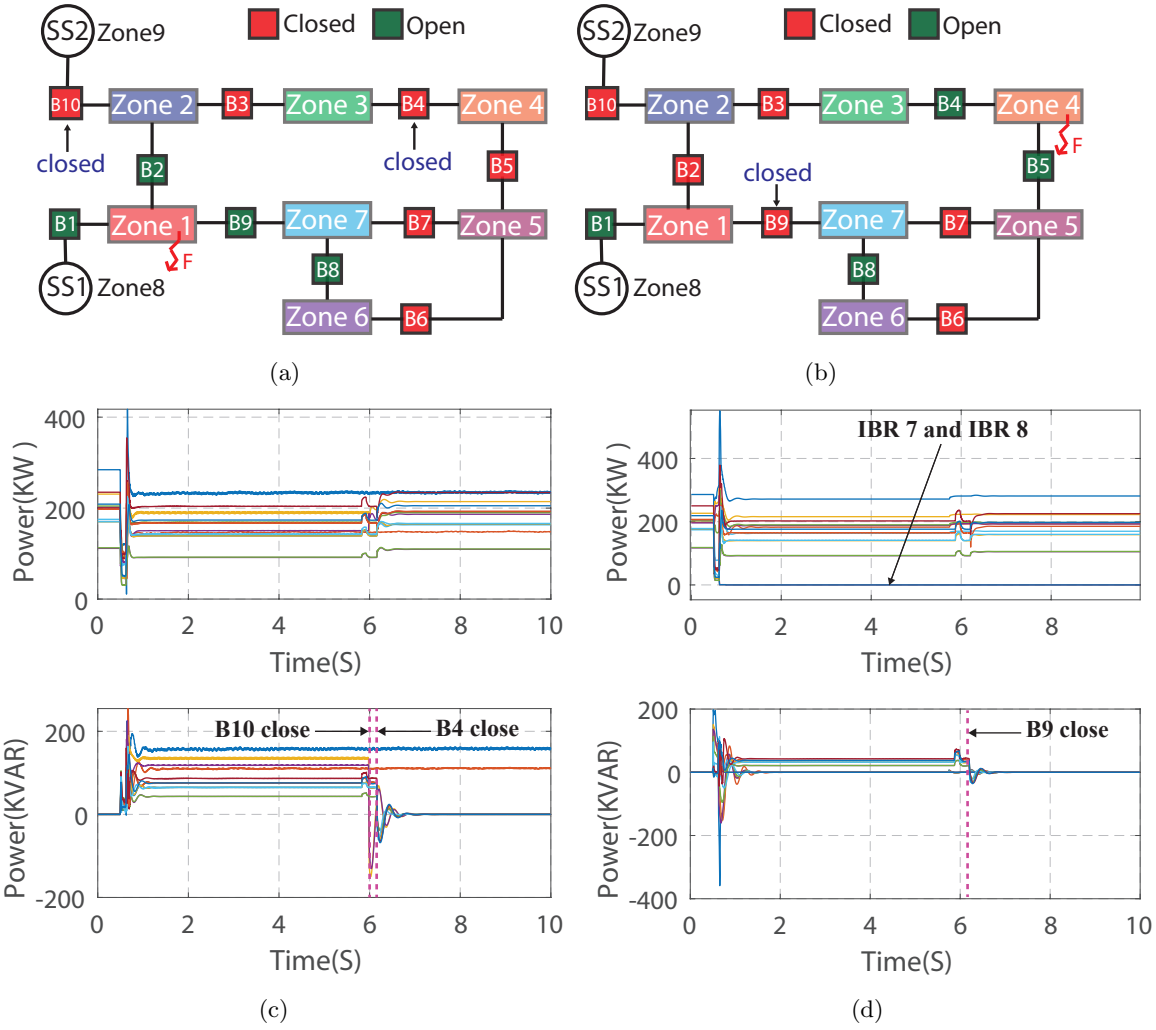

Figure 5.9: (a) Topology post reconfiguration case 1, (b) topology post reconfiguration case 2, (c) IBRs power output for case 1, (d) IBRs power output for case 2

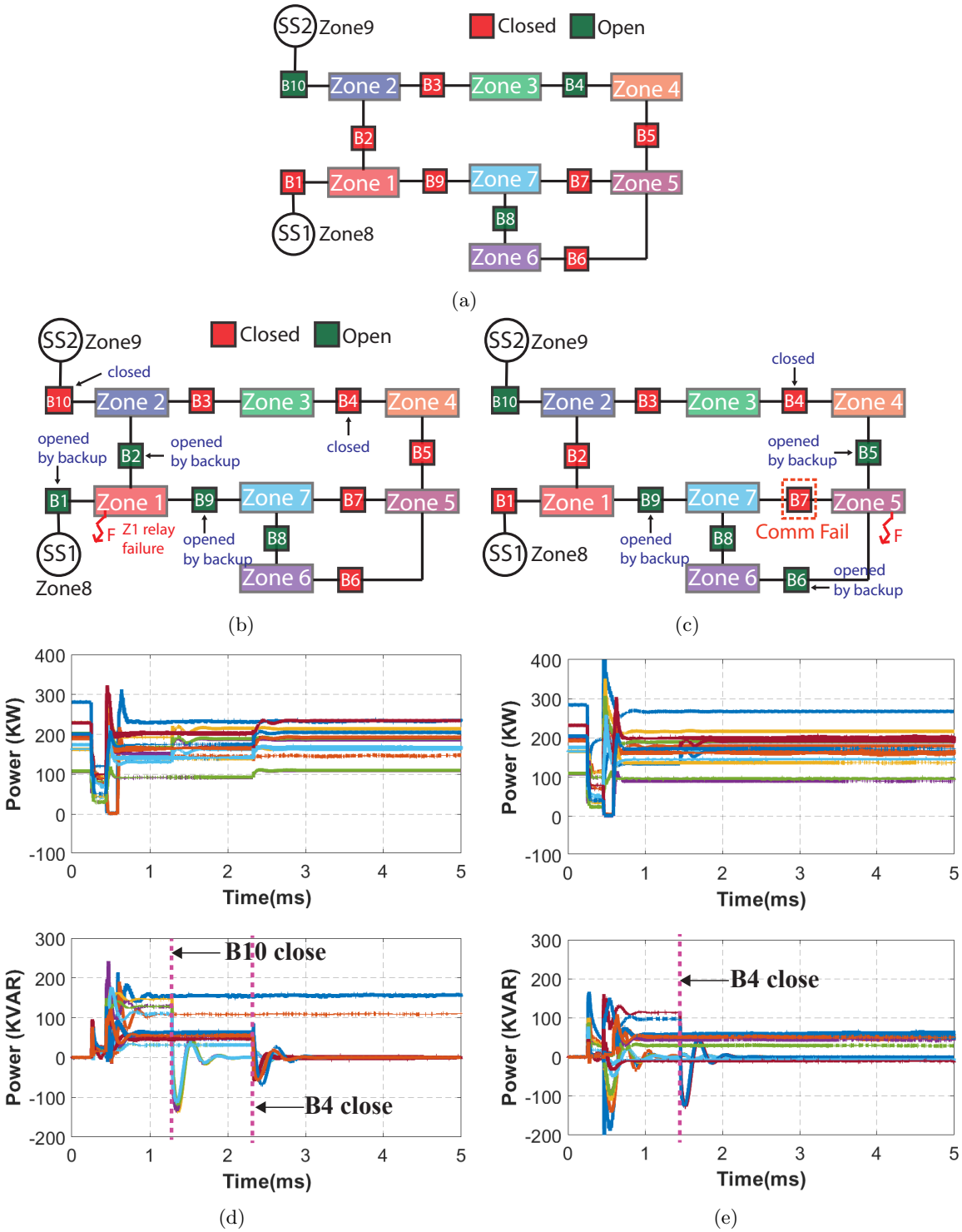

Figure 5.10: (a) base case topology, (b) Topology after reconfiguration case 1, (c) Topology after reconfiguration case 2, (d) IBRs power output for case 1, (e) IBRs power output for case 2

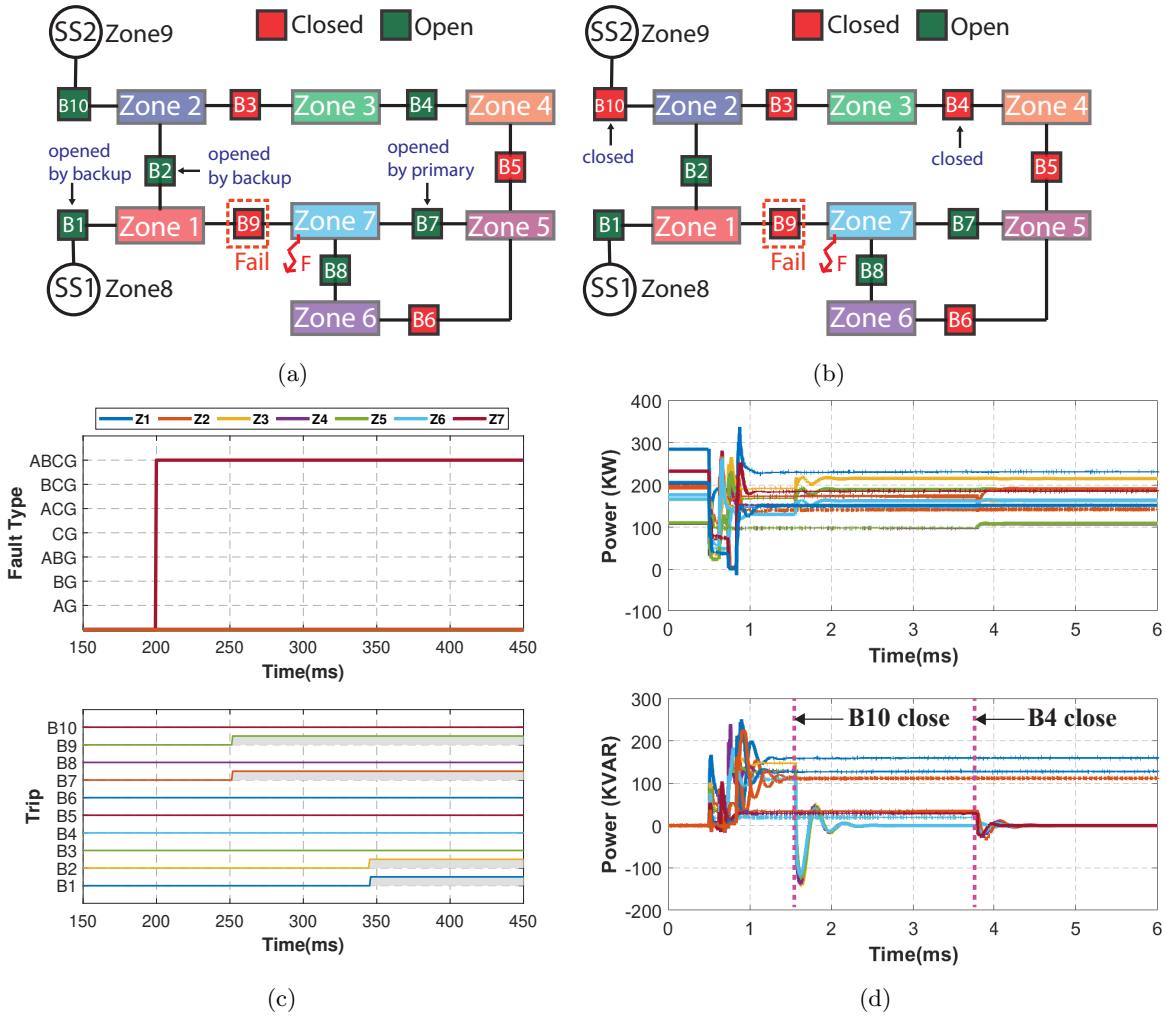

Figure 5.11: (a) Topology after fault isolation, (b) Topology after reconfiguration, (c) protection system response, (d) IBRs power output

this case.

Case 2- Resiliency for IED communication failure: The second case is to demonstrate the case for communication failure to a field IED. When an IED fails to communicate, the primary protection of the zones connected to that respective breaker will fail and backup protection will take care of protecting the combined region. To demonstrate the scenario, the communication to IED at breaker B9 is disabled and a fault is applied in zone 5 on the base case topology shown in Figure 5.10 (a) . The communication failure of B9 will cripple the primary protection of zone 5 and 7. The backup protection system will isolate the fault by opening breakers B5, B6 and B9. This action will lead to the islanding of healthy zone 4. The reconfiguration program closes breaker B4 to connect the healthy zones to the grid source. The topology after reconfiguration in Figure 5.10(c). The power plots shown in Figure 5.10 (e) show stable reconfiguration for this case.

Case 3- Resiliency for Breaker failure: The case will demonstrate the isolation of the faulted zone by backup protection for a breaker failure followed by reconfiguration program self-healing the rest of the healthy system. For a temporary fault in zone 7 on the base case topology shown in Figure. 5.10 (a), the breakers B9 and B7 are tripped by zone 7 relay at 252ms. when breaker B9 fails to operate, the backup protection will clear the faulted region (zone 1 and 7) by opening breakers B1, B2 at 345ms as shown in Figure. 5.11 (a), (c). The reconfiguration program detects two healthy islands (zone 2, 3 and zone 4, 5 ,6) and loss of grid source SS1. It connects the healthy island zones 2, 3 to next available grid source SS2 by closing breaker B10 at 1.6s and the other island of healthy zones 4, 5, and 6 by closing breaker B4 at 3.8s. The topology after reconfiguration is shown in Figure 5.11(b). The power plots for these events of fault isolation and stable reconfiguration are shown in Figure 5.11 (d).

5.5 Summary

This chapter proposed a HIL platform capable of modeling the data flow between the RTDS and physical protective devices to protect a utility-scale microgrid. The co-simulation framework utilizes a real communication network built using IEC61850 for the primary protection and TCP/IP protocol for the backup protection and reconfiguration. The significance of this framework is that it can not only integrate commercially available protective relays, but also protection and control logic programmed on a generic computer to validate the protection methods in real-time. The successful

testing of the protection scheme on IEEE 123 node feeder in real-time demonstrates the smooth flow of data between the cyber and physical parts in the system to protect and self-heal the microgrid under test.

Chapter 6

Guidelines for Implementation of the Protection Scheme

6.1 Introduction

Although implicit in the method described in Chapter 3, this section explicitly provides the guidelines for a utility engineer to successfully implement the proposed protection scheme on any microgrid. Further, to demonstrate the topology-agnostic and scalability aspects, the proposed protection scheme is implemented on a different topology using these guidelines and results are documented, showing successful implementation.

6.2 Guidelines

Step 1: Given a microgrid network, the first task for the design engineer is to define zones of protection. Smaller zone will provide better selectivity, but also require more breakers. It is recommended to perform a load study to determine critical loads and select the part of feeder to include enough generation to feed these critical loads within the zone during zone definition. The problem of optimizing the number and locations of the breakers depends largely on the project scope, its budget, and engineering judgement. It should be noted that the scheme provides flexibility of revisiting the zone definitions as the microgrid network evolves with more gener-

ation and changes in criticality of loads. This way a larger zone definition constrained by cost in the present network can be reduced to smaller zones in the future, based on changes.

The breaker has to be an intelligent recloser/breaker that has inbuilt current and voltage sensors. The breaker is usually attached to an IED with computation capabilities and has communication compatibility with various industry standard protocols like IEC61850, DNP3, and TCP/IP. In addition, the breakers should have check-synchronization capability. One such commercial breaker is described in [48]. Based on breaker locations, the microgrid can be divided into zones as described in section 3.2.

Step 2: In each zone, the location of IBRs can be determined either based on engineering judgment or location restrictions, or optimization principles [63], or using feasibility studies [64]. It should be noted that the protection scheme is agnostic to topology, and DER placement will not affect the protection scheme settings.

Step 3: To ensure stable islands formation in the system,

1. implement a load shedding scheme, if needed, to ensure load-generation balance in each zone, in case of islanding. This can be achieved by dis-connecting the non-critical loads obtained from the recommended load study in step 1.
2. The primary control of DERs has to be equipped with a droop control of choice and should ride through faults as per IEEE 1547 std [1]. This will enable stable island formation with power-sharing among DERs.
3. In each zone, at least one of the DER should have the grid forming capability, e.g., grid forming inverter, diesel generator, etc. In case of diesel generator, its negative sequence capability must be adequate to handle the negative sequence currents during islanded conditions.

Step 4: Select a microgrid controller that acts as a secondary controller and performs duties in accordance with IEEE 2030.7 std [65]. The backup protection and reconfiguration program can be hosted in the same microgrid controller.

Step 5: Since communication is the backbone of the protection implementation, design the communication network carefully:

1. Implement PRP (Parallel Redundancy Protocol) or HSR (High-availability Seamless Redundancy) protocol to attain zero recovery time for network failures [66].
2. Perform latency studies on the communication network to ensure acceptable round trip delays in accordance with The IEC 60834-1: Teleprotection Equipment of Power Systems [67].

Step 6: The communication networks should be OT (operation technology) hardened according to critical infrastructure protection standards to protect against cyber-physical attacks. So, all cyber security policies, plans, and procedures must be implemented on the network.

6.3 Implementation Example

For this example, the IEEE 123 node feeder topology is modified from the previous chapter 5, where the entire network was divided into seven zones. Along with the breaker locations, IBR locations are also changed to demonstrate the topology agnostic characteristic of the protection scheme. The breakers and IBR ratings are shown in Figure. 6.1 (a). In this example, the network is divided into three zones based on the breaker locations. The sleek zonal view with three zones is shown in Figure. 6.1 (b).

For the system with three zones, the protection scheme is tested in real-time for different faults in different parts of the 123-bus feeder in both grid-connected and islanded modes. The response of the scheme in detecting, locating, and clearing the faulted zone at three randomly selected locations on the feeder in grid-connected mode is shown in Figure. 6.2 (a), and results for islanded mode are shown in Figure. 6.2 (b). The same relay settings as discussed in section 5.3 are used. It can be seen that in both modes of operation, correct zonal protection is detecting the fault and sending the trip signal. For example, in Figure. 6.2 (a), an ABCG fault at 200 ms in zone 1 is detected by the zone 1 relay (blue color), and the zone trip signal is received by corresponding breakers B1, B2 and B5 at 250 ms in RTDS run time. The operation time of 50 ms includes the pickup, relay operation, and round trip communication delay. It should be noted that the breaker opens 35ms after receiving the trip signal because of the breaker opening delay as discussed in section 5.3.

As mentioned in the section 5.3, to co-ordinate with the primary protection, a time delay of

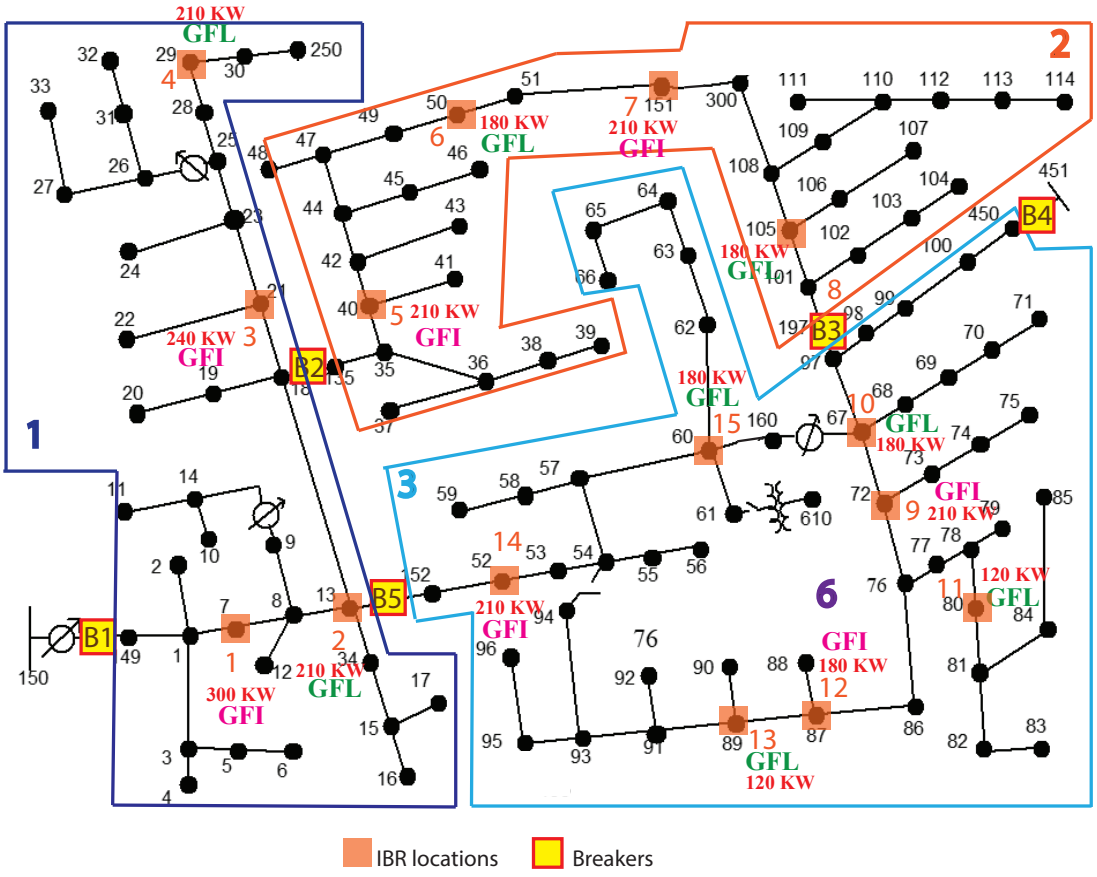

(a)

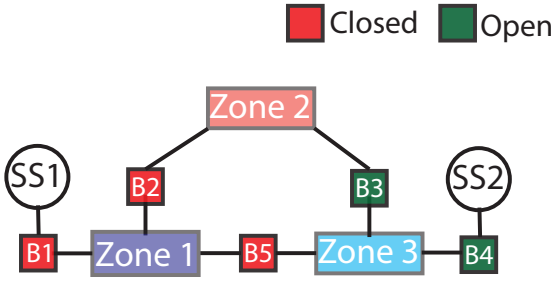

(b)

Figure 6.1: (a) 123 node test feeder with IBR placement and zone divisions, (b) sleek zonal view.

6 cycles (100ms) is used in the backup protection logic. For a primary protection failure, the response of the backup protection for detecting, locating, and clearing the faulted zone at three randomly selected locations on the feeder in grid-connected mode is shown in Figure. 6.3. For example, for an ACG fault in zone 1 at 200ms, the backup protection will trip the breakers B1, B2, and B5 at

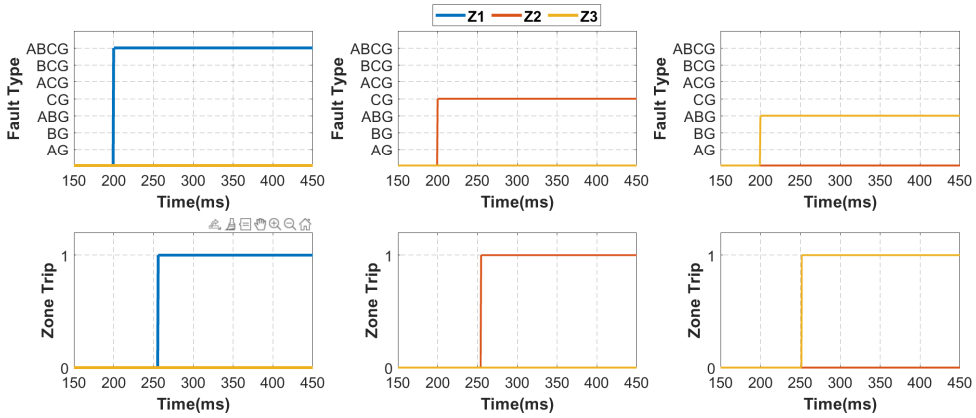

(a)

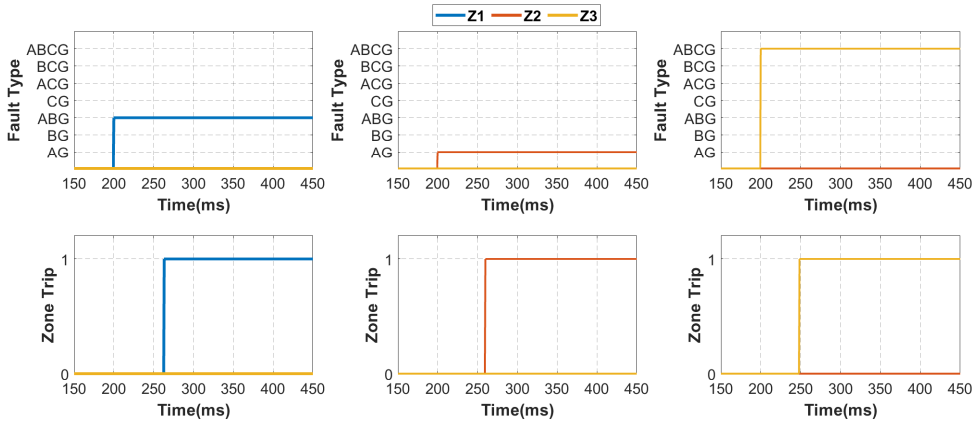

(b)

Figure 6.2: Primary protection response: (a) grid connected mode, (b) islanded mode

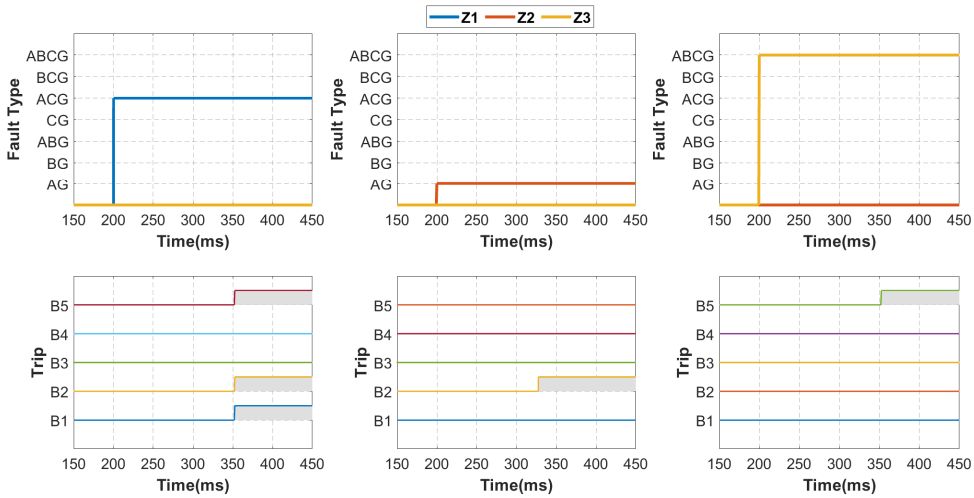

Figure 6.3: Backup protection response to primary protection failure

350ms and isolate zone 1. The operation time of 150 ms includes the 100 ms of time delay plus 50 ms for relay pickup time, backup protection operation, and communication delay.

Chapter 7

Conclusions and Discussion

7.1 Overview of Work

The protection of microgrids is a significant technical obstacle that needs to be addressed for successful implementation. Most of the microgrid protection schemes found in published literature suffer from a lack of generality or tend to be too complicated, expensive, or both. In this dissertation to overcome these drawbacks, a topology-agnostic, scalable, and cost-aware protection based on fundamental principles is developed, validated and implemented in real-time HIL. The protection system also implements stable automatic dynamic reconfiguration of the healthy sections of the system after clearance of fault, thus increasing resilience by self-healing.

7.2 Research Conclusions

In the first chapter, detailed IBR models are developed that can operate in unbalanced networks in grid-connected and islanded modes as a prerequisite to testing the protection scheme. The IBRs share power without conflicting controls using droop control and can ride through faults while limiting fault currents. The working of the inverters with a combination of grid forming and grid following operation modes is shown using the IEEE 13 bus system with 4 IBRs treated as a microgrid. With the proposed primary control design and combination of inverter operation modes, stable operation of the microgrid is achieved in grid-connected and islanded modes, including transition, as well as for changes in load and faults.

In the second chapter, an insight is gained into the performance of PR and PI based controller designs as it relates to inverters used in highly unbalanced microgrids. The PR controller's dynamic performance is found to be superior under all test cases, even when the PI controller performance is enhanced by choosing bulkier filters. Based on the findings in the chapter, the PR based average IBR models are used to construct the IEEE 123 node feeder microgrid system with 15 IBRs to test the proposed protection scheme.

Chapter 3 and 4 lay out the conceptualization, design and performance evaluation of microgrid's primary protection, backup protection, and reconfiguration (self-healing) in grid-connected and islanded modes on PSCAD platform. The novel features of the developed protection scheme formulation are 1) topology independence, 2) scalability and 3) cost-awareness. The Primary protection is formulated locally within each zone to ensure reliability and speed, but backup and reconfiguration are effectively merged with the microgrid controller. Reliable operation of primary and backup protection is demonstrated without needing any adaptive changes in settings for grid-connected or islanded mode using 420 faults on the IEEE 123 node test feeder with 15 IBRs acting as a microgrid.

Since the proposed scheme requires communication between devices, a HIL platform capable of modeling the data flow between the RTDS and physical protective devices is described in chapter 5. The co-simulation framework is built with a real communication network using IEC61850 for the primary protection and TCP/IP protocol for the backup protection and reconfiguration. The significance of this framework is that it can integrate not only commercially available protective relays but also protection and control logic programmed on a generic computer to validate the protection methods in real-time. The proposed framework enabled the successful implementation of the protection scheme using an SEL-421 relay for the IEEE 123 node test feeder in real-time and self-healing scheme utilizing a PC acting as a microgrid controller that hosts a backup and reconfiguration program.

Finally, in chapter 6, the guidelines for a utility engineer to implement the protection scheme for any microgrid are laid out. Using the guidelines protection of a microgrid with completely different topology is successfully demonstrated on a real-time platform.

7.3 Future Work

The main protection issues regarding microgrids are reduced fault current contributions from IBRs compared to conventional DERs, bi-directional power flow, and multi-mode operation. In addition, the ever-changing grid configurations add to the complexity of the problem. The protection scheme described in this dissertation addresses these issues. However, additional features can be incorporated into the fault detection logic for the designed protection framework to improve the scheme's security for exclusive system-specific scenarios, for example, prolonged transformer and/or motor inrush currents. As the inverter control technology and grid integration standards evolve, they can provide additional features that can be used in the fault detection logic. In addition, research should be carried out on inverter controls to make them act predictably for different dynamic scenarios so relays can be set with better knowledge of what to expect.

Since the scheme requires communication between devices, network reliability and cyber security will be a concern and should be addressed. The smart grid devices in a microgrid will create a lot of data flow for different applications traveling over the same communication links, potentially causing congestion. Further research is needed to mitigate the congestion and assign appropriate latencies to diverse data based on the application. In addition, the cyber attack surface is increasing with the increase in the number of DERs and IEDs in the network. More the devices, more the potential cyber-attack vectors would be. Till recently, the cyber security of small networks like microgrids is rarely given the same scrutiny as bulk electrical systems (BES). But, with critical applications like protection depending on communication networks, additional research must be done to harden cyber security without losing reliability and speed.

Appendices

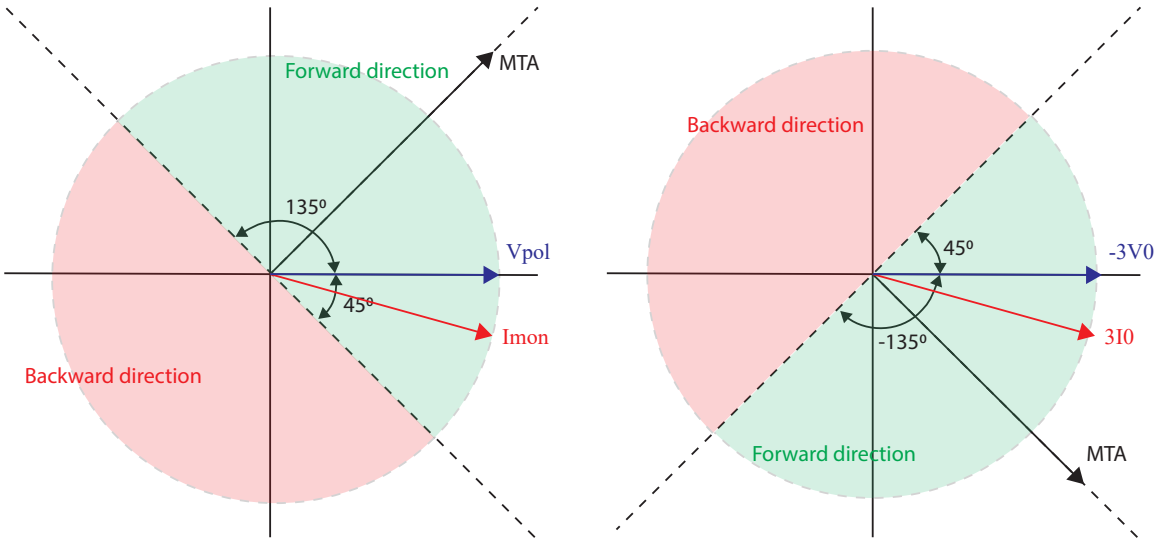

Figure 1: (a) Phase directional element, (b) ground directional element.

Appendix A Directional element calculation

The appendix is created to give more insight into the proposed protection scheme. The operation of the phase directional element and ground directional element is shown in Figure. 1. The phase directional element uses a (90^0-45^0) connection. It will have an operating zone of monitoring current (phase current) leading by 135^0 to 45^0 lagging the polarizing voltage (line voltage). The MTA of ground directional element is shifted by 45^0 clockwise and it has an operating zone of monitoring current (3I0) leading by 45^0 to 135^0 lagging the polarizing voltage (-3V0). The following table shows the polarizing voltage and monitoring current selected for phase and ground elements.

		Polarizing Voltage (V_{pol})	***Monitoring Current*** (I_{mon})
Phase element	Phase A	V_{bc}	I_a
	Phase B	V_{ca}	I_b
	Phase C	V_{ab}	I_c
Ground element		$-3V_0 = V_a + V_b + V_c$	$3I_0 = I_a + I_b + I_c$

Once the direction is determined, if the current is going into the zone, the result of the direction element is '1' and if the current is going out of the zone, it is '0'. This result of the current direction element is used in the fault detection logic in Figure. 3.5 of the paper.

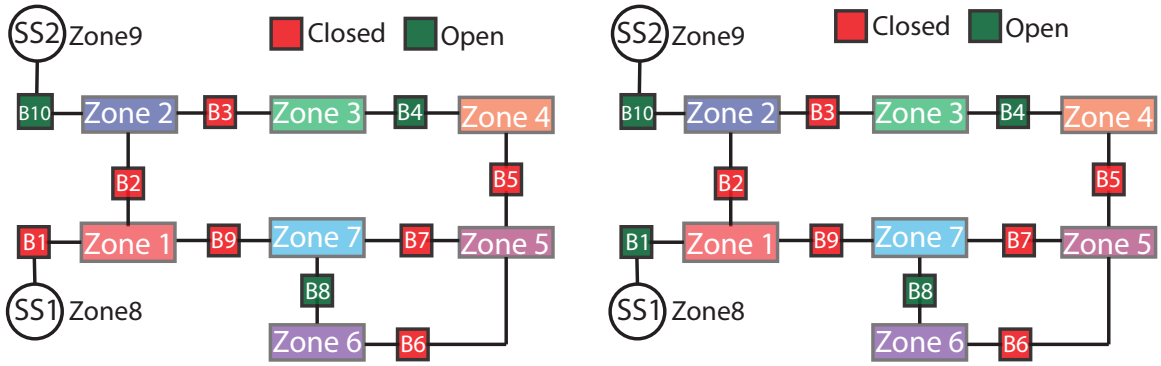

Figure 2: Topology status: (a) grid connected mode, (b) islanded mode.

A.1 Examples of the fault detection logic operation:

To demonstrate the working of the directional element, all four types of faults are created in zone 1 in grid connected and islanded mode of operation. All faults are created at 1s into the simulation and values are recorded at 1.05s. The base case topology for both modes of operation is shown in Figure. 2 The summary of the results for grid connected mode and islanded mode are tabulated below.

Grid connected mode:

AG fault in zone 1:

- $Va < 0.88PU$ (from voltage profile shown below)
- Ia and I0 are coming into the zone 1 from all boundary breakers B1, B2, and B9.
- Operating Elements: Phase A and ground
- Observation: Only zone 1 has the currents coming in from all boundary breakers in phase A.

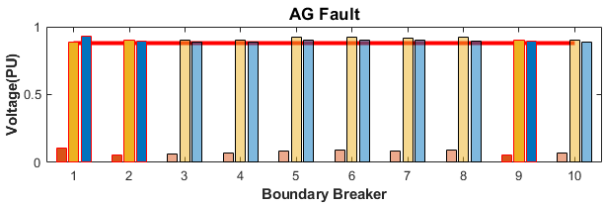

Breaker	Phase	AG fault in Zone 1			
		$\angle V_{pol}$	$\angle I_{mon}$	$\angle I_{mon}$-$\angle V_{pol}$	result
B1($SS \rightarrow Z1$)	A	150.31	151.91	1.60	Forward
	Gnd	247.57	158.28	-89.29	Forward
B2($Z1 \rightarrow Z2$)	A	150.75	28.08	-122.68	Reverse
	Gnd	246.03	-3.17	-249.20	Reverse
B3($Z2 \rightarrow Z3$)	A	150.95	30.54	-120.41	Reverse
	Gnd	248.21	-1.12	-249.33	Reverse
B5($Z5 \rightarrow Z4$)	A	151.44	43.48	-107.97	Reverse
	Gnd	215.74	-21.55	-237.29	Reverse
B6($Z6 \rightarrow Z5$)	A	151.45	-140.89	-292.34	Forward
	Gnd	217.76	151.04	-66.72	Forward
B7($Z7 \rightarrow Z5$)	A	151.35	40.33	-111.01	Reverse
	Gnd	212.69	-38.17	-250.86	Reverse
B9($Z1 \rightarrow Z7$)	A	150.75	30.21	-120.54	Reverse
	Gnd	246.03	-9.67	-255.70	Reverse

BCG fault in zone 1:

- $Vb, Vc < 0.88PU$
- Ib, Ic and I0 are coming into the zone 1 from all boundary breakers B1, B2, and B9.
- Operating Elements: Phase B, Phase C and ground
- Observation: Only zone 1 has the currents coming in from all boundary breakers.

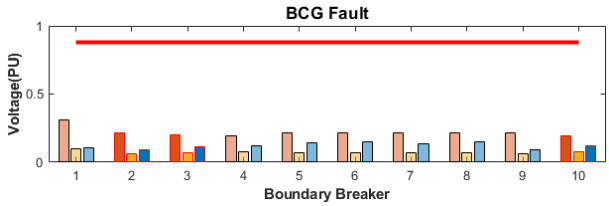

Breaker	Phase	BCG fault in Zone 1			
		$\angle V_{pol}$	$\angle I_{mon}$	$\angle I_{mon}$-$\angle V_{pol}$	result
B1($SS \rightarrow Z1$)	B	46.60	28.14	-18.45	Forward
	C	-119.64	-85.34	34.29	Forward
	Gnd	66.42	-23.18	-89.60	Forward
B2($Z1 \rightarrow Z2$)	B	60.07	-152.87	-212.94	Reverse
	C	-118.27	175.60	293.88	Reverse
	Gnd	65.03	176.50	111.48	Reverse
B3($Z2 \rightarrow Z3$)	B	60.50	-149.51	-210.01	Reverse
	C	-117.20	177.21	294.41	Reverse
	Gnd	66.36	177.34	110.98	Reverse
B5($Z5 \rightarrow Z4$)	B	62.23	-64.26	-126.49	Reverse
	C	-112.93	174.28	287.22	Reverse
	Gnd	87.89	-173.95	-261.84	Reverse
B6($Z6 \rightarrow Z5$)	B	62.42	120.63	58.21	Forward
	C	-112.40	0.34	112.74	Forward
	Gnd	86.95	21.07	-65.88	Forward
B7($Z7 \rightarrow Z5$)	B	61.95	-68.11	-130.06	Reverse
	C	-113.85	175.41	289.26	Reverse
	Gnd	76.60	-177.50	-254.10	Reverse
B9($Z1 \rightarrow Z7$)	B	60.07	-101.45	-161.52	Reverse
	C	-118.27	173.03	291.30	Reverse
	Gnd	65.03	172.23	107.20	Reverse

AC fault in zone 1:

- $Va, Vc < 0.88PU$
- Ia and Ic are coming into the zone 1 from all boundary breakers B1, B2, and B9.
- Operating Elements: Phase A, and Phase C.
- Observation: Only zone 1 has the currents coming in from all boundary breakers in phase A and phase C.

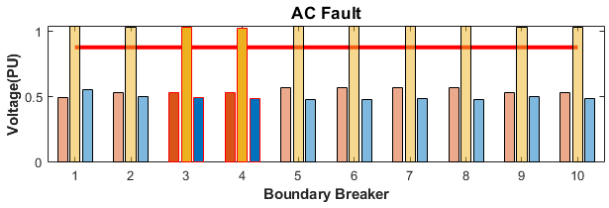

Breaker	Phase	AC fault in Zone 1			
		$\angle V_{pol}$	$\angle I_{mon}$	$\angle I_{mon}$-$\angle V_{pol}$	result
B1($SS \rightarrow Z1$)	A	122.92	122.30	-0.62	Forward
	C	-62.42	-61.41	1.01	Forward
B2($Z1 \rightarrow Z2$)	A	121.17	42.35	-78.82	Reverse
	C	-59.55	-168.25	-108.70	Reverse
B3($Z2 \rightarrow Z3$)	A	121.53	43.55	-77.98	Reverse
	C	-59.41	-166.21	-106.80	Reverse
B5($Z5 \rightarrow Z4$)	A	122.34	3.23	-119.12	Reverse
	C	-59.56	-151.90	-92.35	Reverse
B6($Z6 \rightarrow Z5$)	A	122.40	-170.94	-293.33	Forward
	C	-59.61	20.41	80.02	Forward
B7($Z7 \rightarrow Z5$)	A	122.14	20.73	-101.42	Reverse
	C	-59.58	-155.59	-96.01	Reverse
B9($Z1 \rightarrow Z7$)	A	121.17	27.56	-93.61	Reverse
	C	-59.55	-162.31	-102.76	Reverse

ABCG fault in zone 1:

- $Va, Vb, Vc < 0.88PU$
- Ia, Ib, Ic and I0 are coming into the zone 1 from all boundary breakers B1, B2, and B9.
- Operating Elements: Phase A, Phase B, Phase C and ground
- Observation: Only zone 1 has the currents coming in from all boundary breakers in all phases.

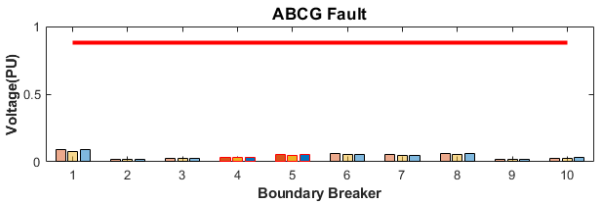

Breaker	Phase	ABCG fault in Zone 1			
		$\angle V_{pol}$	$\angle I_{mon}$	$\angle I_{mon}$-$\angle V_{pol}$	result
B1($SS \rightarrow Z1$)	A	129.46	151.82	22.35	Forward
	B	3.89	30.84	26.94	Forward
	C	-120.07	-89.77	30.31	Forward
	Gnd	2.38	-86.96	-89.34	Forward
B2($Z1 \rightarrow Z2$)	A	-142.34	59.72	202.06	Reverse
	B	89.82	-61.32	-151.14	Reverse
	C	-33.63	177.93	211.55	Reverse
	Gnd	75.14	-117.40	-192.54	Reverse
B3($Z2 \rightarrow Z3$)	A	-144.20	61.28	205.49	Reverse
	B	89.02	-61.76	-150.78	Reverse
	C	-30.36	177.11	207.46	Reverse
	Gnd	127.07	-173.22	-300.29	Reverse
B5($Z5 \rightarrow Z4$)	A	-145.98	57.09	203.06	Reverse
	B	91.70	-61.31	-153.01	Reverse
	C	-32.77	177.97	210.74	Reverse
	Gnd	171.83	12.74	-159.09	Reverse
B6($Z6 \rightarrow Z5$)	A	-146.42	-123.10	23.31	Forward
	B	91.90	118.74	26.85	Forward
	C	-32.64	-2.21	30.43	Forward
	Gnd	308.34	167.54	-140.80	Reverse
B7($Z7 \rightarrow Z5$)	A	-145.15	55.79	200.94	Reverse
	B	91.73	-62.49	-154.22	Reverse
	C	-33.60	177.91	211.52	Reverse
	Gnd	128.14	-86.81	-214.94	Reverse
B9($Z1 \rightarrow Z7$)	A	-142.34	56.63	198.97	Reverse
	B	89.82	-62.66	-152.48	Reverse
	C	-33.63	177.75	211.38	Reverse
	Gnd	75.14	175.87	100.74	Reverse

Islanded mode:

AG fault in zone 1:

- $Va < 0.88PU$ (from voltage profile shown below)
- Ia and I0 are coming into the zone 1 from all boundary breakers B1, B2, and B9.
- Operating Elements: Phase A and ground
- Observation: Only zone 1 has the currents coming in from all boundary breakers

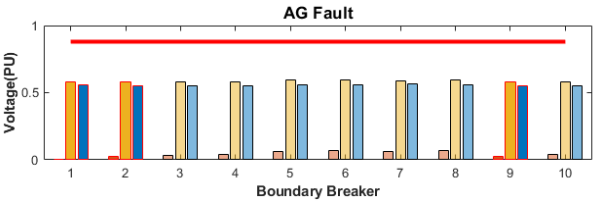

Breaker	Phase	AG fault in Zone 1			
		$\angle V_{pol}$	$\angle I_{mon}$	$\angle I_{mon}$-$\angle V_{pol}$	result
B2($Z1 \rightarrow Z2$)	A	-3.95	-110.97	-107.02	Reverse
	Gnd	151.30	-98.26	-249.56	Reverse
B3($Z2 \rightarrow Z3$)	A	-3.89	-114.36	-110.46	Reverse
	Gnd	154.13	-94.89	-249.02	Reverse
B5($Z5 \rightarrow Z4$)	A	-4.21	-127.10	-122.89	Reverse
	Gnd	11.61	153.26	141.65	Reverse
B6($Z6 \rightarrow Z5$)	A	-4.34	47.29	51.63	Forward
	Gnd	37.90	-50.97	-88.87	Forward
B7($Z7 \rightarrow Z5$)	A	-4.13	-128.85	-124.72	Reverse
	Gnd	7.55	112.28	104.73	Reverse
B9($Z1 \rightarrow Z7$)	A	-3.95	-123.82	-119.87	Reverse
	Gnd	151.30	-102.87	-254.17	Reverse

BCG fault in zone 1:

- $Vb, Vc < 0.88PU$
- Ib, Ic and I0 are coming into the zone 1 from all boundary breakers B2, and B9.
- Operating Elements: Phase B, Phase C and ground
- Observation: Only zone 1 has the currents coming in from all boundary breakers.

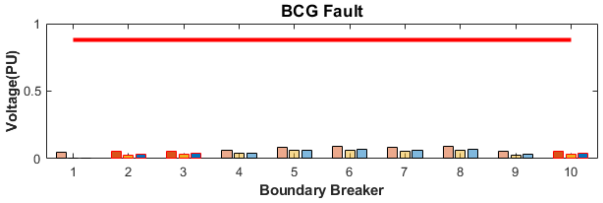

Breaker	Phase	BCG fault in Zone 1			
		$\angle V_{pol}$	$\angle I_{mon}$	$\angle I_{mon}$-$\angle V_{pol}$	result
B2($Z1 \rightarrow Z2$)	B	-62.84	101.73	164.58	Reverse
	C	130.25	14.61	-115.64	Reverse
	Gnd	312.94	65.10	-247.84	Reverse
B3($Z2 \rightarrow Z3$)	B	-65.34	102.75	168.10	Reverse
	C	131.63	13.59	-118.05	Reverse
	Gnd	314.98	65.13	-249.85	Reverse
B5($Z5 \rightarrow Z4$)	B	-70.82	115.47	186.28	Reverse
	C	133.64	-2.49	-136.13	Reverse
	Gnd	335.54	76.52	-259.03	Reverse
B6($Z6 \rightarrow Z5$)	B	-71.35	-63.05	8.30	Forward
	C	133.91	176.99	43.08	Forward
	Gnd	337.06	-85.32	-422.38	Forward
B7($Z7 \rightarrow Z5$)	B	-69.87	113.31	183.18	Reverse
	C	132.88	-1.21	-134.09	Reverse
	Gnd	322.03	72.12	-249.91	Reverse
B9($Z1 \rightarrow Z7$)	B	-62.84	108.34	171.18	Reverse
	C	130.25	3.22	-127.03	Reverse
	Gnd	312.94	58.92	-254.02	Reverse

AC fault in zone 1:

- $Va, Vc < 0.88PU$
- Ia and Ic are coming into the zone 1 from all boundary breakers B2, and B9.
- Operating Elements: Phase A, and Phase C.
- Observation: Only zone 1 has the currents coming in from all boundary breakers (B2, B9) in phases A and C.

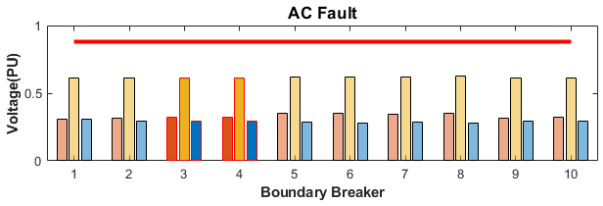

Breaker	Phase	AC fault in Zone 1			
		$\angle V_{pol}$	$\angle I_{mon}$	$\angle I_{mon}$-$\angle V_{pol}$	result
B2($Z1 \rightarrow Z2$)	A	-35.33	-151.65	-116.32	Reverse
	C	142.89	20.31	-122.57	Reverse
B3($Z2 \rightarrow Z3$)	A	-34.96	-148.36	-113.40	Reverse
	C	142.73	23.03	-119.69	Reverse
B5($Z5 \rightarrow Z4$)	A	-34.26	-167.57	-133.32	Reverse
	C	141.16	41.69	-99.46	Reverse
B6($Z6 \rightarrow Z5$)	A	-34.27	9.17	43.44	Forward
	C	140.87	-140.07	-280.94	Forward
B7($Z7 \rightarrow Z5$)	A	-34.41	-162.42	-128.02	Reverse
	C	141.41	37.18	-104.23	Reverse
B9($Z1 \rightarrow Z7$)	A	-35.33	-157.11	-121.78	Reverse
	C	142.89	29.96	-112.92	Reverse

ABCG fault in zone 1:

- $V_a, V_b, V_c < 0.88PU$
- $I_a, I_b, I_c and I_0$ are coming into the zone 1 from all boundary breakers B2, and B9.
- Operating Elements: Phase A, Phase B, Phase C and ground
- Observation: Only zone 1 has the currents coming in from all boundary breakers in all phases.

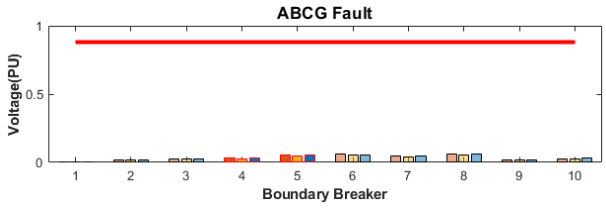

Breaker	Phase	ABCG fault in Zone 1			
		$\angle V_{pol}$	$\angle I_{mon}$	$\angle I_{mon}$-$\angle V_{pol}$	result
B1($SS \rightarrow Z1$)	A	33.30	-122.15	-155.45	Reverse
	B	-93.15	117.85	210.99	Reverse
	C	142.90	-2.15	-145.05	Reverse
	Gnd	255.58	-104.42	-360.00	Forward
B2($Z1 \rightarrow Z2$)	A	34.37	-129.91	-164.28	Reverse
	B	-95.16	116.47	211.62	Reverse
	C	141.75	-6.09	-147.84	Reverse
	Gnd	258.46	57.86	-200.59	Reverse
B3($Z2 \rightarrow Z3$)	A	33.06	-129.49	-162.56	Reverse
	B	-96.40	116.00	212.40	Reverse
	C	144.70	-6.33	-151.03	Reverse
	Gnd	301.84	-4.13	-305.97	Reverse
B5($Z5 \rightarrow Z4$)	A	29.75	-126.48	-156.23	Reverse
	B	-92.15	112.99	205.14	Reverse
	C	143.27	-6.37	-149.64	Reverse
	Gnd	344.47	111.73	-232.74	Reverse
B6($Z6 \rightarrow Z5$)	A	29.24	53.12	23.88	Forward
	B	-91.93	-66.93	25.00	Forward
	C	143.39	173.28	29.89	Forward
	Gnd	130.26	-42.71	-172.97	Reverse
B7($Z7 \rightarrow Z5$)	A	30.70	-126.61	-157.31	Reverse
	B	-92.25	112.45	204.70	Reverse
	C	142.39	-6.31	-148.70	Reverse
	Gnd	310.16	88.77	-221.39	Reverse
B9($Z1 \rightarrow Z7$)	A	34.37	-126.81	-161.18	Reverse
	B	-95.16	112.94	208.10	Reverse
	C	141.75	-6.49	-148.24	Reverse
	Gnd	258.46	-15.85	-274.30	Reverse

Appendix B Breadth First Search Algorithm

Breadth-first search (BFS) is an algorithm that is used for traversing a graph or a tree. A tree can be considered as a subset of a graph that contains multiple loops. The topology of a microgrid network discussed in chapter 3 resembles a graph when open breakers are considered. Hence, BFS algorithm can be used to construct the shortest path between two nodes.

A graph consists of nodes (vertices) and branches (edges). The BFS algorithm efficiently visits each node in an accurate breadth wise fashion and mark them in memory along with path information. A primary node or source point need to be specified for the algorithm to start with (substation node can be considered as primary node). Once the algorithm starts and marks the primary node, it moves to towards the next un-visited nodes. Once visited, each node will be marked as visited and its parent node is noted. This iterations continue until all nodes of the graph have been successfully visited and marked. An example of the algorithm on a graph with 6 nodes and 9 branches is shown in Figure. 3. Please note that although a graphical example is shown here, the traversal along the graph is done using the AM matrix to find the next un-visited nodes.

The reasons to use the BFS Algorithm are [54]:

- It has simple and robust architecture.
- It is useful for constructing the shortest path by traversing through the graph in the smallest number of iterations.
- The result of the BFS algorithm holds a high level of accuracy in comparison to other search algorithms.
- There is no possibility of BFS algorithm getting caught up in an infinite loop problem.

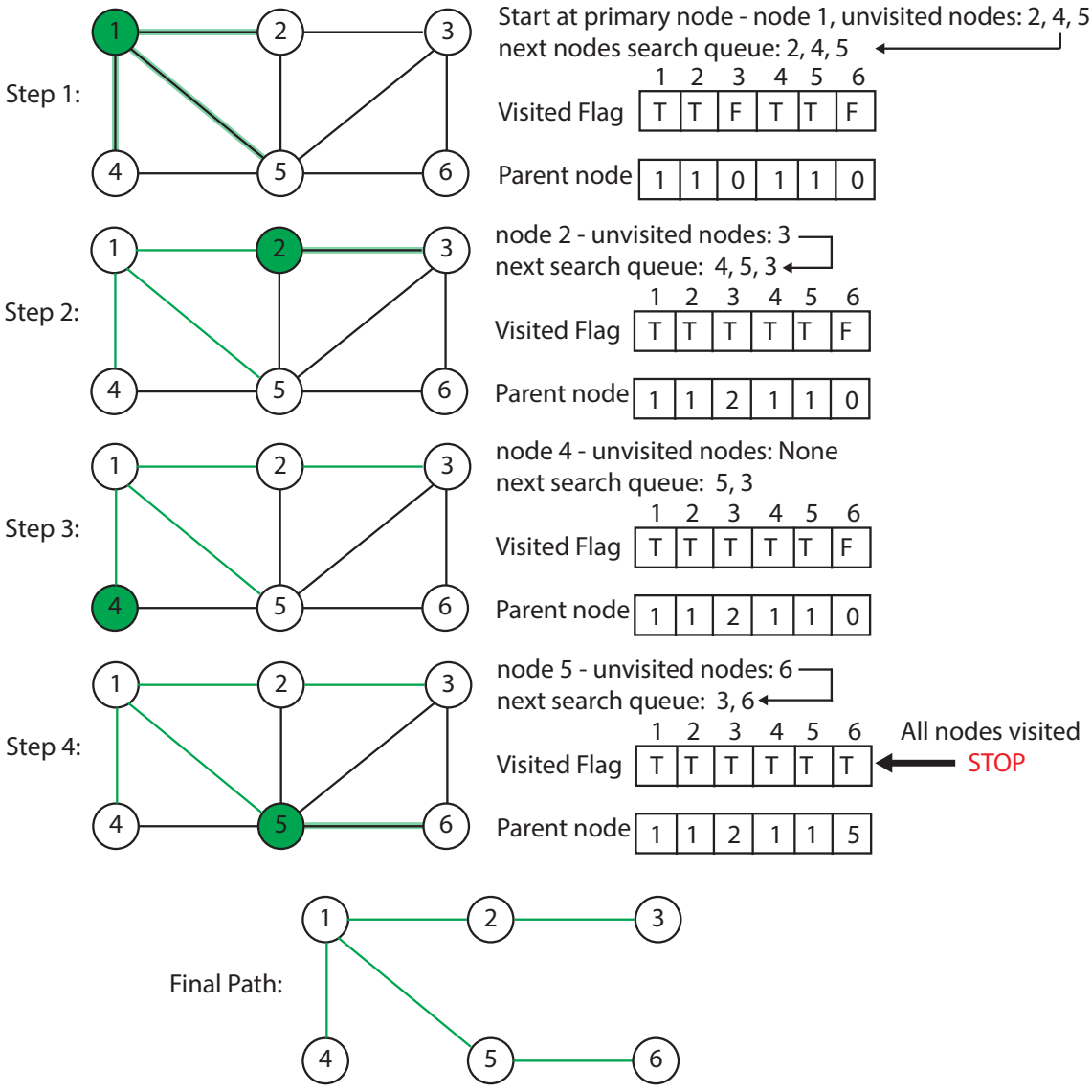

Figure 3: BFS algorithm example.

Appendix C Publications

1. **P. H. Gadde** and S. Brahma, "Realistic Microgrid Test Bed for Protection and Resiliency Studies," 2019 North American Power Symposium (NAPS), 2019, pp. 1-6.

2. **P. H. Gadde** and S. Brahma, "Comparison of PR and PI Controllers for Inverter Control in an Unbalanced Microgrid," 2020 52nd North American Power Symposium (NAPS), 2021, pp. 1-6

3. T. Patel, **P. Gadde**, S. Brahma, J. Hernandez-Alvidrez and M. J. Reno, "Real-time Microgrid Test Bed for Protection and Resiliency Studies," 2020 52nd North American Power Symposium (NAPS), 2021, pp. 1-6.

4. **P. H. Gadde** and S. M. Brahma, "Topology-Agnostic, Scalable, Self-Healing and Cost-Aware Protection of Microgrids," in IEEE Transactions on Power Delivery. IEEE Early access: https://ieeexplore.ieee.org/abstract/document/9618855

5. **P. H. Gadde**, S. Brahma and T. Patel, "Scalable Protection and Self-Healing of Microgrids: Hardware In The Loop Co-Simulation," 2022 IEEE Texas Power and Energy Conference (TPEC), 2022, pp. 1-6, doi: 10.1109/TPEC54980.2022.9750681.

6. **P. H. Gadde** and S. Brahma, "Unbalance Compensation Using single-phase Inverters in Inverter-Dominated Microgrids," 2022 IEEE Industry Applications Society Annual Meeting (IAS), 2022. (Accepted)

7. **P. H. Gadde** ,S. M. Brahma, T. Patel, "Scalable Protection and Self-Healing of Microgrids: Hardware In The Loop Co-Simulation," in IEEE Transactions on Industry Applications.(In review)

Bibliography

[1] IEEE standard for interconnection and interoperability of distributed energy resources with associated electric power systems interfaces. IEEE Std 1547-2018 (Revision of IEEE Std 1547-2003), pages 1–138, April 2018.

[2] Andreas Poullikkas. A comparative overview of large-scale battery systems for electricity storage. Renewable and Sustainable Energy Reviews, 27:778–788, Jan 2013.

[3] J. Rocabert, A. Luna, F. Blaabjerg, and P. Rodríguez. Control of power converters in ac microgrids. IEEE Transactions on Power Electronics, 27(11):4734–4749, Nov 2012.

[4] S. M. Brahma, J. Trejo, and J. Stamp. Insight into microgrid protection. In IEEE PES Innovative Smart Grid Technologies, Europe, pages 1–6, Oct 2014.

[5] E. Sortomme, G. J. Mapes, B. A. Foster, and S. S. Venkata. Fault analysis and protection of a microgrid. In 2008 40th North American Power Symposium, pages 1–6, Sep. 2008.

[6] Wei Du, Robert H. Lasseter, and Amrit S. Khalsa. Survivability of autonomous microgrid during overload events. IEEE Transactions on Smart Grid, 10(4):3515–3524, 2019.

[7] Peng Li, Bai Dan, Kang Yong, and Chen Jian. Research on three-phase inverter with unbalanced load. In Nineteenth Annual IEEE Applied Power Electronics Conference and Exposition, 2004. APEC '04., volume 1, pages 128–133, Feb 2004.

[8] Hongtao Shi, Fang Zhuo, Hao Yi, and Zhiqing Geng. Control strategy for microgrid under three-phase unbalance condition. Journal of Modern Power Systems and Clean Energy, 4(1):94–102, Jan 2016.

[9] I. Ali and S. Kucuksari. Voltage regulation of unbalanced distribution network with distributed generators. In 2016 North American Power Symposium (NAPS), pages 1–6, Sep. 2016.

[10] M. B. Delghavi and A. Yazdani. Islanded-mode control of electronically coupled distributed-resource units under unbalanced and nonlinear load conditions. IEEE Transactions on Power Delivery, 26(2):661–673, April 2011.

[11] S. Gonzalez, N. Gurule, M. J. Reno, and J. Johnson. Fault current experimental results of photovoltaic inverters operating with grid-support functionality. In 2018 IEEE 7th World Conference on Photovoltaic Energy Conversion (WCPEC) (A Joint Conference of 45th IEEE PVSC, 28th PVSEC 34th EU PVSEC), pages 1406–1411, June 2018.

[12] Q. Zhong. Robust droop controller for accurate proportional load sharing among inverters operated in parallel. IEEE Transactions on Industrial Electronics, 60(4):1281–1290, April 2013.

[13] Q. Zhong and Y. Zeng. Universal droop control of inverters with different types of output impedance. IEEE Access, 4:702–712, 2016.

[14] S. Brahma, N. Pragallapati, and M. Nagpal. Protection of islanded microgrid fed by inverters. In 2018 IEEE Power Energy Society General Meeting (PESGM), pages 1–5, Aug 2018.

[15] J. Svensson, M. Bongiorno, and A. Sannino. Practical implementation of delayed signal cancellation method for phase-sequence separation. IEEE Transactions on Power Delivery, 22(1):18–26, Jan 2007.

[16] IEEE PES Distribution System Analysis Subcommittee. Distribution test feeders. `http://sites.ieee.org/pes-testfeeders/resources/`.

[17] T. L. Vandoorn, J. C. Vasquez, J. De Kooning, J. M. Guerrero, and L. Vandevelde. Microgrids: Hierarchical control and an overview of the control and reserve management strategies. IEEE Industrial Electronics Magazine, 7(4):42–55, 2013.

[18] Phani Harsha Gadde, Munim Bin Gani, and Johan H. Enslin. An ac/dc hybrid campus microgrid: Modelling, control and financial analysis. In 2021 IEEE 12th International Symposium on Power Electronics for Distributed Generation Systems (PEDG), pages 1–7, 2021.

[19] R. Teodorescu, F. Blaabjerg, M. Liserre, and P. C. Loh. Proportional-resonant controllers and filters for grid-connected voltage-source converters. IEE Proceedings - Electric Power Applications, 153(5):750–762, 2006.

[20] M. Parvez, M. F. M. Elias, and N. A. Rahim. Performance analysis of pr current controller for single-phase inverters. In 4th IET Clean Energy and Technology Conference (CEAT 2016), pages 1–8, 2016.

[21] R. Teodorescu, F. Blaabjerg, M. Liserre, and A. Dell'Aquila. A stable three-phase lcl-filter based active rectifier without damping. In 38th IAS Annual Meeting on Conference Record of the Industry Applications Conference, 2003., volume 3, pages 1552–1557 vol.3, 2003.

[22] Phani Harsha Gadde and Sukumar Brahma. Realistic microgrid test bed for protection and resiliency studies. In 2019 North American Power Symposium (NAPS), pages 1–6, 2019.

[23] Q. Zhong and D. Boroyevich. A droop controller is intrinsically a phase-locked loop. In IECON 2013 - 39th Annual Conference of the IEEE Industrial Electronics Society, pages 5916–5921, 2013.

[24] S. Brahma, N. Pragallapati, and M. Nagpal. Protection of islanded microgrid fed by inverters. In 2018 IEEE Power Energy Society General Meeting (PESGM), pages 1–5, 2018.

[25] N. Bottrell and T. C. Green. Comparison of current-limiting strategies during fault ride-through of inverters to prevent latch-up and wind-up. IEEE Transactions on Power Electronics, 29(7):3786–3797, July 2014.

[26] D. T. Ton and M. A. Smith. The U.S. department of energy's microgrid initiative. The Electricity Journal, 25(8):84–94, April 2012.

[27] S. S. Venkata, M. Reno, W. Bower, S. Manson, J. Reilly, and G. W. Sey Jr. Microgrid protection: Advancing the state of the art. Sandia National Laboratorie, Tech. Rep., mar 2019.

[28] R. Haron, A. Mohamed, and H. Shareef. A review on protection schemes and coordination techniques in microgrid system. Journal of Applied Sciences, 12:101–112, feb 2012.

[29] J. Shiles, E. Wong, S. Rao, C. Sanden, M. A. Zamani, M. Davari, and F. Katiraei. Microgrid protection: An overview of protection strategies in north american microgrid projects. In 2017 IEEE Power Energy Society General Meeting, pages 1–5, 2017.

[30] H. Al-Nasseri and M. A. Redfern. Harmonics content based protection scheme for micro-grids dominated by solid state converters. In 2008 12th International Middle-East Power System Conference, pages 50–56, 2008.

[31] J. Duan, K. Zhang, and L. Cheng. A novel method of fault location for single-phase microgrids. IEEE Transactions on Smart Grid, 7(2):915–925, 2016.

[32] X. Li, A. Dyśko, and G. M. Burt. Traveling wave-based protection scheme for inverter-dominated microgrid using mathematical morphology. IEEE Transactions on Smart Grid, 5(5):2211–2218, 2014.

[33] Hannu Laaksonen, Dmitry Ishchenko, and Alexandre Oudalov. Adaptive protection and microgrid control design for hailuoto island. IEEE Transactions on Smart Grid, 5(3):1486–1493, 2014.

[34] J. Gu, M. Yang, J. Chen, H. Chung, C. Wang, Y. Chang, Y. Lee, C. Chan, and C. Hsu. Application of multi-agent systems to microgrid fault protection coordination. In 2016 International Symposium on Computer, Consumer and Control (IS3C), pages 188–191, 2016.

[35] N. Fawzy, H. F. Habib, O. Mohammed, and S. Brahma. Protection of microgrids with distributed generation based on multiagent system. In 2020 IEEE International Conference on Environment and Electrical Engineering and 2020 IEEE Industrial and Commercial Power Systems Europe (EEEIC / I CPS Europe), pages 1–5, 2020.

[36] C. Yuan, K. Lai, M. S. Illindala, M. A. Haj-ahmed, and A. S. Khalsa. Multilayered protection strategy for developing community microgrids in village distribution systems. IEEE Transactions on Power Delivery, 32(1):495–503, 2017.

[37] S. B. A. Bukhari, C. Kim, K. K. Mehmood, R. Haider, and M. Saeed Uz Zaman. Convolutional neural network-based intelligent protection strategy for microgrids. IET Generation, Transmission Distribution, 14(7):1177–1185, 2020.

[38] S. Mirsaeidi, D. M. Said, M. W. Mustafa, M. H. Habibuddin, and K. Ghaffari. Progress and problems in micro-grid protection schemes. Renewable and Sustainable Energy Reviews, 37:834–839, 2014.

[39] T. Patel, S. Brahma, J. Hernandez-Alvidrez, and M. J. Reno. Adaptive protection scheme for a real-world microgrid with 100inverter-based resources. In 2020 IEEE Kansas Power and Energy Conference (KPEC), pages 1–6, 2020.

[40] T. Patel, P. H. Gadde, S. Brahma, J. Hernandez-Alvidrez, and M. Reno. Real-time microgrid test bed for protection and resiliency studies. In 2020 North American Power Symposium (NAPS), pages 1–6, 2020.

[41] IEEE 123-bus Feeder. `https://site.ieee.org/pes-testfeeders/resources/`.

[42] Advancements in centralized protection and control within a substation. IEEE Transactions on Power Delivery, 31(4):1945–1952, 2016.

[43] Matthew J. Reno, Sukumar Brahma, Ali Bidram, and Michael E. Ropp. Influence of inverter-based resources on microgrid protection: Part 1: Microgrids in radial distribution systems. IEEE Power and Energy Magazine, 19(3):36–46, 2021.

[44] V. Valdivia, A. Barrado, A. LÁzaro, P. Zumel, C. Raga, and C. FernÁndez. Simple modeling and identification procedures for "black-box" behavioral modeling of power converters based on transient response analysis. IEEE Transactions on Power Electronics, 24(12):2776–2790, 2009.

[45] H. Kanaan, K. Al-Haddad, and F. Fnaiech. Modelling and control of three-phase/switch/level fixed-frequency pwm rectifier: state-space averaged model. IEE Proceedings - Electric Power Applications, 152(3):551–557, 2005.

[46] S. Hiti. Modeling and control of three-phase PWM converters. PhD thesis, Virginia Polytechnic Institute and State University, Blacksburg, VA, 1995.

[47] D. L. Ransom. Get in step with synchronization. In 2014 67th Annual Conference for Protective Relay Engineers, pages 401–407, 2014.

[48] Siemens AG. Siemens Vacuum Recloser 3AD. https://assets.new.siemens.com/siemens/assets/api/uuid:2573ed46-a618-45e5-bcdf-40b8f511dd5f/hg-11-42-en.pdf.

[49] B. Falahati and E. Chua. Failure modes in iec 61850-enabled substation automation systems. In 2016 IEEE/PES Transmission and Distribution Conference and Exposition (T&D), pages 1–5, 2016.

[50] J. L. Blackburn and T. J. Domin. Protective Relaying, Principles and Applications, chapter 3, pages 94–101. CRC Press, New York, 3rd ed. edition, 2006.

[51] IEEE guide for protective relay applications to transmission lines. IEEE Std C37.113-2015 (Revision of IEEE Std C37.113-1999), 2016.

[52] S. Brahma. Protection of distribution system islands fed by inverter-interfaced sources. In 2019 IEEE Milan PowerTech, pages 1–6, 2019.

[53] Siemens. SIRIUS soft starter. https://assets.new.siemens.com/siemens/assets/api/uuid:db1bd0a0-8d3a-4e13-ae6a-3f9427f554c3/siep-b10001-00sirius3rweghflyerenus-72.pdf.

[54] D. C. Kozen. The Design and Analysis of Algorithms, chapter 4, pages 19–30. Springer New York, New York, 1st ed. edition, 1992.

[55] K sidwall and P Forsyth. Advancements in real-time simulation for the validation of grid modernization technologies. Energies, 13(16):4036, 2020.

[56] Hany F. Habib, Nevin Fawzy, and Sukumar Brahma. Performance testing and assessment of protection scheme using real-time hardware-in-the-loop and iec 61850 standard. IEEE Transactions on Industry Applications, 57(5):4569–4578, 2021.

[57] RTDS Technologies. RTDS Hardware Manual, 03 2020.

[58] Fanny Clavel, Eric Savary, Philippe Angays, and Alain Vieux-Melchior. Integration of a new standard: A network simulator of iec 61850 architectures for electrical substations. IEEE Industry Applications Magazine, 21(1):41–48, 2015.

[59] RTDS Technologies. RSCAD IEC61850 IED configuration tool, 03 2020.

[60] Javier Martín Herrera, Matias Sanchez Mingarro, Santiago López Barba, David Dolezilek, Fernando Calero, Amandeep Kalra, and Brian Waldron. Case study of time-domain automation and communications: Field-proven benefits to automation, control, monitoring, and special protection schemes. In 2017 Saudi Arabia Smart Grid (SASG), pages 1–8, 2017.

[61] Gelli Ravikumar, Dan Ameme, Satyajayant Misra, Sukumar Brahma, and Reza Tourani. ¡italic¿icasm¡/italic¿: An information-centric network architecture for wide area measurement systems. IEEE Transactions on Smart Grid, 11(4):3418–3427, 2020.

[62] THE GRID CODE - National Grid Electricity System Operator Limited.

[63] Al-Attar Ali Mohamed, Shimaa Mohamed Ali, A.M. Hemeida, and Abdalla Ahmed Ibrahim. Optimal placement of distributed energy resources including different load models using different optimization techniques. In 2019 International Conference on Innovative Trends in Computer Engineering (ITCE), pages 389–395, 2019.

[64] Ashoke Kumar Basu, Sunetra Chowdhury, and S. P. Chowdhury. Impact of strategic deployment of chp-based ders on microgrid reliability. IEEE Transactions on Power Delivery, 25(3):1697–1705, 2010.

[65] Ieee standard for the specification of microgrid controllers. IEEE Std 2030.7-2017, pages 1–43, 2018.

[66] Industrial communication networks - high availability automation networks - part 3: Parallel redundancy protocol (prp) and high-availability seamless redundancy (hsr). IEC 62439-3:2021, pages 493–500, 2021.

[67] Teleprotection equipment of power systems - performance and testing - part 1: Command systems. IEC 60834-1:1999, pages 1–500, 1999.